Appliance-level Demand Side Management for Power Network Stress Mitigation

Ren Kang
St Hilda's College

Department of Engineering Science
University of Oxford

Dissertation submitted for the degree of
Doctor of Philosophy

Michaelmas 2016

Abstract

Power networks are under increasing pressure to maintain operation within permissible voltage and current limits with higher penetrations of renewable energy. This thesis aims to develop and evaluate a practical and economical way to control key domestic appliances to alleviate stress caused by high level of renewable energy penetration.

The first objective in this thesis is to develop a network stress identification technique that does not rely on communication infrastructure. Traditionally, there is an emphasis on using centralized control strategies for demand side management (DSM) involving a central brain which collects information from each individual device and sends out commands to them which schedules their operation. This approach relies heavily on communication infrastructure and introduces security challenges, which are not problems for distributed or decentralised control. Whilst the latter two approaches have the virtue of scalability and flexibility, they require a good network model or good estimation of network condition without real time communication for effective control. A tap change detection approach via local voltage measurement has been developed and validated to enable the domestic smart appliance to perceive the network stress in three different levels across the power network without any real-time communication.

The second objective is to explore the economic benefits associated with the usage of electric hot water tanks (EHWTs) as an alternative to home batteries or electric vehicles for demand response. To do this, an optimization approach for sizing of the EHWT is proposed. Real-world hot water usage data is analysed and applied, revealing four typical hot water usage patterns and 100-litre as the most common optimal tank size for UK consumer.

Finally, since increasing PV generation has risen voltage concerns in various locations across the UK, such as in Cornwall, this thesis investigated to what extend intelligent EHWTs can be used to alleviate the LV network stress caused by the high level of PV penetration. A Monte-Carlo simulation is carried out on real UK LV networks, showing that the presence of intelligent EHWTs could improve both the voltage and current performance of the LV network and allow 50% more PV installations beyond the network's original capacity.

Acknowledgements

Firstly, I am deeply grateful to my supervisor, Professor Malcolm McCulloch, for his guidance and support throughout my study at Oxford. He taught me how to do research, and gave me the freedom to pursue the subject that I am interested in.

I would like to acknowledge my colleagues, especially Richard Wong and Peter Armstrong for their valuable discussion and feedback to my thesis. My thanks also extend to my collaborators, Professor Stephen Duncan, Professor Antonis Papachristodoulou and Xuan Zhang, with whom I gained valuable insights in control theory and its applications. A special thanks to my girlfriend Chen Zou, who has always been around and supported me with care and love.

Finally, I would like to express my deepest gratitude to my family, my mother Lan Zhang and my father Canhua Kang, for their love and support. Without them I would never be this far, and this thesis is dedicated to them.

Declaration

The work presented in this thesis was carried out by the author between October 2012 to December 2016 under the supervision of Professor Malcolm McCulloch. Where any work of others has been used, appropriate reference and acknowledgement were made in the text.

This thesis has not been submitted towards the completion of another degree at the University of Oxford or elsewhere. Parts of the thesis have been submitted to or published in the following scientific journals or conference presentations:

1. R. Kang and M. D. McCulloch, "Identification of Electric Power System Stress through Feeder Voltage Measurement," in *Innovative Smart Grid Technologies Europe (ISGT EUROPE), 2013 4th IEEE/PES*, 2014, pp. 1–6.
2. X. Zhang, R. Kang, M. McCulloch, and A. Papachristodoulou, "Real-time active and reactive power regulation in power systems with tap-changing transformers and controllable loads," *Sustain. Energy, Grids Networks*, vol. 5, pp. 27–38, 2016.
3. R. Kang, X. Zhang, A. Papachristodoulou, M. McCulloch, "Indicating Low Voltage Network Stress Using Tap Change Detection" *IET Gener. Transm. Distrib.*, manuscript submitted and awaiting for review.
4. R. Kang, M. McCulloch, "Identification of Electric Power System Stress through Local Voltage Measurement," in *Manchester Electrical Energy and Power Systems (MEEPS) workshop*, Nov, 2015 (Oral presentation).
5. R. Kang, M. McCulloch, "Sizing Design and Usage Profile Clustering for Domestic Hot Water Storage Systems", in preparation.
6. R. Kang, M. McCulloch, "Probabilistic Impact Assessment of Electric Hot Water Tanks in LV Distribution Network", in preparation.

Nomenclature

The variables are defined as follows:

n_z	The largest sampling integer before the zero-crossing
n	Number of sampling points between two zero-crossings
V_n	Voltage at the nth sampling point (V)
V_{n+1}	Voltage at the n+1th sampling point (V)
f	System frequency (Hz)
$V_{\mathrm{rms}(1/2)}$	Half-cycle RMS voltage (V)
V_i	The ith voltage between two zero-crossings (V)
V_{diff}	Voltage different in six half cycles (V)
δ	Threshold for event detector (V*)*
S_0	Cumulative sum
α_n	Threshold value for CUMSUM algorithm
z_{tp}	z-score for tap positions
TP	Tap positions
σ_{tp}	Standard deviation of tap positions in 24 hours
P	Active power (W)
Q	Reactive power (VAr)
V_{measured}	Measured mains voltage (V)
V_{app}	Apparent voltage (V)
E_{dsin}	Feed-in renewable energy (kWh)
E_{dsout}	Energy demand from the household (kWh)
E_{egin}	Energy supplied from the grid (kWh)
E_{egout}	Energy exported from the storage system to the grid (kWh)
C	Energy capacity of the storage system (kWh)
S	State of charge of the energy storage system

E_{sl}	Energy storage loss (kWh)
m	Water mass that has been used (litre)
C_{p}	Heat capacity of the water ($\mathrm{J}/(\mathrm{kg}\cdot\mathrm{K})$)
T_{out}	Tank outlet temperature (°C)
T_{in}	Tank inlet temperature (°C)
C_{pi}	Electricity price (£/kWh)
C_{pe}	Export tariff (£/kWh)
C_{rn}	Normalized daily capital cost of the renewable generation unit (£/day)
C_{es}	Normalized daily capital cost of the energy storage unit (£/day)
C_{t}	Capital cost of the tank (£)
μ	Daily equivalent interest rate
E_{c}	Thermal energy in the tank (kWh)
M	Mass of water in the tank (litre)
T_{t}	Water temperature in the tank (°C)
T_{a}	Ambient (reference) temperature (°C)
M_{est}	Estimated optimal tank size (litre)
A	PV panel size (kWp)
H	Irradiance projected onto the PV panel (kWh/m^2)
η	Scaling factor for the PV panel
V_{ut}	Upper voltage threshold to enable over-voltage protection (V)
V_{hs}	Household voltage supply (V)
V_{lt}	lower voltage threshold to enable under-voltage protection (V)

Acronyms:

DSM	Demand Side Management
EHWT	Electric Hot Water Tank
LV	Low Voltage
MV	Medium Voltage
HV	High Voltage
OLTC	On-load Tap Change (Transformer)
MLP	Multilayer Perceptron
PV	Photovoltaic
EST	Energy and Saving Trust
DNO	Distribution Network Operator

Table of Contents

List of Figures

List of Tables

Chapter 1. Introduction

This thesis explores the question: "*Is there an effective and economical way of using key domestic appliances which will allow the power network to operate within permissible thermal and voltage limits, with higher penetration of intermittent renewable energy sources?*". This chapter sets out the high-level research themes, and followed in the next chapter by a more detailed literature review and gap analysis.

Section 1.1 begins with an introduction of the environmental context which motivates the study of this dissertation. *Section 1.2* introduces the scope of the study, including demand side management (DSM) and the use of electric hot water tanks (EHWTs). Finally, details of the roadmap and structure for the thesis are provided in *Section 1.3*.

1.1 Motivation: The Environmental Context

CO_2 is the primary greenhouse gas, the one which is believed to be the major cause of global warming [1]. Atmospheric CO_2 can be produced either by natural sources as part of the Earth's carbon cycle or by human activities such as the combustion of fossil fuels. Since the industrial revolution, human activities are considered as the major contributor to the CO_2 increase in the atmosphere, and the main sources of CO_2 emission through human activities are electricity generation, transport and industrial process [1].

The Intergovernmental Panel and Climate Change has claimed that "the net damage costs of climate change (temperature rising caused by greenhouse gas) are likely to be significant and to increase over time" [2]. It is predicted by Allen et al. [3] that 1 trillion tons of CO_2 emission would results in 1.1 to 2.7 °C of warming. To avoid such temperature increases, CO_2 emissions therefore need to be curtailed. The International Energy Agency

[4] stated that although many countries are on track to achieve the carbon targets set in the pledges of the Paris Agreement, more efforts still need to be made to keep temperature increase by 2100 below 2 °C, the figure which is generally considered to represent a manageable level that does not constitute a danger to world climate stability.

As the UK has committed to reduce greenhouse gas emissions by at least 80% by 2050, relative to 1990 levels [5], which is equivalent to a reduction in energy consumption of between 26 and 43%, a wide range of energy saving measures must be deployed to achieve this target. According to the Department for Business, Energy & Industrial Strategy [6], in 2015, the most common fuel types for energy consumption in the UK are solid fuels, electricity, gas, and petroleum. Even though petroleum and gas still account for a higher portion of energy consumption (45% and 30% respectively) than electricity (20%), they have in the last decade, been decreasing, while the proportion for electricity has remained stable (at around 26,000 ktoe per annum). In terms of end use, in 2015, gas and electricity accounted for 63% and 23% respectively of total energy consumption (39,623 ktoe) in the domestic sector. In the industrial sector, gas and electricity were approximately the same at 7800 ktoe, and in the transport sector, the primary source of energy consumption was oil (97% of 54,810 ktoe). The proportion of electricity in these sectors would, however, increase in future, given that the UK is integrating more renewable generation units, adopting more EVs, and expecting to decommission its gas network by 2050 [7]. ***Figure 1.1*** shows the trends in electricity consumption in the UK for different sectors: residential, industrial and other (transport, public administration, agricultural and commercial) sectors. The residential sector represents the largest portion of total electricity consumption of 109 TWh in 2015. Furthermore, the use of electric vehicles and the electrification of the heating sector (as natural gas declines as the source of heating) will increase the percentage of electricity consumption in the residential sector. Given that decarbonization is not just

about reducing energy demand, but also improving efficiency, the motivation behind this thesis is the need to find low carbon technologies which could enable better use of clean renewable energy.

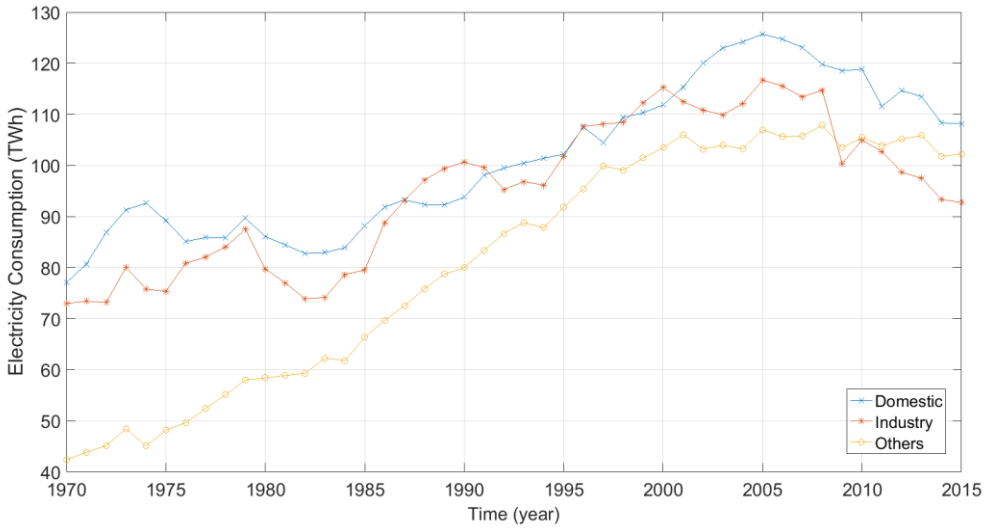

Figure 1.1 Electricity consumption by sectors in the UK [8]

1.2 Towards a Low Carbon Network

Various measures, including increased installation of renewable energy, have been taken within power networks to reduce the carbon footprint. ***Figure 1.2*** shows electrical generation capacity in the UK for renewable energy, with a significant increase in the use of solar PV and wind since 2010. This, on the one hand, reduces the carbon emissions associated with electricity generation which would otherwise have been generated by fossil fuels. But on the other hand, it leads to voltage or thermal issues for the network due to surplus PV and intermittent wind generation. This limits the renewable generation capacity that a network is able to withstand [9].

Demand side management (DSM), which is used by utility companies to optimize energy consumption on the user side to match available and planned energy generation, has

emerged in recent years as a solution which allows to accommodate higher level of renewable generations. Given that the residential sector is responsible for the largest share of electricity consumption, the objective of this thesis is to explore economic and practical DSM techniques at residential level, with a view to enabling enhanced utilization of renewable energy.

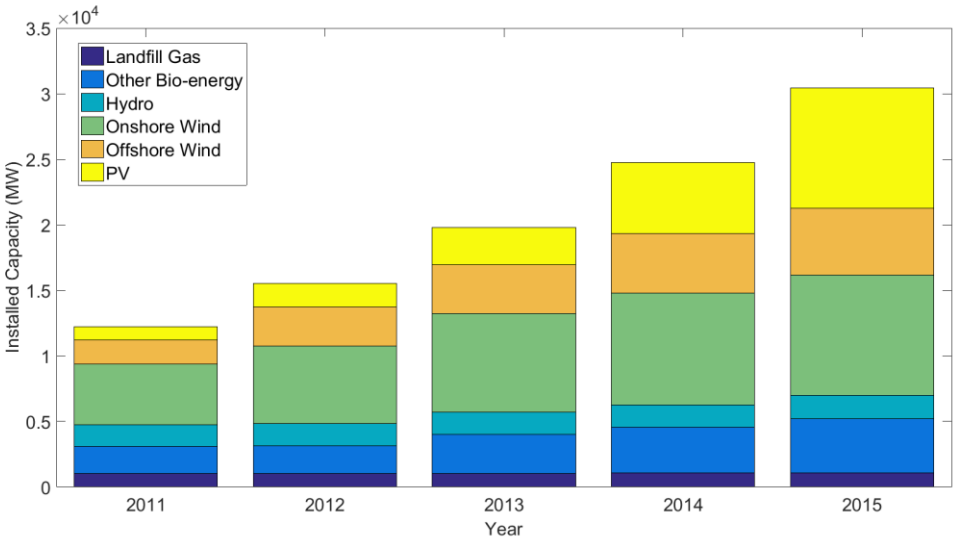

Figure 1.2 Electrical generation capacity for renewable energy in the UK [10]

1.2.1 DSM schemes

DSM has become important in the field of smart grid for energy conservation and power network control. Earlier research by Zehir et al. [11] claimed that the cost of controlling load was lower than the construction of a new power plant or the setup and use of an energy storage system. As DSM is capable of controlling the load directly or indirectly, reducing peak demand and smoothing the demand curve, it can be used as a practical and cost-effective approach to resolving the capacity and efficiency issues in the power system. Many countries, such as the USA, the UK and France, have already adopted time-of-use tariff [12], which is considered as an indirect DSM approach. Another aspect to consider as regards the acceptance of DSM is smart meter infrastructure, which allows the implementation of more sophisticated DSM schemes [13]. ***Figure 1.3*** shows the

regulatory situation and progress of smart meter implementation in Europe. It can be seen from the figure that many countries, including the UK, are either actively rolling out the smart meter scheme or planning to do so.

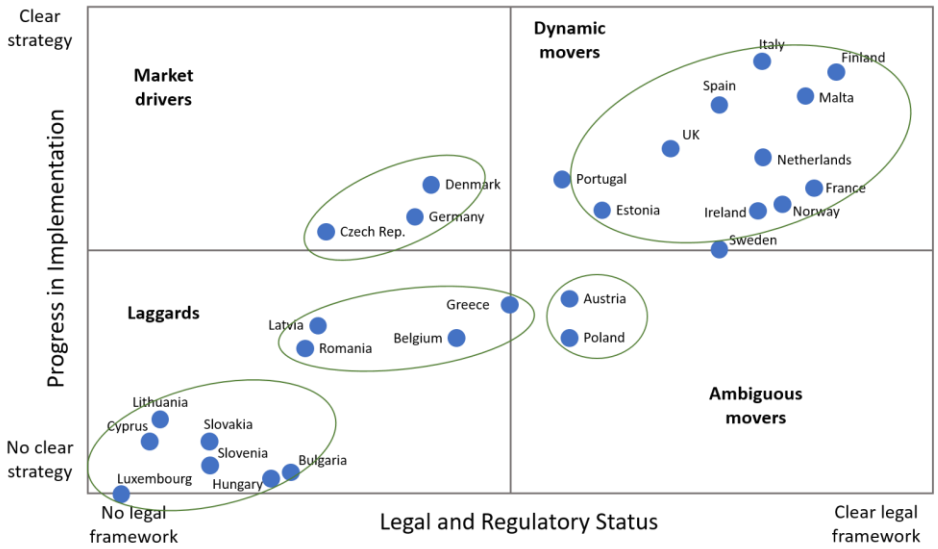

Figure 1.3 Smart meter implementation progress in Europe (reproduced from [14]**)**

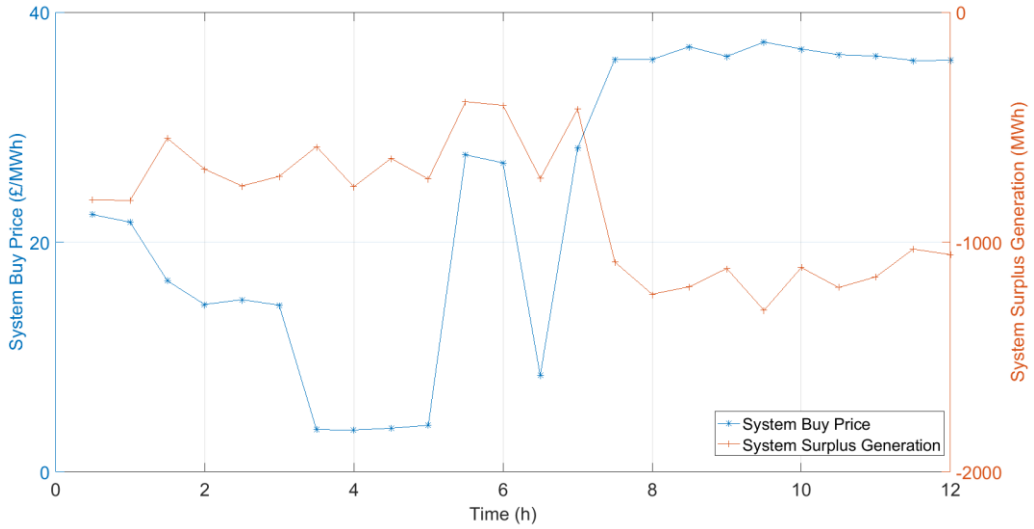

Figure 1.4 UK System buy price and surplus generation in January 2nd, 2015 [15]

To tackle the overall imbalance between generation and demand, the UK introduced an energy balancing market as one of the DSM approaches, in which the National Grid can accept a 'bid' or 'offer' to increase or decrease generation or demand based on the

discrepancy between electricity supplied and consumed [16]. ***Figure 1.4*** shows the UK energy market system buy price and surplus generation on 2nd January, 2015, with price and surplus generation trends showing an inverse proportional relationship. This approach helps the National Grid to balance the energy network more effectively in real time, but this usually does not solve the local stress and often does not involve load control on domestic consumer side.

The topology and further details of DSM schemes are reviewed in *Section 2.3.4*. There are more DSM approaches currently on trial or being researched. In this thesis, we aim to develop techniques which could enable more efficient and effective DSM schemes for local network stress mitigation.

1.2.2 Potential of EHWTs

At residential level, DSM approaches usually involve changing the consumer's energy usage behaviour, controlling appliances or devices, and the use of domestic energy storage systems. There is an overlap between the latter two approaches, as energy storage systems can sometimes also be appliances, for instance, hot water storage tanks or electric vehicles.

Both storage and service-based devices can be used as DSM assets. Home battery systems have been gaining attention lately as domestic energy storage devices [17]. Despite significant improvements in performance in battery chemistry technologies in recent years (notably from lead acid to lithium-ion cells where energy density increased from 30-40 Wh/kg to 110-175 Wh/kg [18]), there are still challenges involved in the widespread adoption of home battery systems, such as the high cost [18].

A complimentary approach to home battery systems is the use of existing hot water tank fleets in the domestic sector. The energy storage potential associated with these tanks is significant. In England alone, for example, 55% of the 23 million households have hot

water storage tanks [19], and 50% of these tanks use an electric immersion heater either as a primary or secondary source of heat [20]. Assuming all these tanks are the typical size of 120-litre, with operating and ambient temperatures 60 °C and 20 °C respectively, the total storage capacity for tanks with electrical immersion heaters is approximately 35 GWh. To put this capacity into perspective, the largest system surplus power generation in a day in the UK in 2016 was 2.2GWh on 22nd of March [21], which could be absorbed by using only 6% of the hot water tank capacity.

Domestic energy consumption, divided by end use, is shown in ***Figure 1.5***, with 80% of total energy used for water and space heating, out of which approximately 10%, or 25353 GWh [6], was supplied by electricity. However, given the decarbonization target which the UK government has committed to, the gas network in the UK is expected have been decommissioned by 2050 [7]. If this does happen, it is likely that there will be an increased uptake of electrical load associated with water heating. Given the reasons above, it is our belief that domestic EHWTs will in future take on a more important role in DSM planning.

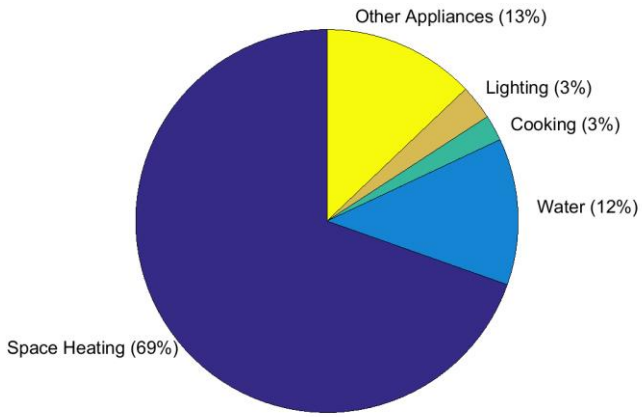

Figure 1.5 Domestic energy consumption by end user in 2016 [6]

1.3 Objectives of The Thesis

Given the background introduction in the previous sections, the aim of this thesis is to use intelligent domestic appliances to mitigate the LV network stress caused by PV penetration. More specifically, the aim can be broken down into answering the following four research questions (objectives):

1. "*Is there a technique that can enable domestic devices to perceive the stress across the network in real time without the need to further invest into the communication infrastructure?*"
2. *"How to determine the optimal tank size to provide customers with greater economic benefits, given the pattern of their hot water usage?"*
3. *"What are the typical patterns of hot water usage and the most common optimal tank size for UK consumers?"*
4. "*To what extent can intelligent EHWTs be used to alleviate voltage and thermal problems in the LV network caused by excessive PV generation?*"

Figure 1.6 illustrates how objectives connected and covered by thesis chapters. The details and connection of each chapter are further explained in the next section.

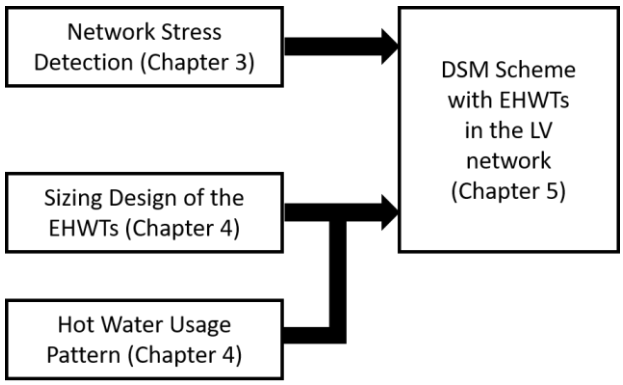

Figure 1.6 Illustration of connections among the scopes in the thesis

1.4 Thesis Structure

The remainder of this thesis is organized as follows:

Chapter 2 presents a gap analysis of the challenges surrounding the question proposed at the beginning of the thesis, and sets out a roadmap for the following chapters. A review of the literature, focusing on existing power network issues, identifies the major challenges involved in the increase in distributed generation. A variety of solutions for tackling such challenges are then compared, and DSM is identified as a practical solution, bearing in mind cost and ease of implementation. Various DSM assets are further compared, and gaps as regards the sizing design of EHWTs identified. Finally, to evaluate the performance of the proposed techniques at network level, past network simulation techniques are reviewed, and a gap identified for performance evaluation of EHWTs.

With a view to better facilitating the operation of decentralised DSM devices and answering the first research question: "*Is there a technique that can enable domestic devices to perceive the stress across the network in real time without the need to further invest into the communication infrastructure?*", *Chapter 3* proposes a technique that identifies the network stress condition without any external communication. This chapter begins with the definition of network stress at three different levels across the power network, namely, high voltage (system-wide), medium and low voltage. The techniques for using the information extracted from local voltage measurement for stress identification at the three levels are proposed and validated in the following sections. The significance of these techniques for DSM planning is further explained at the end of this chapter.

Once the appliance can perceive the stress, the next step is to investigate the particular appliance that could be used as DSM asset. In our case, the benefit of EHWT is explored. A sizing design for domestic EHWTs is proposed in *Chapter 4*, addressing the second and third research questions: *"1. How to determine the optimal tank size to provide customers*

with greater economic benefits, given the pattern of their hot water usage? 2. What are the typical patterns of hot water usage and the most common optimal tank size for UK consumers?". A sizing optimization problem is formulated and real-world hot water demand data is used as input to produce realistic optimal tank sizes for UK consumers. The hot water demand pattern and its relationship with the household occupancy feature is also investigated. The outcomes of this chapter provide guidelines for the inputs required for the network simulation in the following chapter.

To combine the techniques developed in the previous two chapters, *Chapter 5* proposed a probabilistic assessment approach to evaluate the performance of EHWTs under different control scenarios in the LV network. Instead of looking at stress at all levels, we focus on investigating the impact of LV network stress. A DSM control scheme responding only to voltage is therefore used, instead of the DSM scheme incorporating the stress identification technique in C*hapter 3*. Case studies using real UK networks are carried out using validated demand and generation profiles, and the performance results are analysed in the final section. This addresses the question "*To what extent can intelligent EHWTs be used to alleviate voltage and thermal problems caused by excessive PV generation?*".

The final chapter summarises the work carried out in this thesis, along with the conclusion remarks. Recommendations for future work are also suggested.

Chapter 2. A Review of Power Network Issues and Demand Side Management

2.1 Introduction

Electric power networks are complex adaptive systems which continually evolve as demands on them change. This chapter identifies the challenges around the question raised at the beginning of the thesis: *"Is there an effective and economical way of using key domestic appliances which will allow the power network to operate within permissible thermal and voltage limits, with higher penetration of intermittent renewable energy sources?"*. We first explain the difference between the conventional and modern power network in *Section 2.2.1*, followed by the discussion of major challenges around power network operation in *Section 2.2.2*. To tackle these challenges, a list of solutions is discussed in *Section 2.3*. Among these solutions, Demand Side Management (DSM), and in particular decentralised DSM, is highlighted as one of the most economic strategies to address challenges in power distribution networks. *Section 2.5* extends the discussion to devices that could be used as DSM assets, particularly home batteries, refrigerators & freezers, and electric hot water tanks. Finally, to determine the impact of domestic DSM assets on the operation of power distribution networks, *Section 2.6* presents an overview of impact assessment techniques from the literature that has been undertaken in the past.

2.2 Power Networks and Major Issues

2.2.1 Evolving Power Networks

A typical conventional electrical power system in the UK is illustrated in ***Figure 2.1***. Electric power plants convert energy from primary sources, such as coal and gas, into electrical power which is supplied to the transmission network through step-up

transformers. Electricity is then carried to the distribution substation via the transmission network. The distribution network has two subnetworks, primary (medium voltage) and secondary (low voltage) [22]. In terms of the physical structure, the distribution substation is at the top level of the distribution network and directly connects to the transmission network. It steps down the voltage from 132kV and above to 66kV or less and feeds it into the primary distribution network. A typical primary distribution, or medium voltage (MV) network, consists of a step-down on-load tap-changing (OLTC) transformer which has multiple feeders connecting to distribution transformers. The distribution transformers supply secondary distribution, or low voltage (LV) networks. These networks consist of step-down three-phase transformers, for example 11kV / 415V in the UK, which supply individual households and light commercial consumers on a single phase 230 V connection via three-phase, four wire networks [23]. The overall intent behind the design of conventional networks is to supply power in a unidirectional way as it flows from centralized generating units to end users. In conventional, unidirectional networks, power is usually generated to match demand since there is little or no energy storage and some control algorithms that are embedded in the OLTC transformers can have difficulties handling large reverse power flows [24]. This scheme is commonly referred to as "Generation Following Demand".

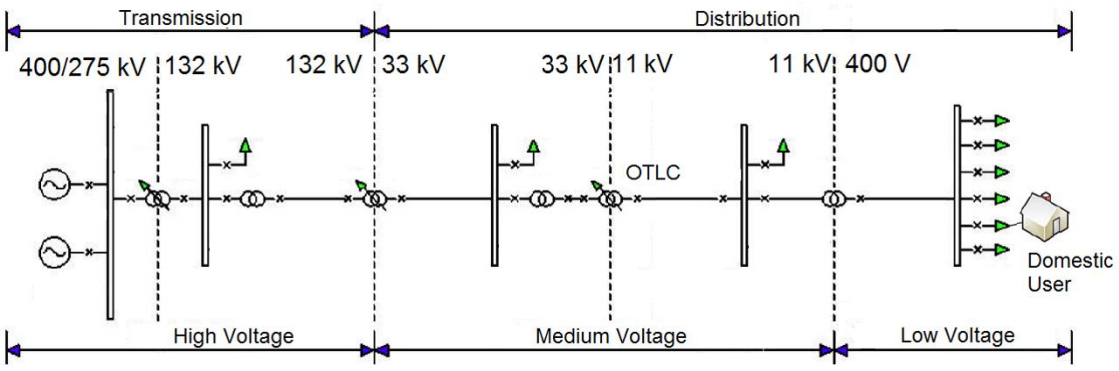

Figure 2.1 Structure of the conventional power network in the UK [25]

Over the past decades, power networks have undergone extensive changes. Power networks today are evolving towards the structure shown in ***Figure 2.2***. At the MV level, more distributed energy resources, such as wind or solar photovoltaic (PV) farms, combined heat and power plants, and biomass generation have been connected to the grid. At the LV voltage level, apart from increasing installation of small scale distributed generation systems, in particular roof-top PV panels, there is also an increasing uptake of domestic energy storage systems such as home batteries and electric vehicles. These low carbon technologies lead to a bidirectional power flow within the network [25]. Meanwhile a smart meter scheme is being rolled out in the UK. The ambition is that every household will have a smart meter by 2020 [26]. This will create a platform which would enable user data to be collected and the remote control of user devices. Such a platform would help facilitate the transition from a "Generation Following Demand" to a "Demand Following Generation" power network.

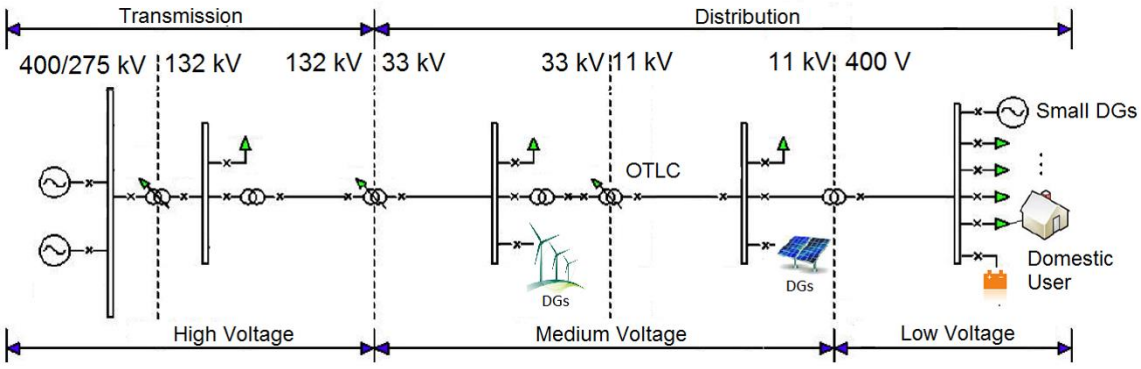

Figure 2.2 Structure of the modern power networks in the UK

2.2.2 Challenges of Existing Power Networks

In the UK, the total energy losses in transmission and distribution networks, in 2011, were 30,843 GWh which is 8.7% of total energy generated [27]. Studies in [28]–[30] show

that conventional transmission networks operate with a higher efficiency in comparison with distribution networks with losses in the region of 2% and 10% respectively.

A key challenge is that the supporting infrastructure is not expanding fast enough to meet growing demand. It has been estimated by the International Energy Agency that global domestic energy demand will increase by 12% in 2020 compared to 2010 [31], whereas the current infrastructure is predicted to grow by only 6% [32]. As the demand is constrained by network capacity, during peak hours (typically around 6pm in the UK [33]), there is increasing attention around the idea of introducing localised demand response to reduce peak demand so that upgrade of the network infrastructure can be deferred [34].

Another challenge is maintaining network operation stability as the penetration of distributed or renewable generation increases. This is becoming a reality in the UK which is targeted to deliver 15% of its energy demand from renewable resources by 2020 [35]). As most renewable resources are non-dispatchable and prone to intermittency, the imbalance between energy supply and demand introduces various problems in networks with distributed generation [36]. It has been reported that the integration of distributed generators and bi-directional power flows associated with batteries can cause challenges around maintaining system frequency, voltage and thermal limits and fault current levels within the network [37]–[40]. Changing power flow caused by local renewable generation, such as solar PV, can cause voltage to rise locally, exceeding its permissible limits, 230V +10/-6% [41]. Local feeder transformers are usually pre-set by distribution network operators (DNOs) to keep the voltage at the end of distribution line within permissible limits assuming no or little renewable generation. Demirok et al. suggested that excessive PV with inverters in the LV network could cause various problems such as voltage rise, harmonics and unbalanced voltages [42]. In some regions in the UK, such as Cornwall, power networks are encountering voltage and thermal problems due to large surplus PV

generation to the extent that the network capacity limits have been reached [43]. This has resulted in network restriction for new renewable connections and an export limit on PV generation has been imposed within some of WPD regions [43].

In addition to local network problems such as the breach of voltage and thermal limits, the system frequency can also be adversely affected by high penetrations of wind and solar PV generation [44]. The combined rotating mass of conventional synchronous generators provides significant system inertia which helps to regulate the operating frequency (50Hz in the UK). Wind or solar PV generation connection to the grid via power electronics however contribute much less to the system inertia compared to the conventional generators [45]. It therefore imposes a challenge to maintain the system frequency and respond to transient events such as faults and power outages [46], [47].

In summary, renewable generation within the distribution networks causes challenges at both the system and local scale. This thesis is concerned with issues around the distribution network in particular network stress and how to accommodate increasing capacity of renewable generation. The following literature therefore focuses on the solutions to those challenges within distribution networks.

2.3 Common Solutions to distribution network problems

This section discusses the solutions for two major challenges in the distribution network: voltage and thermal limits. To compare the practicality of each solution, cost, flexibility, and reliability are discussed.

2.3.1 Cable (conductor) reinforcement

Given that distribution losses and thermal limits are directly related to the series resistance (R) of distribution cables, the most direct way to reduce energy losses and increase thermal limits is to reduce R. This can be achieved by reinforcing existing primary and secondary distribution cables by increasing the cross-section of their conductors, a practice referred to as re-conductoring [29]. Sarfi et al. [48] reported that by implementing re-conductoring, a municipal utility was able to reduce distribution network losses to 2%, which is considerably lower than the majority of the utilities' loss in the same region that varies from 4 to 13%. Unfortunately no benchmark measurement was taken prior to the network upgrades and so definitive conclusions cannot be drawn. An optimal conductor selection algorithm for specifying radial power networks was proposed by Tram et al. [49]. In this work, it was claimed that by replacing the conductor selected by the algorithm, a real feeder network in the USA could reduce the maximum voltage drop across the network from 6.4% to 4.5%.

Whilst re-conductoring might be the most direct way to reduce distribution network losses, this approach can be expensive, disruptive and time-consuming [50]. Furthermore, changing the conductor size may necessitate further upgrades of other network assets such as transformers and protection circuits, which adds more cost. Studies in [51] and [52] suggested that re-conductoring is the most expensive solution compared to other approaches such as reactive power support or re-insulation.

Given the expense and other challenges associated with re-conductoring, other approaches are often explored when increasing distribution network capacity, such as reactive power compensation.

2.3.2 Reactive power compensation

Total power consumed in the electricity power network consists of two components: active power (*P*) and reactive power (*Q*). Power consumed by the resistive part of the load is considered *active* and is the power that performs actual work. Power consumed by the inductive part of the load is defined as *Q* and is an inherent part of the total power that doesn't do actual work. As the current on the network cable is determined by the total power, if reactive power consumption can be reduced, cable losses will drop.

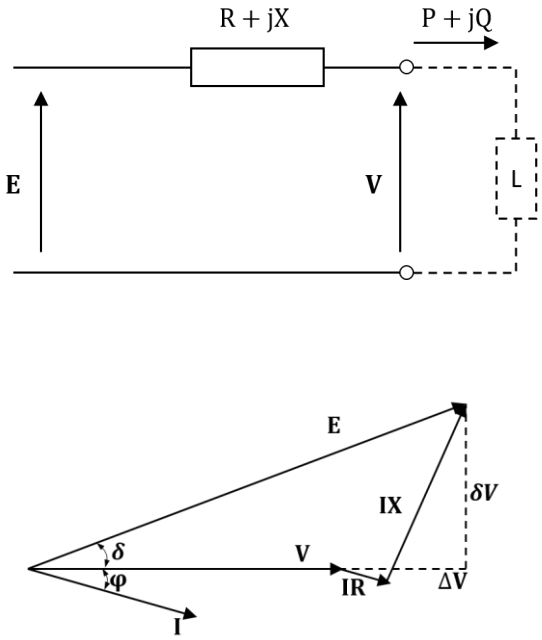

Figure 2.3 Circuit and phasor diagrams for power flow calculation [23]

Figure 2.3 shows simplified power flow circuit and phasor diagrams [23], and the voltage drop on the cable can be derived as follows:

$$E^2 = (V + \Delta V)^2 + \delta V^2 \quad \textbf{(2.1)}$$

where

$$\Delta V = RI\cos\varphi + XI\sin\varphi = \frac{RP+XQ}{V} \quad \textbf{(2.2)}$$

and

$$\delta V = XI\cos\varphi - RI\sin\varphi = \frac{XP-RQ}{V} \quad \textbf{(2.3)}$$

If

$$\delta V \ll V + \Delta V$$

$$E^2 = (V + \Delta V)^2$$

Given ***equation (2.2)***, the voltage drop can be approximately expressed as:

$$E - V = \Delta V = \frac{RP + XQ}{V} \quad \textbf{(2.4)}$$

In the transmission network, R is negligible compared to X, and therefore the voltage can be controlled by reactive power Q. The X/R ratio of the distribution network (which could be as low as 0.3 [53]) is, however, much lower than that of the transmission network, and consequently the reactive power compensation becomes less effective in the distribution network.

Another reason of not using capacitors in distribution networks for voltage control is its cost for implementation. As reactive power demand varies throughout the LV network and it can become uneconomical to install capacitors at every location. The locations and sizes of capacitors need to be strategically planned to avoid excessive cost. Studies have been carried out to determine the optimal size and location of capacitors in a number of LV radial networks [56], [57]. Recently, a centralized reactive power compensation approach was proposed by Chen [58]. However, this approach is only applicable to small LV distribution networks because reactive power cannot travel over long distances.

Overall, being one of the most fundamental and common methods to manage distribution network voltages, reactive power compensation still lacks the flexibility and economy of transformer tap changing (a subject which is introduced in the next section), especially for distribution network voltage control. It is hence only used in schemes where transformers alone will not suffice to maintain nominal network operation [23].

2.3.3 Voltage regulator (OLTC transformer)

DNOs are held responsible for maintaining the voltage within permissible limits across their distribution network. On-Load Tap Changer (OLTC) transformers are widely used between multiple voltage levels to regulate the voltage downstream of its secondary windings [23]. In the UK, OLTC transformers are generally located in MV substations to transform voltages down from 33kV to 11kV [59].

To ensure the voltage is within statutory limits all the way to the end user, OLTC transformers are embedded with automatic voltage control (AVC) and sometimes include a line drop compensation (LDC) algorithm. ***Figure 2.4*** shows how an AVC takes a voltage measurement from the secondary side of the transformer and then compares it with a pre-set voltage reference. If the difference exceeds a certain dead band, the transformer will switch the tap to change the winding ratio between the primary and secondary side after a short time delay, this will keep voltage within an allowable range. An example of the voltage response and its corresponding tap position are plotted in ***Figure 2.5***, where tap changes down with 10 seconds pre-set time delay after OLTC transformer's secondary voltage surpassed its upper band limit. The LDC scheme also monitors the voltage and current at the secondary side of the transformer. As shown in ***Figure 2.6***, with a pre-set impendence model of the distribution network, the transformer can calculate an estimated voltage at the feeder end and adjust the tap to compensate the voltage drop accordingly.

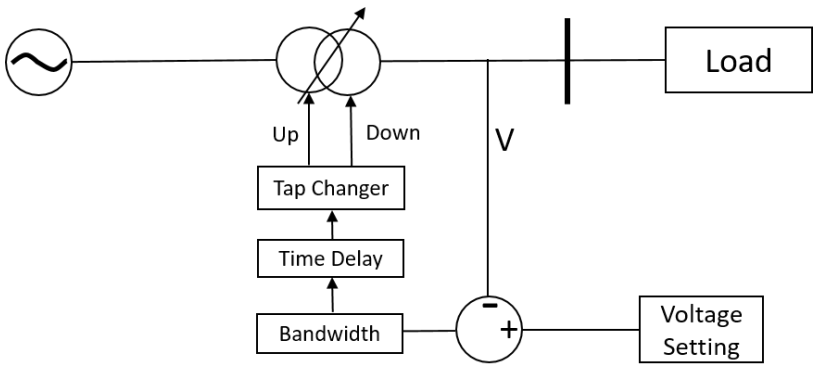

Figure 2.4 Schematic block diagram of OLTC transformer with automatic voltage control (AVC) after [59]

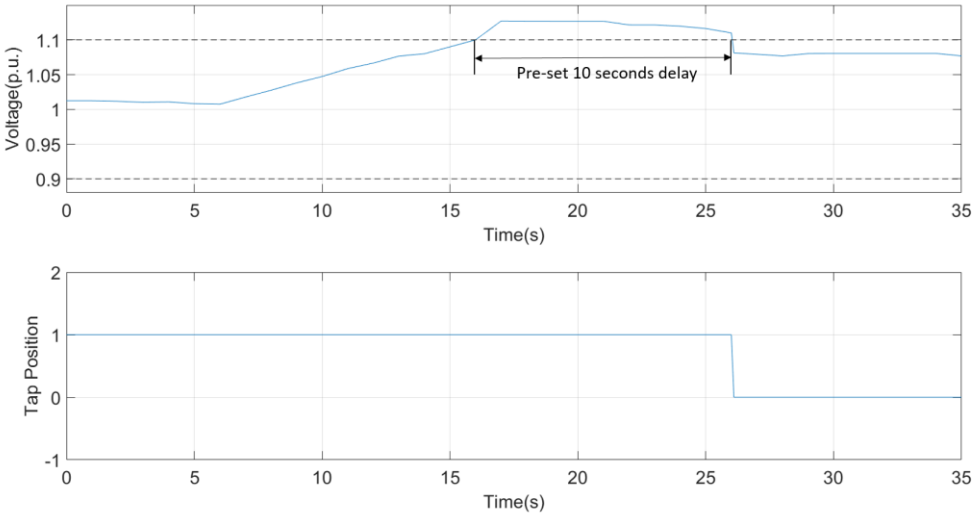

Figure 2.5 OLTC transformer's secondary voltage (top) and corresponding tap position (bottom)

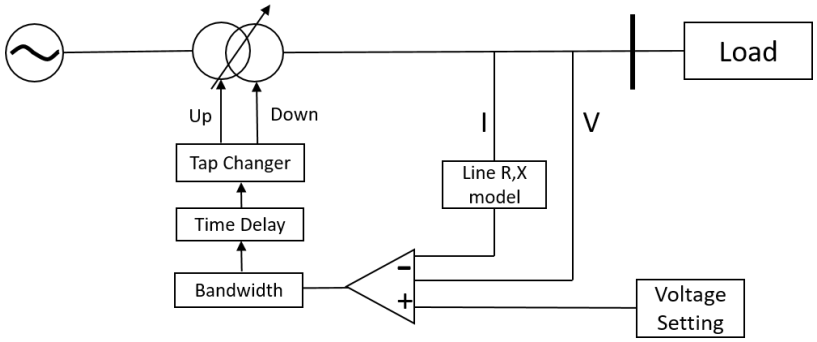

Figure 2.6 Schematic block diagram of OLTC transformer with line drop compensation (LDC) after [59]

Whilst OLTCs are one of the most popular and widely used voltage control devices, they can only compensate for the voltage measured at their secondary windings and infer the voltage downstream via a fixed network model. This, compounded with a lack of telemetry which might enable more intelligent, centralised control, means that OLTC transformers are sometimes not sufficient to be used alone to maintain voltage throughout the network. It has been pointed out in [60] that local rooftop PV installations can cause a complex voltage profile across the network which could disrupt the normal operation of OLTC transformers. Coordinated control of OLTC transformers, distributed generators and

energy storage devices have been highlighted in recent years as a solution to distribution network problems [61], [62]. Active voltage control strategies have also been proposed to minimize tap change switching events and network losses in [63] and [64] respectively. In [65] and [62], different control strategies have been studied for the operation of energy storage devices (i.e. batteries and electric vehicles) along with OLTC transformers to allow an increase in DG penetration in the LV distribution network. A study in a real UK distribution network suggested that using a combination of an OLTC transformer along with a number of energy storage systems would facilitate an increase in PV penetration from 30% to 50% before voltage problems were encountered [60]. Controlling OLTCs however demands a degree of telemetry and measurement not always available in legacy systems. This is particularly true in the UK where the average age of the most of distribution network assets is over 45 years [66]. It is therefore advantageous to consider demand side management alone as an alternative to more active OLTC control coupled with energy storage systems.

One advantage of controlling local devices through distributed DSM at the household level against OTLC transformers is that it is possible to achieve management of voltage constraints at a more granular scale [67]. OLTCs Transformers simply raises or lowers the voltage of the entire network downstream of its primary windings. In addition to the use of existing conventional OLTC transformers, distributed DSM of energy storage systems and smart appliances throughout the network could be considered to enable higher penetrations of renewable generation.

2.3.4 Demand side management

In recent years, demand side management (DSM) arose as an approach for utility companies to optimize energy consumption at the user side to match available and planned

power generation. This generally involves shifting load demand from peak to off-peak times in order to smooth the demand curve, encouraging more energy consumption when there is a surplus generation and curtailment during periods of constrained supply. This brings the following benefits to the network including:

1. The ability to delay the need to upgrade power infrastructure to meet growing demand by reducing peak consumption.
2. The distribution network operates more efficiently since peaks are reduced and losses are proportional to the square of the current demand through the cables.
3. Energy storage devices or smart appliances will be able to store or consume the surplus energy generated by renewable resources which would otherwise be spilt.

Figure 2.7 provides a tree topology which highlights the key DSM approaches that are commonly used. The approaches can be divided into two categories, direct and indirect:

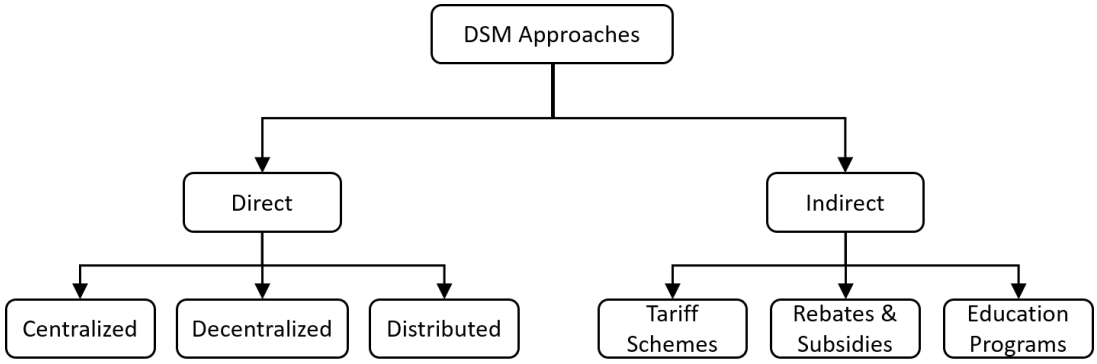

Figure 2.7 Tree topology of DSM approaches [12]

Among indirect DSM approaches, variable tariff schemes are the most common and widely adopted. In this approach, the customer will either get a price discount for load reduction during certain periods of time when demand is high get time based electricity sometimes referred to as real time pricing (RTP), or receive a pre-set electricity price which depends on transition times, such as time of use (TOU) tariffs. Due to the virtues of fast

implementation time and relatively low cost, TOU and RTP schemes are used extensively in countries such as the UK and USA [12]. However, the impact of these schemes on usage behaviour is uncertain as they rely on assumptions around consumer price sensitivity; in other words: 'at what point is electricity so expensive I'll defer my consumption?'. A recent report [68] showed that nearly 30% of surveyed TOU tariff users in the UK were not satisfied with their tariff scheme. Consequently, significant effort has been put into direct DSM approaches as its impact to load is more deterministic.

Within direct DSM schemes, DNOs or local controllers can switch customers' devices on or off based on certain technical signals such as frequency or voltage. Autonomous schemes have a number of advantages, in particular, minimal attention is required from both the user and DNOs [69]. Direct DSM approaches can be divided into three different control architectures: centralized, distributed and decentralized control [70]. Centralized control refers to an architecture where all the control actions are computed and determined by a central entity (usually a DNO's facility) on the basis of information and measurements from the devices in the sub-network. Decentralized control is, on the contrary, where all devices within the network operate and make decisions on their own. All the information is collected and used at the device level meaning that no information exchange to a central hub is required. Distributed control is a combination of centralized and decentralized control that only limited information will be exchanged among different devices and any central entities. A more detailed comparison among tariff schemes and different direct DSM approaches are listed in ***Table 2.1*** [71], [72].

Table 2.1 Feature comparison among different DSM approaches (tariff scheme, centralized, decentralized and distributed control)

Options	Advantages	Disadvantages
Tariff scheme	Easy and fast to implement. Low cost.	Lack of flexibility. Inaccuracy in reflecting the real time supply and demand relationship. Uncertainty around the real impact on users' energy usage
Centralized direct control	Direct Impact on loads. Full network information. Global cost efficiency.	High complexity. Expensive to implement (requires full telemetry infrastructure). Communicate delay. Data security. Less scalable.
Decentralized direct control	Direct Impact on loads. Low Complexity. Low cost (No communication required). Immediate response	Local information. Local cost efficiency
Distributed direct control	Direct Impact on loads. Medium complexity and cost. Partial visibility network information.	Requires certain level of communication. Data security.

In summary, given the benefits around security, reliability, scalability and cost, decentralised, direct DSM would be desirable if the technical challenges can be overcome.

2.4 Network Stress Identification

Monitoring and estimating the level of power network stress is an essential part of network operation. It is also critical for planning DSM schemes so that devices know when to turn on or off.

One of the common approaches is to install Phase Measurement Units (PMUs) at multiple locations across both the transmission [73] and distribution [74] networks to measure the voltage, current, phase angle and other parameters such as harmonic content, which is then passed to a control centre in real-time. These devices use a common time source for synchronization with high-resolution time sampling, thus providing a comprehensive picture of real-time network conditions. However, this approach faces challenges around security, for instance, Shepard et al. [75] demonstrated that an existing PMU-based automatic control scheme could be breached by a GPS spoofing attack to trip a primary generator. Centralised DSM using PMUs is also expensive due to the complexity of PMUs and the cost of the communication infrastructure required. Li et al. estimated that a network typically needs to have PMUs installed across one third of the bus bars in service to achieve adequate network observability [76]. Since the installation of PMUs at these numbers is costly and impractical, in practice, state estimation algorithms are used to supplement smaller numbers of PMUs with inferences made about network conditions throughout.

An alternative way to provide visibility of network conditions is to incorporate monitoring algorithms into smart meters that are installed in domestic households. Music et al. [77] demonstrated a successful project that used domestic smart meters along with a SCADA system to monitor the power quality throughout the distribution network. However, privacy has been increasingly raised as a concern regarding to the data exchange facilitated by smart meters [78].

Given the challenges above, recent attention has been paid to decentralised or distributed control techniques, which can be implemented into smart meters with minimal data communicate. In *Chapter 3*, a network stress identification technique that does not require real time communication based solely on local mains voltage measurements is

proposed. In order to facilitate this, it is important to consider the devices that could defer meaningful amounts of energy.

2.5 Devices for Decentralised DSM Control

Numerous appliances such as fridge-freezers, dish washers, tumble dryers, and electric hot water tanks are suitable as DSM assets. This section reviews a number of popular devices that are technically mature and commonly used. The focus of this thesis is on the application of DSM at the domestic level, therefore large scale energy storage systems such as pumped hydro stations and thermal storage plants are not within the scope of this thesis. ***Figure 2.8*** shows the category of the devices that are discussed in the following literature.

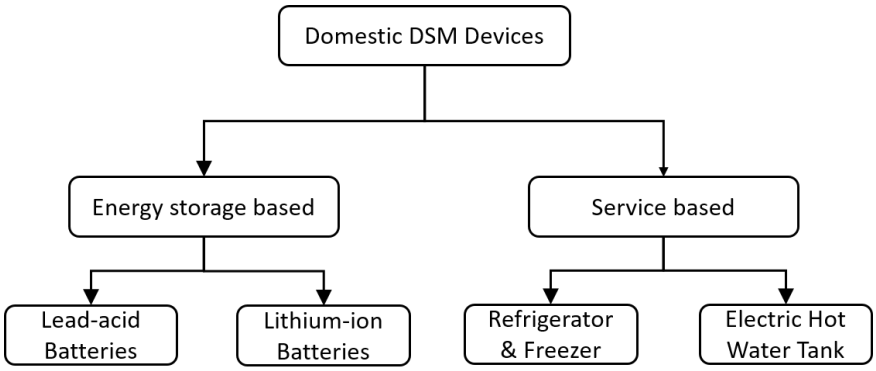

Figure 2.8 Category of the domestic DSM devices that are discussed in the literature

2.5.1 Energy storage based devices

Energy storage devices have the ability to smooth out the load curve, and provide ancillary generation or extra capacity to absorb surplus generation. In recent years, energy storage capacities (include both grid level and domestic level) have grown steadily to the point that capacity worldwide is equivalent to 90 GW, roughly 2.6% of total generation [79]. Recently, there has been increasing emphasis on how domestic energy storage devices,

such as home batteries or batteries within electric vehicles, can play a role in demand response [17], [80].

Lead-acid batteries

There are two main types of domestic storage batteries that are used extensively up-to-date: lead-acid batteries and Lithium-ion batteries [81]. Lead-acid batteries are one of the oldest and most mature rechargeable battery technologies. The energy density of lead-acid batteries is typically between 30-40 Wh/kg and its energy efficiency is around 75% [18]. Whilst lead-acid batteries have virtues such as ease of installation, simple battery management systems, low maintenance requirements and relatively lower capital costs ($120/kWh), they has limiting factors such as low cycle life and battery operational lifetime (1200 to 1800 cycles) [81].

Lithium-ion batteries

Lithium-ion batteries are a more recent battery technology. Lithium Ion systems are at present used primarily in portable devices such as mobile phones and laptops but they are being used increasingly at larger volumes within electric vehicles and home battery storage systems, for instance, the Tesla Powerwall, a lithium-ion based home battery that stores up to 10 kWh of energy at a cost of $3,500 [82]. Lithium-ion batteries outperform lead-acid batteries in terms of energy density and energy efficiency, which are typically 110 to 175Wh/kg and 97% respectively [18]. However, the battery management system within lithium-ion battery systems are far more complex because the lifetime and safety of the lithium-ion is dependent on the charge/dis-charge levels along with the thermal conditions of the battery pack. Packs of lithium ion battery cells need to be monitored and operated under well designed battery management systems otherwise catastrophic thermal runaway

can result; a scenario which can lead to fires or explosions [83]. High cost ($600/kWh [18]) is another major shortcoming for lithium-ion batteries. A study of a real-world UK network suggested that energy storage purely for electrical loss reduction may not be cost effective given the high capital cost [50]. Meanwhile, concerns such as environmental footprint associated with the disposal of old batteries [84] have been raised. Alternative or complementary approaches are therefore sought.

2.5.2 Service based devices

Regardless of what type of energy storage system considered for DSM, its installation introduces an additional cost to the system. A complementary approach to home energy storage systems and DSM of electric vehicles is to use service based domestic appliances as controllable loads. By modifying the firmware or retrofitting a smart controller, these appliances could have great potential to act as DSM assets.

Thermal controllable loads (TCLs) such as fridges, freezers, space heaters and water heaters take up a large portion of energy consumption. Water and space heating alone, account for over 80% of total energy consumption in UK domestic sector [85]. Although wet appliances such as dish washers and washing machines consume a significant amount of energy (16.5% of domestic energy consumption [86]), consumers have little appetite for shifting their wet appliance loads (for instance the noise created by using wet appliances at night was concerned, especially in a small dwelling) [87].

Refrigerators and freezers

Refrigerators and freezers can also be considered as TCLs. The cooling system within refrigeration equipment consists of a compressor, condenser and evaporator. The motor

driving the compressor is an inductive load. The energy demand can be dependent on user behaviour as well as ambient temperature.

Two widely considered approaches for using refrigerators and freezers for DSM purposes are: 1. By directly controlling the cooling schedule of the device. 2. By integrating phase change materials to lengthen the demand cycle. A study undertaken by Zehir et al. [11] tested a simulated fleet of refrigerators and recommended that by controlling the defrost function within them, demand during peak hours can be reduced by 13.6% or more. Where phase change materials have been tested, studies showed that several days of storage time can be achieved for refrigerators with phase change materials [88]. However, these phase change materials haven't been on the market within refrigeration applications due to the lack of commercial viability [88].

Whilst the literature demonstrates that refrigeration plant could be used for DSM, the primary mission of refrigerators and freezers is to preserve perishable goods in fresh and hygienic condition, the controllability of the refrigerators and freezers may therefore be compromised. In addition, it is also worth noting that power consumption of refrigeration plants (typically 80-250W [89]) is much less than water storage heaters (3kW in the UK [90]). The opportunities around using water storage heaters for DSM should therefore be explored.

Electric hot water tanks

Electric hot water tanks (EHWTs) provide a great decoupling mechanism between the time when energy is used and when hot water is needed. In the UK, 50% of households use an electric immersion heater either as a primary or secondary source of heat for hot water production within tanks [20]. A report by Ofgem [91] suggested that EHWTs are the most favoured appliance for domestic users to time shift their load with.

Various research efforts around EHWTs have been undertaken with respect to DSM. Much of the literature is around the physical modelling of the tank. A thermal model comprised of a single mixed lump above a discretized, one-dimension conduction zone was proposed in [92] and indicated that in the UK, tanks may be at risk of bacterial growth within the bottom below the location of the immersion heating element. In [19], the energy efficiency of 5 different types of domestic water heating system (gas boiler, micro CHP, heat pump, electric immersion heater and solar thermal system) in the UK was investigated. It was claimed that on occasion, the electric immersion heater outperforms heat pumps, especially where they were coupled with solar thermal systems.

Another theme in the literature is around tank sizing. Sizing approaches are usually formulated within the context of a combined system delivering hot water and space heating using a tank heated by a variety of energy sources, therefore the tank size is not always the only parameter to optimize in such a scenario. For instance in [93] and [94], a heat pump fired system and solar thermal storage tank were analysed respectively. To understand the optimal sizing for EHWTs in isolation within a DSM scheme, *Chapter 4* presents a methodology for sizing design of the storage tanks based on the real hot water usage profiles and energy tariffs.

2.6 Network Impact Assessment

In order to discern the impact of an aggregated fleet of appliances operating within a DSM scheme, an analysis at the network level must be undertaken.

2.6.1 Empirical studies

Empirical study (or empirical research) is to gain knowledge or evidence by means of direct and indirect observation or experience. In our case, it is the claimed benefit or impact of using HWTs by looking at past or existing applications. In [95], observation of a ripple control trial using HWTs in New Zealand is reviewed. The study observed that inappropriate ripple control during a power outage event raised complaints from the consumers. The effect of demand side control of hot water tanks in 16 regions including several states in the USA, UK, and some European countries are summarized in [87]. However, these summaries focused on the social impact; there is still a lack of technical details surrounding the response of the power network to these programs. For instance, it is claimed that a trial carried out in Ireland achieved 2.5% demand reduction over 12 months without specifying the exact appliance distribution (it only stated that "*some electric and space heating*" as the devices in the trial). To further understand the behaviour of power networks under differing hot water tank DSM schemes, simulations with power network models are required.

2.6.2 Power network Simulation: Top Down

There are two approaches commonly taken when modelling power networks, top-down and bottom up. The top-down approach formulates an overview of the system but does not provide any details with regard to low-level subsystems or components. Different subsystems are usually aggregated and not presented in great detail. For example, in [96], real world energy data has been gathered at 30 second time resolutions to test a novel hot water tank system (supplying to washing machine and dishwasher) incorporated with a control strategy, it is claimed in this work that this approach can save energy consumption by up to 1.2 kWh (with 70 °C hot fill) per day. However, when it comes to network level,

the author extrapolated from a single load to infer the overall energy saving without providing temporal load information or considering the effect on different types of network. Although time series simulation was undertaken in [97], [98] for individual tanks, the overall network impact was still calculated by simply scaling up the number of tanks without regard to interactions within a dynamic power network. Similarly, in [99], when considering the use of wind generation to meet space heating demand, both heating demand and wind generation for the power network were treated as lump sum figures for each analysis. It omitted the technical issues surrounding the network such as thermal limits and voltage constraints.

The literature above demonstrates that whilst a top down approach provides a macro view of the impact that a fleet of devices, it does not consider the dynamics of a real power network. To facilitate this, a more detailed transient bottom up model is required.

2.6.3 Power network simulation: Bottom Up

Bottom up approaches apply load profiles to individual devices, and then integrate their response within a larger network for simulation. This is for a more in depth analysis which might reveal whether any operating constraints or limits are encountered.

Usually bottom up approaches within network simulations are conducted at the household level. Load profiles across multiple appliances within the home are aggregated. Household loads are then integrated into the network model where power flows and their response to network assets and settings are simulated.

In terms of devices, much of the emphasis in the literature regarding network simulation of DSM strategies has been on EV batteries, heat pumps and home energy storage systems. In comparison, conventional EHWTs have received relatively little attention. Callaway et al., however, did consider EHWTs as a subset of thermal storage

systems used as part of a fleet of TCLs using a generic model in [100], [101]. However, the standalone role or impact that EHWTs can make in LV distribution networks is yet to be fully investigated.

In terms of networks that have been used for simulation, a literature review asserted [102] that most of the studies on energy storage systems have focused on the impact on MV networks. It is also claimed in the same literature that "*highly dense residential LV networks, such as those in Europe (multiple feeders, hundreds of customers) are likely to be the first bottleneck and thus corresponding impacts must be investigated*". For this reason, LV networks are considered for the impact assessment.

There are various distribution models in use. Prominent examples include: the Modified IEEE standard bus distribution system [103], [104], a generic UK distribution system [105], [106] and various real distribution networks. The modified IEEE standard bus distribution system, as shown in ***Figure 2.9***, usually represents an American style network structure which typically has fewer users per feeder transformer, as opposed to European networks where there are usually more. The generic UK distribution system model where there is a higher number of users per feeder transformer is shown in ***Figure 2.10***. However, all its LV feeder networks are in uniform length and consisted with same number of customers. The differences in scale that existed in the real LV distribution networks are not captured by the generic model. Researchers at the University of Manchester made 25 real UK LV networks [107] available for studies around the impact of low carbon technologies such as electric vehicle, home batteries and heap pump. In *Chapter 5*, these real LV networks are used in case study for network impact assessment of using intelligent EHWTs.

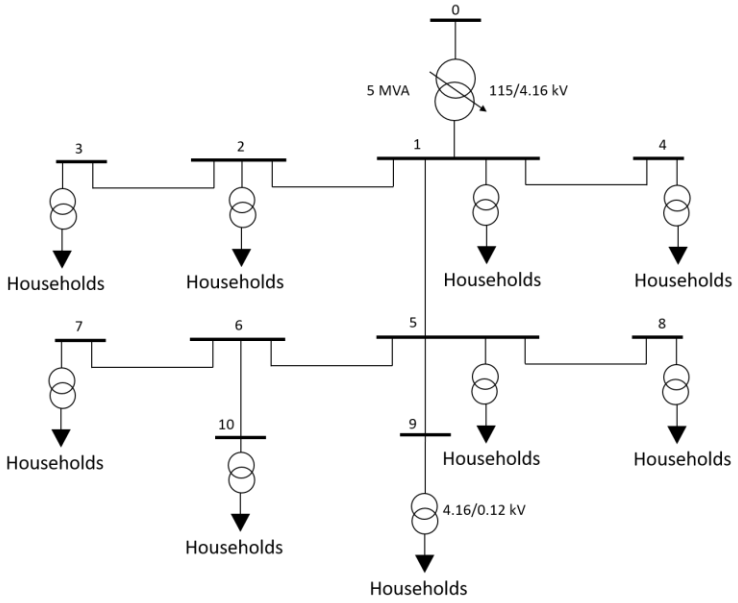

Figure 2.9 Modified IEEE standard distribution system that was used in [104]

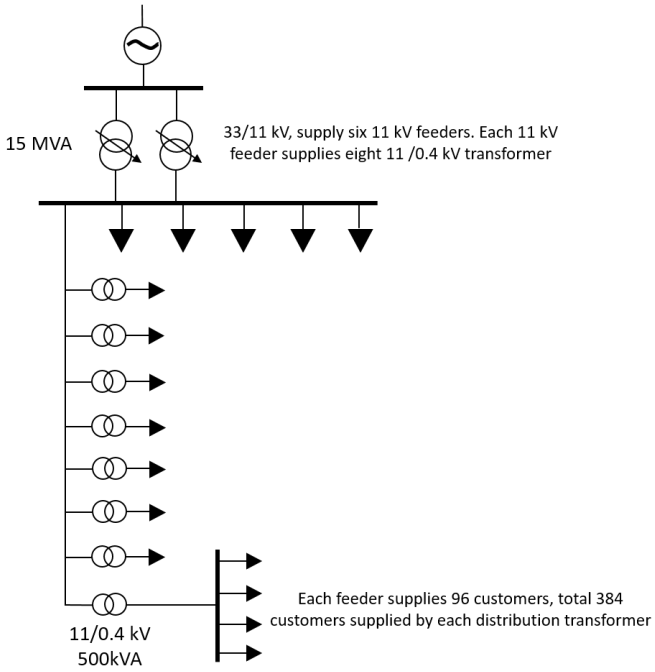

Figure 2.10 Generic UK distribution network that was used in [105], [106]

2.7 Gap Analysis

This chapter set out a roadmap to address the fundamental question posed by this thesis: *"Is there an effective and economical way of using key domestic appliances which will*

allow the power network to operate within permissible thermal and voltage limits, with higher penetration of intermittent renewable energy sources?". Three gaps are identified in the literature review:

1. Decentralized and distributed DSM approaches are becoming desirable as a solution to balance energy supply and demand. However, there are technical challenges to overcome for those approaches. One of the challenges is for the device to estimate the network stress condition without relying on any external communication.
2. Whilst size of the EHWT was mostly considered in the context of combined systems delivering hot water using a tank heated by various energy sources, understanding the optimal size of the EHWT in isolation within DSM has not been explored thoroughly.
3. A bottom up network simulation approach specifically for intelligent EWHT model has not been fully investigated.

This thesis makes three novel contributions to address these gaps respectively:

1. In *Chapter 3*, an approach to detecting power network stress across three different levels relying only on local voltage measurement is demonstrated. This allows smart appliances to perceive network stress without the requirement of real-time communication and potentially making decentralized management schemes more viable.
2. In *Chapter 4*, a sizing optimization method was formulated specifically for EHWTs using a variety of demand profiles to determine the tank volume which minimizes energy cost. To do this, the UK hot water usage behaviour was analysed and different usage patterns have been revealed. By developing a way

to correctly size EHWTs, this contribution further enhances the role that tanks can play in future smart distribution networks.

3. The final contribution of this thesis is to explore the potential benefit that intelligently controlled tanks might deliver to power networks in *Chapter 5*. Different real UK distribution network models incorporating EHWTs with designed control strategy were simulated. Results demonstrate that network capacity for renewable energy generations can be increased by introducing intelligent control of EHWTs.

Chapter 3. Power Network Stress Identification

3.1 Introduction

In the previous chapter, it was claimed that a decentralized DSM approach would be an economic and practical solution to balance power networks. In order to carry out an effective decentralized DSM scheme, minimal communication is desired among different devices. This chapter asks the question: *"Without further investment into the communication infrastructure, is there a technique that can enable domestic devices to perceive the stress across the network in real time?"*. To answer this question, a technique which indicates the stress across the power network using only local voltage measurement at the connection point of a domestic DSM asset was proposed. Such a technique would provide the opportunity to implement decentralised DSM schemes more cost-effectively, and without the communication overheads that would otherwise be required with a centralised DSM scheme.

To understand which parameters or conditions DSM assets should detect within a decentralised approach, *Section 3.2* introduces two types of stress that exist either at a local level within low voltage distribution networks or across the entire system. The former type of stress is related to the limitations around cables and transformers, while the latter originates in the disparity between demand and supply across the entire system.

The remaining sections propose a technique which detects these two stress types via measurement of the mains voltage at the connection point of a domestic DSM asset. Firstly, in *Section 3.4*, a technique to determine frequency from the mains is introduced and validated in order to provide an indication of the stress at system level. To discern local stresses, the key enabling technique is to detect tap changing events that occur within the on-load tap changer (OLTC) transformer in the MV substation which regulates the

operating voltage of the network in response to changes in demand. By inferring to what extend the OLTC intervenes to regulate the distribution network voltage, inference of the stress at a local level becomes possible. *Section 3.5* goes on to propose a novel classification system to detect such tap changing events. A particular embodiment of this arrangement, discussed in *Section 3.5.6*, is the multi-layer neural network. This is a critical part of the classification system which functions as a pattern recognition tool for the detection of voltage features associated with tap changing events. A collaboration was established with Scottish and Southern Energy (SSE) in order to determine the success rate of this classification system.

Lastly, to enable the device to perceive local stress within the distribution network, an algorithm making use of the inferred tap changes derived from the classification scheme above was used to determine the voltage that would have prevailed without the OLTC (in *Section 3.6*). This 'uncompensated' voltage is then used to indicate the local distribution network stress by comparison with a daily average with a standard deviation bandwidth. To close, *Section 3.7* explains the estimation of stress would affect the DSM scheme.

3.2 Power Network Stress

This section introduces two types of stress that exist across three levels of power network, and explains how they can be inferred by different network parameters.

3.2.1 Type I: Stress in the HV network

Type I stress may occur when there is a tendency towards imbalance between generation and demand. Grid frequency changes in large scale power networks are a direct result of an imbalance between the load and power generation supplied by or demanded

from the grid [108]. On a system-wide level, Type I stress therefore reflects the generation capacity.

Owing to the physics of the synchronous machines, the frequency of the generator voltage is directly related to the rotation speed. The rotor motion of the synchronous machine can be expressed in ***equation (3.1)*** [23],

$$J\frac{\mathrm{d}^2\delta_\mathrm{m}}{\mathrm{d}t^2} = T_\mathrm{m} - T_\mathrm{e} \qquad \textbf{(3.1)}$$

where

J is the total moment of inertia of the rotor mass

δ_m is the angular position with respect to the synchronously rotating reference frame axis

T_m is the mechanical torque of the rotor

T_e is the electrical torque output of the alternator

Equation (3.1) can be further derived into ***equation (3.2)***, which is known as swing equation, to describe the rotor dynamics of the synchronous machine.

$$\frac{2H}{\omega_\mathrm{s}}\frac{\mathrm{d}^2\delta_\mathrm{m}}{\mathrm{d}t^2} = P_\mathrm{m} - P_\mathrm{e} = \Delta P \qquad \textbf{(3.2)}$$

where

ω_s is the synchronous electrical angular velocity of the rotor

H is the inertia constant, which is determined by the ratio of stored energy at rated speed and machine rating in MVA

P_m is the mechanical power

P_e is the electrical power

If the generator output is lower than demand, the rate of change of generator rotation speed is negative and consequently the speed, and therefore the frequency, will fall. The same is true in the opposite scenario: when generator output exceeds demand, frequency will rise. Synchronous generators in the UK are designed to operate between 49 and 51 Hz,

but can operate for short periods between 47.5 and 51.5 Hz [109]. As most of the generation stations are synchronously connected, frequency should be the same anywhere in the network [110] so that the frequency and phase of all conventional power generators remain synchronous at all times [111] (i.e. all synchronous generators rotate at the same speed). A significant frequency deviation could lead to undesirable effects on the power networks, damaging equipment, degrading load performance, disrupting system protection operations, and eventually, causing instability in the network or even its collapse [110]. However, frequency control is gradually becoming more complex due to the system's migration from large conventional synchronous machines to distributed renewable generation such as wind and solar PV. The inertia associated with the distributed generation, especially for those which connect to the grid by power electronics, is in relatively terms lower than synchronous machines. This leads to increasing challenges related to the frequency control and system-level stability. In the UK, the National Grid mandates the grid frequency to operate between 49.5 to 50.5 Hz [109], but it also tenders out additional services [112], [113] to maintain the frequency within a much narrower band, as shown in ***Figure 3.1***. Grid frequency should therefore be closely monitored, and it could be used to indicate system-wide stress.

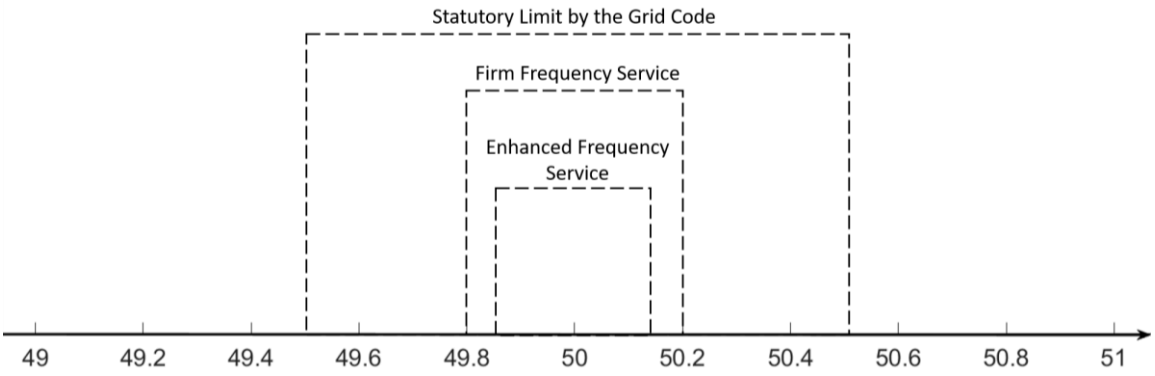

Figure 3.1 Statutory frequency and frequency response services tendered by the National Grid

3.2.2 Type II.A: Stress in the MV network

Type II stress occurs when the distribution cable delivers power close to its limit, leading to excessive loss and heating along the cable and within network assets such as transformers and regulators. This type of stress can lead to voltages straying outside their nominal levels and insulation temperatures exceeding operational limits.

Type II stress exists at both medium (MV) and low voltage (LV) and levels. At the MV or regional level, there are devices which operate to maintain the voltage within stable limits. One common example of this in the UK is the 33/11 kV on-load tap changer (OLTC) transformers in the distribution substation [59]. As reviewed in *Section 2.3.3* (***Figure 2.3 and Figure 2.4***), OLTC transformers are usually embedded with the automatic voltage control algorithm, which measures the voltage at the secondary side and compares it with a voltage reference. If the voltage deviation exceeds a pre-set deadband due to load or supply changes within the MV network, the transformer will move its tap to a different winding contact in order to compensate the MV or LV voltage.

There are two factors that may affect the secondary voltage of the OLTC transformer:

1. The transformer voltage drop which is associated with the internal impedance and current demanded by downstream loads; and
2. Voltage fluctuation on the primary side.

The OLTC transformer usually has a high internal impedance, and a typical impedance drop with full load could be up to 30% for a 30MVA transformer (see ***Appendix 3.1***). The upstream voltage, on the other hand, fluctuates within a much smaller range (3.5% variation on a daily basis, see ***Appendix 3.2***). The impact of primary voltage is therefore assumed to be negligible compared to the voltage fluctuation associated with the current demanded by downstream load. In this case, when heavier loads are demanded within the distribution network, the voltage drop within the transformer and along the length of the distribution

cable will increase. The OTLC transformer then needs to move the tap up to maintain the voltage on its secondary side and downstream. Therefore, knowing the tap position of the OLTC transformer will enable the inference of how much load is being demanded by the regional distribution network.

3.2.3 Type II.B: Stress in the LV network

As with the MV network, Type II stress also exists in the LV, or regional network. Across the LV network, demand has a direct impact on the voltage at the same node. Without the intervention of the OLTC transformer, there should be an inverse proportional relationship between the voltage and power consumed at the same node (this will be demonstrated later, in *Section 3.6*). However, the tap change of the OLTC compensates for changes in load and masks the real behaviour of local voltage. In order to indicate stress in the LV network, the impact of the tap change events must be accounted for so that it is possible to determine uncompensated voltage behaviour at each node. It is noticeable that, although there are OLTC transformers across different levels of the network, 132/33 kV OLTC transformers change their taps much less frequently than 33/11 kV transformers (approximately twice a day and ten times a day respectively, according to a conversation with Martin Lee, Survey and Planning Manager at SSE). For this reason, to show the uncompensated voltage only the voltage change associated with the 33/11 kV tap change is removed, as this is sufficient to provide knowledges of the local stress.

In summary, stresses across different levels of the power network can be translated into different parameters derived from the mains voltage (nominally 230 V in the UK) at the customer side, as shown in ***Figure 3.2***.

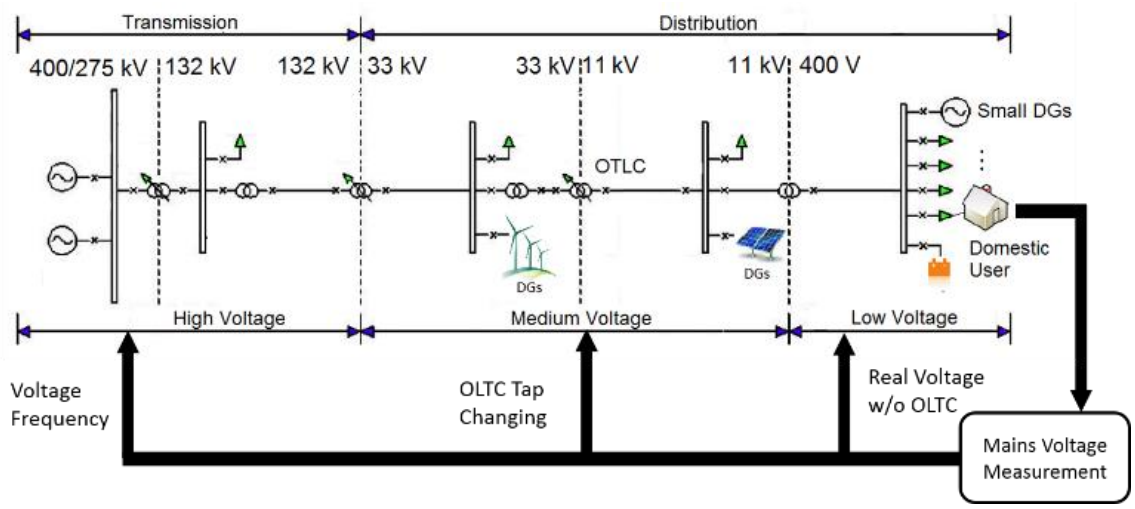

Figure 3.2 Scheme of the stress identification at three levels through mains voltage measurement

3.3 Data available for stress identification

A data logger shown in ***Figure 3.3*** was set up to measure voltage and current measurement in three different locations in the UK; an office site in Reading, premises of Christ Church College in Oxford, and a feeder for a community of domestic users in Bath. Single-phase voltage sampling at 10 kHz was recorded in Oxford and Reading and three-phase voltage and current sampling at the same rate were recorded in Bath. Although the stress identification technique used in this chapter only requires measurement of voltage, current measurement was taken to calculate power consumption at the same location for the purpose of LV network stress validation. A collaboration was established with Scottish & Southern Energy (SSE) to obtain the ground truth data of tap change events, such that the time and direction data when a tap change event occurred were provided during the voltage recording in Reading. The quality and details of the data is further explained in *Section 3.5.4*

It is worth noting that in practice, the sampling frequency of the power data does not need to be as high as 10 *kHz* to provide the information that is required by the stress

identification approach. A standard energy chip available in the market at a retail price between £1.5 and £4 (such as Cirrus Logic CS5480 [114] or Analog Device ADE7816 [115]) could meet the data precision requirements.

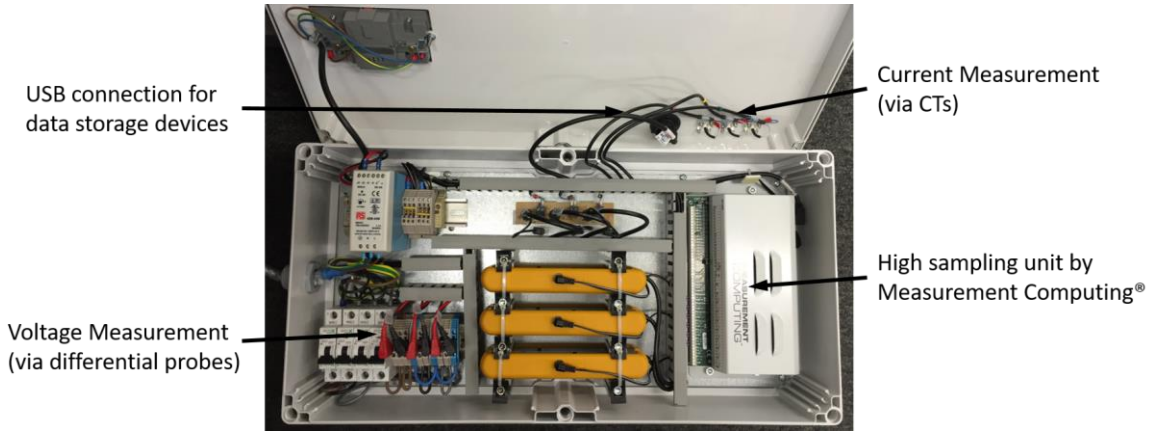

Figure 3.3 The power data logger used to record voltage and current with high sampling rate

3.4 Detecting the Stress in HV network

This section introduces the techniques that are used to process measured voltage data to determine the system frequency so that the system-wide, HV network stress can be inferred.

It starts with zero crossing detection in *Section 3.4.1* to calculate the frequency. A quantization error was, however, observed in the result. A low pass filter was therefore specified and applied in *Section 3.4.2* to ensure closer proximity between the processed frequency and the actual value. A frequency boundary based on the grid code and tendered services offered by the National Grid, is established in *Section 3.4.3* to indicate system-wide stress.

It is worth noting that although zero crossing is a straightforward way to measure system frequency, it could be affected by the error introduced by the voltage harmonic distortions. A variety of other methods could therefore be used for a more accurate

measurement, including discrete Fourier transform and FIR filtering [116], phase-locked loop [117], Kalman filtering [118], modified zero crossing [119].

3.4.1 Estimation of frequency from voltage data

The logged mains voltage is a series of discrete values at the rate of 10,000 per second. As the mains voltage alternates between positive and negative values (like a sine wave if without harmonics), zero crossing points was detected to calculate the frequency. The linear interpolation method shown in ***Figure 3.4*** is used to determine zero crossings where voltage changes from negative to positive. If the voltage at the n^{th} and $(n+1)^{th}$ sampling point are negative and positive respectively, then zero crossing is calculated by ***equation (3.3)***:

$$n_z = n + V_n/(V_{n+1} + V_n) \quad \textbf{(3.3)}$$

where n is the largest sampling integer before the zero crossing, V_n and V_{n+1} are the voltage values at n^{th} and $(n+1)^{th}$ sampling point, and n_z is the zero-crossing value with double-precision.

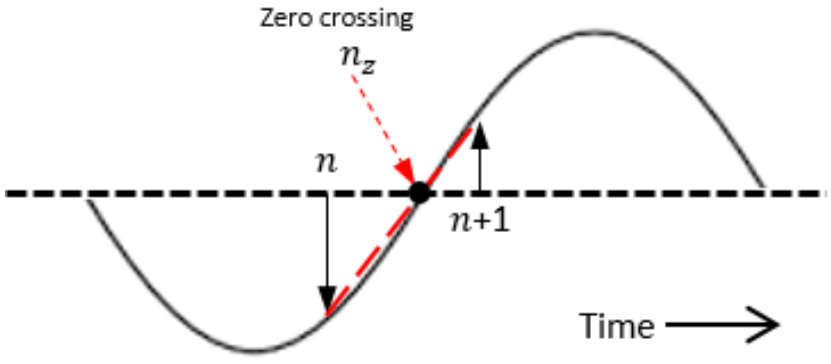

Figure 3.4 Zero crossing point detection using linear interpolation

The next zero crossing n_{z+1} can also be calculated using the same method, and the frequency during the two adjacent zero crossings may thus be calculated in ***equation (3.4)***:

$$f = 10000/(n_{z+1} - n_z) \quad \textbf{(3.4)}$$

As the frequency calculated in this approach is based on discretized value, the result is imposed with a quantization error as shown in ***Figure 3.5***, which plots frequency in both 24-hours and 12-minute resolution. It is therefore necessary to apply a low pass filter to minimize such error and show a more realistic approximated frequency.

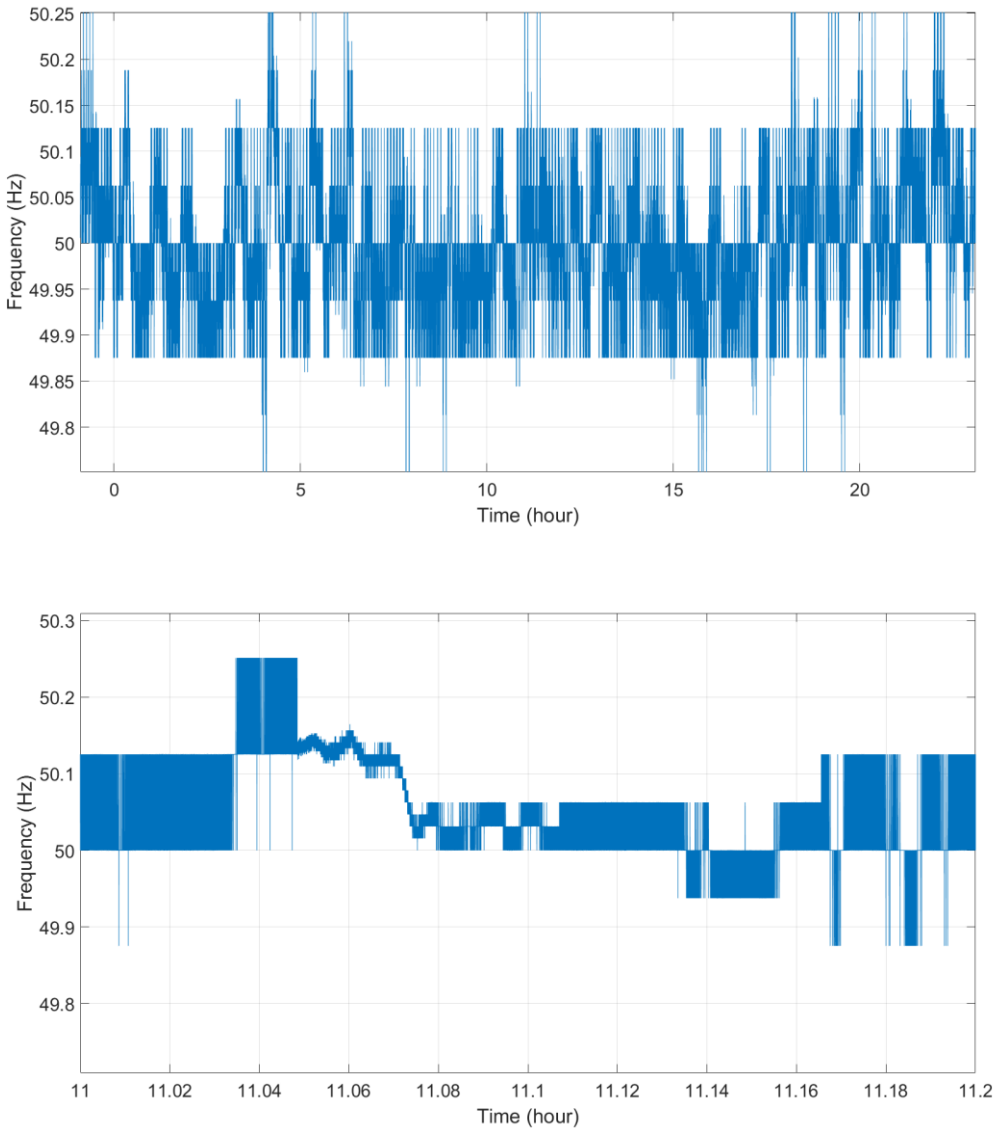

Figure 3.5 Top: Frequency calculated from a zero crossing by a linear interpolation approach through 24 hours. Bottom: resolution between 11 and 11.2 hours

3.4.2 Frequency low pass filtering

Linear filters such as a moving average or the Butterworth filter are used to process time-varying signals to smooth the curve and reduce noise. The Butterworth filter has been used to reduce quantization errors in signal processing on various occasions [120], [121] because it is designed to have a very flat frequency response within the passband. Akke [122] applied a third-order Butterworth low pass filter to a measured power system frequency both in forward and backward direction, demonstrating that the filtered frequency displays a close proximity to the actual frequency without any time delay.

A similar approach in [122] is adopted in this thesis to filter the calculated frequency, using a 3rd-order Butterworth low pass filter with a normalized cut-off frequency of 0.1 to reduce the quantization error introduced by zero crossing detection. The reason why a 3rd-order filter was chosen over other orders is because it provides quicker falloff frequency response than 1st and 2nd order whilst any other higher orders do not show a significant improvement in noise attenuations.

To validate the accuracy of the estimation algorithm, frequency data over the same period of time from National Grid's SCADA system was used for the purpose of comparison. As the National Grid only updates system frequency every 15 minutes, the SCADA frequency has been interpolated linearly to achieve the same resolution with the estimated value. ***Figure 3.6*** shows the frequency during the same time period as ***Figure 3.5***, and it is clear that the results demonstrate a consistency between the estimated frequency from the algorithm and the frequency provided by the National Grid. It can also be observed that the measurement results showed a small phase lag (approximately 9 seconds) which was introduced by the use of a low pass filter. This phase lag, however, does lie within the 30-second frequency response requirement specified by the National Grid [123], and is therefore, acceptable for DSM application.

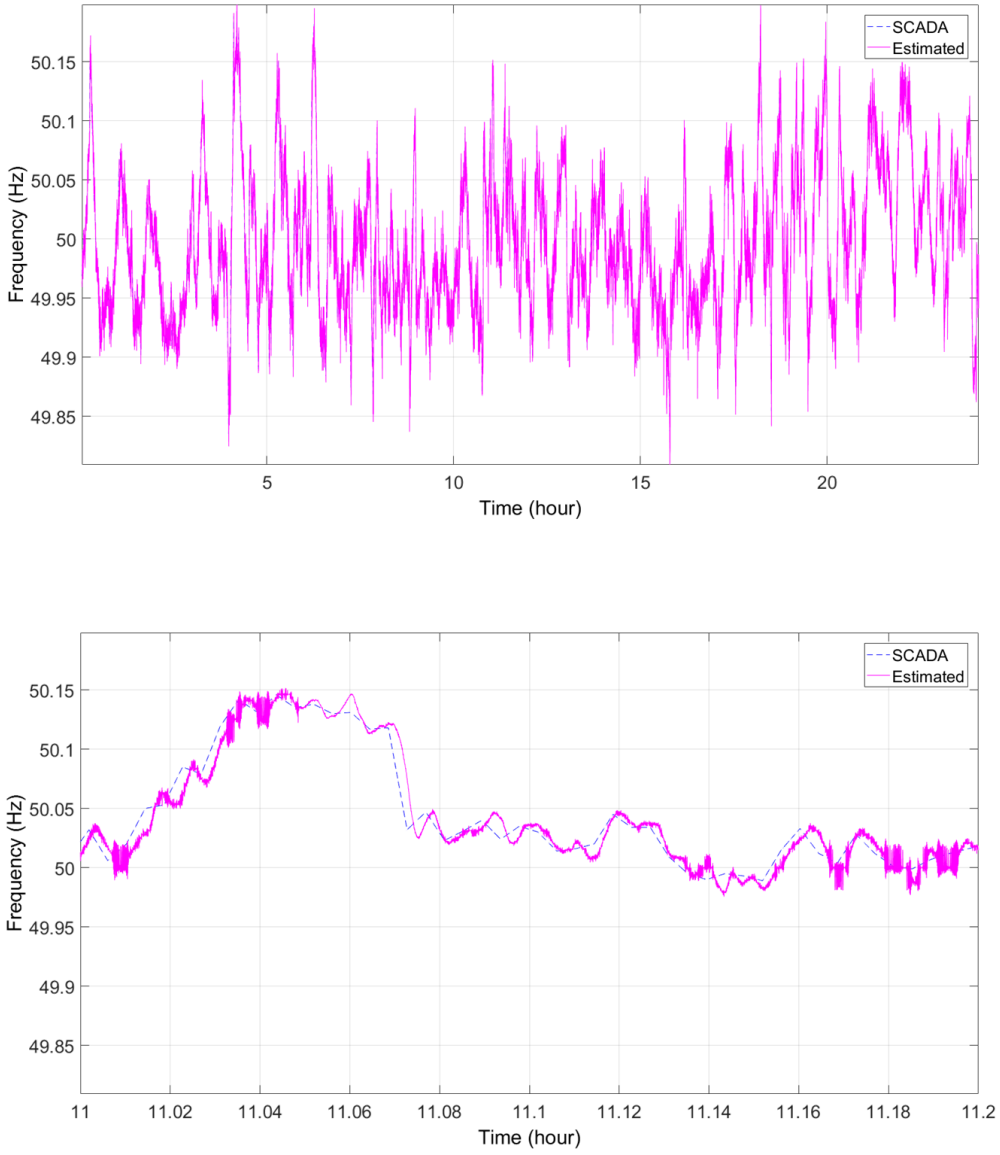

Figure 3.6 Low pass filtered frequency in comparison with the frequency recorded by the National SCADA system during the same time period.

3.4.3 Indication of HV network stress

As is explained in *Section 3.2*, frequency reflects the tendency of the imbalance between the overall generation and demand within the power network. The severity of system-wide stress can be defined by absolute value of the system frequency or by its deviation from its nominal value. In the UK, for instance, it is specified that the network shall be controlled within the limits of 49.50 – 50.50 Hz except under exceptional

circumstances, when the frequency is temporarily allowed to rise to 52 Hz or fall to 47 Hz [109]. In practice, though, these frequency limits are rarely reached, with only two low frequency events (below 49 Hz) and one high frequency event (above 51 Hz) occurring in the UK since 1976 [109]. The transmission network operator usually takes action to control either load or generation long before the frequency reaches such limits. The National Grid (the transmission network operator in the UK) tenders out different load control services when frequency deviates ± 0.2 Hz (Firm frequency response [112]) or ± 0.15 Hz (Enhance frequency response [113]). To coordinate stress detection with the DSM scheme, the stress indication boundary is set in accordance with the narrower band of the two frequency response services: 50 ± 0.15 Hz. ***Figure 3.7***, for example, shows indicated system stress in the UK on the day 29/08/2013, with the red zones above 50.15 Hz indicating that the system is underloaded, and below 49.85 *Hz* that it is overloaded. Such data provides valuable information on when to turn on or off a fleet of loads based on system condition.

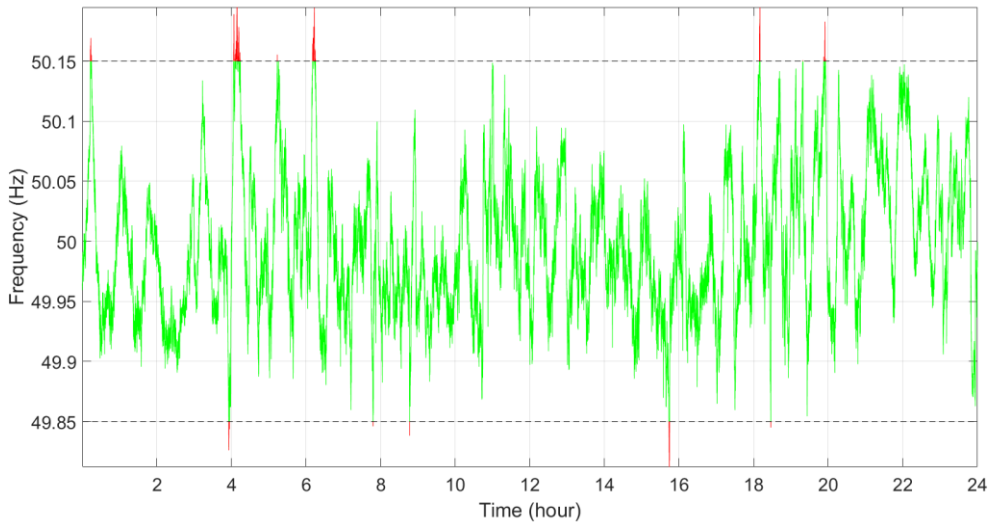

Figure 3.7 Frequency and indication of system wide-stress in the UK.

3.5 Tap Change Detection for Indicating Stress in MV networks

Section 3.2.2 explained how the tap position of the OLTC transformer could be used to indicate the stress in the MV network. This section proposes a novel classification system which uses local mains voltage measurement to detect tap changing events, enabling the customer to perceive MV network stress without any communications with the DNO. The core component of this classification system is a multi-layer perceptron (MLP) neural network, which functions as a pattern recognition tool to differentiate the voltage signature during a tap change from other network events such as load shedding. The reason a machine learning algorithm was used was its generalization capability. As the voltage signatures associated with upstream tap change events may vary in different locations, a simple rule based or decision tree approach was found to be insufficient to detect tap changes across all locations (i.e. there was no generalization capability). While other pattern recognition tools such as support vector machine are available, the MLP neural network was chosen because of its simpler design and lower computational demand.

The flow structure of the classification system and training data preparation are shown in ***Figure 3.8***, where the rectangle and the rectangle with the rounded corners stand for system components and data respectively. The classification system consists of the following components: event detector; change point detection and data normalization; feature selection; and finally, MLP network for classification. The raw RMS voltage data first passes through an event detector to extract all the voltage data of the potential tap change events. Change point detection and data normalization are then applied to the data to normalize it into the same range and format. Finally, the feature vector is determined from the normalized training data to train the MLP network for tap change classification. The output of the classification is either 1 (tap change event) or 0 (non-tap change event) for the corresponding input. It should be noted that because tap up and tap down events

have different voltage signatures, there will be two separate classification systems designed for each tap change direction. The data processing and analysis was carried out offline in MATLAB on a daily basis.

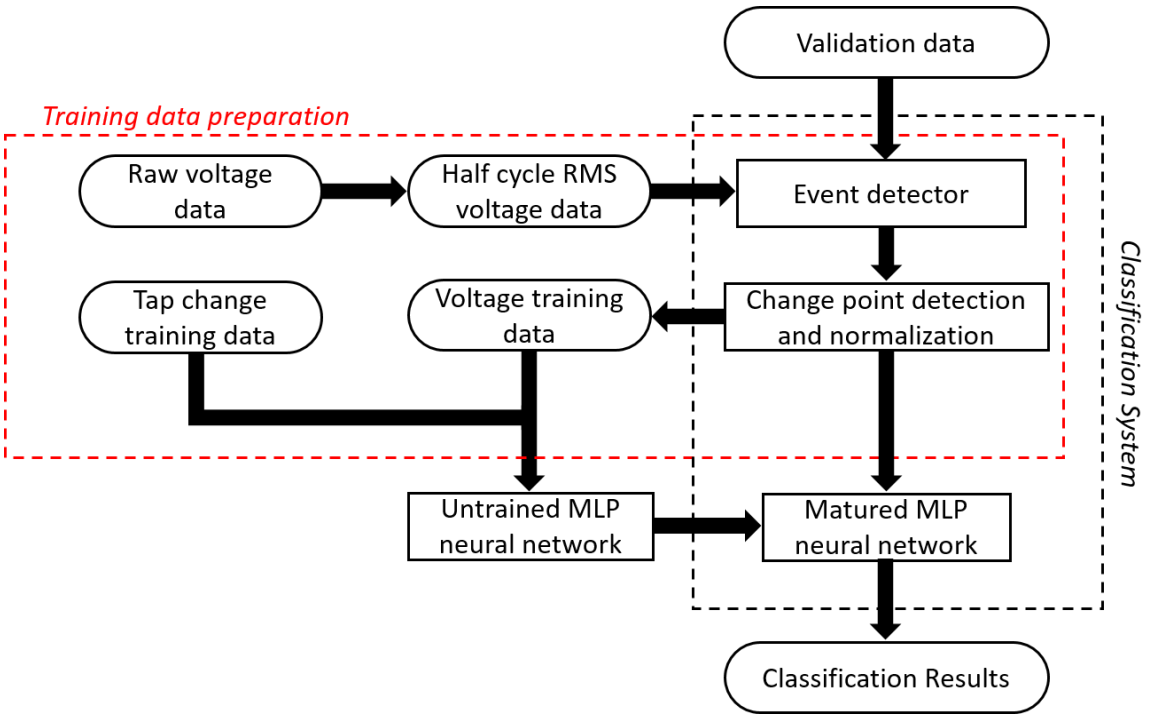

Figure 3.8 Structure of the classification system (black dashed zone) and the training of MLP neural network (red dashed zone)

3.5.1 Raw voltage data processing

The original voltage data was collected at a sampling rate of 10 kHz, the processing of which would require a significant amount of computing and processing power. The voltage data therefore needed to be pre-processed before it could be used for tap change classification.

A previous study [124] by Bollen et al. showed that although RMS voltage can be used for many voltage event classifications such as motor start, transformer saturation, etc., it might suffer from precision issues when being used to detect small voltage changes with short transient duration. ***Figure 3.9*** shows the RMS voltage calculated for every full and half cycle during the same tap change event. It can be seen that the full-cycle RMS voltage

does not show any voltage overshoot during a tap change event, and for this reason, half-cycle RMS voltage is used in this study, taking into account both error minimization and computational complexity.

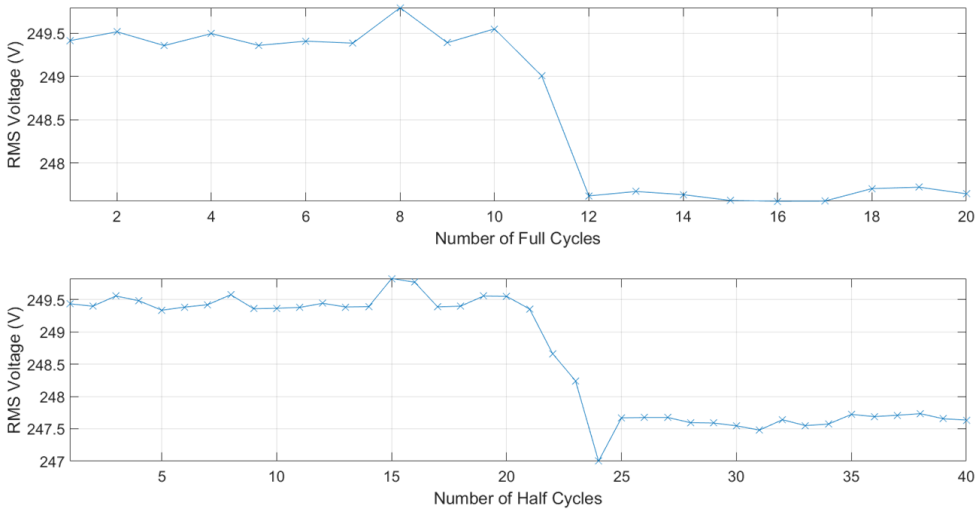

Figure 3.9 The RMS voltage with one cycle (top) and half cycle (bottom) calculation during a tap change event.

To calculate half cycle RMS voltage from the measured voltage, zero crossing detection with linear interpolation was used initially to determine two adjacent zero crossing points. It is worth noting that the zero-crossing used here is different from that used in frequency calculation; in this section, it is the point where the sign of the voltage changes, either from positive to negative or from negative to positive. Assuming there are m sampling points between the two adjacent zero crossings, half-cycle RMS voltage $V_{\mathrm{rms}(1/2)}$ can be calculated using ***equation (3.5)***:

$$V_{\mathrm{rms}(1/2)} = \sqrt{(\sum_1^m V_i^2)/m} \qquad \textbf{(3.5)}$$

where V_i is the i^{th} sampling voltage between the two zero-crossings.

Once the instantaneous voltage is converted to half cycle RMS value, the data is ready to be used for the classification system.

3.5.2 Event detector

Up to this point the data have been processed into a time series half-cycle RMS voltage on a daily basis. These data are still so bulky that not all of them are required for use as the inputs for the MLP neural network. The event detector and change point detection and normalization in the following section are used to narrow down the data to the voltage changes potentially associated with the tap change events. The data processed by these algorithms could then be used as both training and validation datasets.

An event detector is designed to detect any abrupt voltage change from the half-cycle RMS voltage data. This allows the real-time application of the classification system and ensures that the MLP network will only process and classify voltage change data which could potentially be associated with a tap change event. The computational requirement of the system is thus reduced significantly. It also determines which classifier (tap down or tap up) the voltage data needs to be sent to. A previous study [125] by Erbrink showed that the OLTC transformer completed its tap switching within around 60 milliseconds (six half-cycles), which indicates that the voltage change associated with the tap changing should be within the same time scope. A detection index, V_{diff}, is obtained by calculating the difference between two half-cycle RMS voltages with a distance of six half-cycles (60 milliseconds) as shown in ***equation (3.6)***:

$$V_{\text{diff}}(i) = |V_{\text{rms}(1/2)}(i) - V_{\text{rms}(1/2)}(i-6)\,| \qquad \textbf{(3.6)}$$

where i indicates the i^{th} half-cycle sampling point. A threshold δ needs to be determined for each sampling location that:

- If $V_{\text{diff}}(i) \geq \delta$: the voltage change at i^{th} point is potentially caused by tap change.
- If $V_{\text{diff}}(i) < \delta$: the voltage change at i^{th} point is not caused by tap change.

For a typical OLTC, each tap step is between 1.43 to 1.67% [126]. However, as a typical UK distribution network usually has two OLTC transformers operating in parallel, the voltage impact on the mains voltage downstream is expected to be halved (0.71 – 0.83%). To provide some headroom which allows us to obtain all potential data, δ is set at 1 V, or approximately 0.45% of local voltage in this case. Any voltage change larger than 1 V is therefore considered to be a potential tap change event. A sliding window is then created by using V_{diff}, which is calculated at each newly measured half cycle RMS voltage to compare with δ (1 V in this case) to determine whether this voltage point is a potential start of a tap change event. Once a voltage change event is detected at i^{th} point, 14 sampling points before and 15 after will be taken out to form a 30 sampling point event window.

3.5.3 Change point detection and normalization

The event detection method in the previous section can identify potential tap change events. However, voltage changes in different event windows are not always aligned within the same time period. In order to provide consistent voltage change training data, a change detection algorithm is used to fix voltage change at the same temporal position in all event windows.

The cumulative sum (CUSUM) method is a sequential analysis technique developed by Grigg et al. for detecting changes from a time series event [127]. At the n^{th} point, the sum is calculated as follows:

$$S_0 = 0 \tag{3.7}$$

$$S_{n+1} = S_n + x_n - \alpha_n \tag{3.8}$$

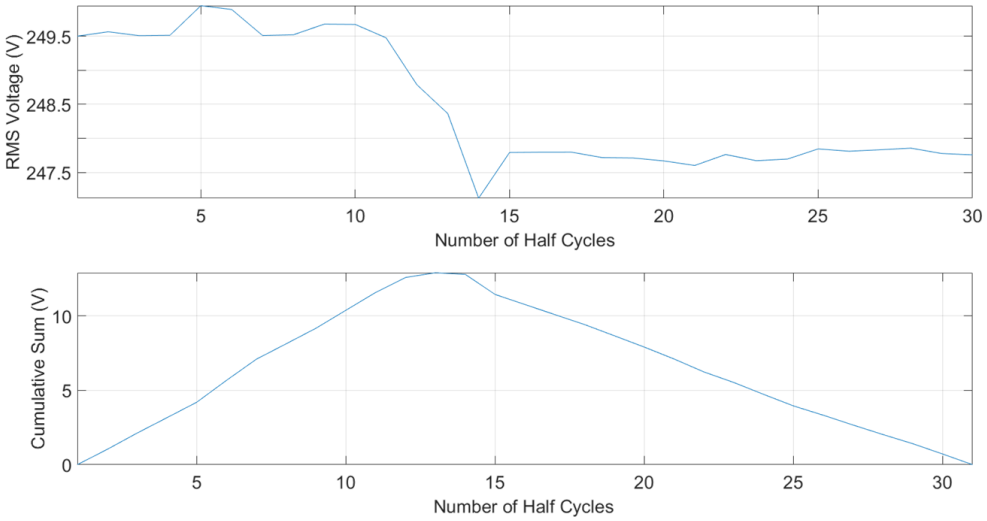

Figure 3.10 RMS voltage (top) and corresponding CUMSUM (bottom) plots during a tap down change event, showing a change point detected at the 13th point.

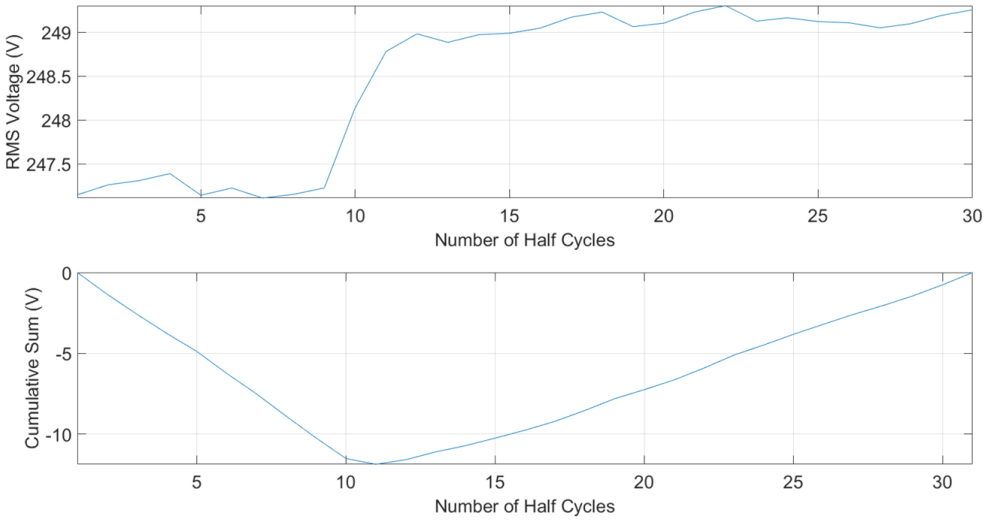

Figure 3.11 RMS voltage (top) and corresponding CUMSUM (bottom) plots during a tap up change event, showing a change point detected at the 11th point.

where α_n is the threshold value. In this case, α_n is set as the mean value of the 30 points within the event window. In a tap down (decreasing voltage) change event, the point with the largest sum is defined as the change point. Similarly, in a tap up (increasing voltage) change event, the minimum sum is used as an indication for the change point detection. A decreasing and increasing voltage plot and their corresponding cumulative sum plots are shown in ***Figure 3.10*** and ***Figure 3.11***, where decreasing and increasing voltage change

points are detected at the 13th and 11th point respectively. Once the change point is detected, all the training data are re-aligned by taking 14 sampling points before and 15 after the change point.

As the real world measurements [128] showed that the local voltage fluctuated from 240V to 250V throughout the day, the voltage window extracted using the technique above would show different voltage ranges. This would result in an ill-conditioned neural network. Data normalization is thus required before using this training data. A normalization approach commonly used for battery voltage pattern recognition is 'initial starting voltage point fixation' [129]. Instead of having different values for initial points, this approach offsets all training data to a consistent initial value, in our case, set to zero. This provides more consistent voltage signatures including mean and standard variation, thus guaranteeing a more stable convergence of weights and biases in the neural network. The effect of normalization can be seen in ***Figure 3.12*** in the following section, that all voltages start at 0 V.

3.5.4 Obtaining training and validation data

As stated in *Section 3.3*, data from three locations were available for training and validation; Christ Church, Reading and Bath. The data from Christ Church and Reading were used as training sets, whereas the data from Bath was used as a validation set to evaluate the performance of the classification system. SSE provided tap change signals for the training data. Using the methods described in *Section 3.5.2* and *Section 3.5.3*, all voltage changes over a certain threshold were detected and normalized to form the training dataset. As each voltage change came with a time stamp, those voltage changes which matched the tap changing time suggested by DNO were selected as the positive data. The rest of the training data were then considered as negative data. The size of the training dataset,

including both the negative and positive data, is shown in ***Table 3.1***. The positive tap up and tap down voltage training data are shown in ***Figure 3.12***.

Table 3.1 Training Data from Christ Church and Reading

Event	Training Data		
	Total	***Positive (1)***	***Negative (0)***
Tap Up	1020	126	894
Tap Down	1039	115	924

Positive (1) indicates a tap change event and negative (0) indicates a non-tap change event

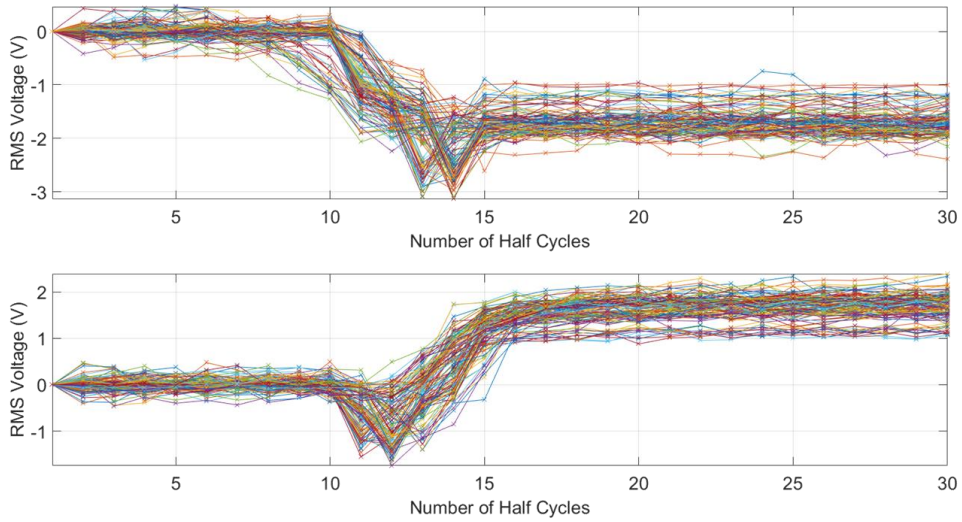

Figure 3.12 Normalized tap down (top) and tap up (bottom) positive training data

In terms of validation data, there are three days of voltage data from Reading. The data were recorded in a domestic community which is assumed to have no heavy three-phase industrial load. Therefore, whenever there is a consistent voltage change across all three phases, as shown in ***Figure 3.13***, this is assumed to be caused by a tap change event. This approach thus allows us to obtain tap change information without recoursing to the DNO. The details of the validation data are further explained in ***Table 3.2***.

Table 3.2 Validation Data from Bath

Event	Validation Data		
	Total	***Positive (1)***	***Negative (0)***
Tap Up	1328	38	1290
Tap Down	2829	32	2797

Positive (1) indicates a tap change event and negative (0) indicates a non-tap change event

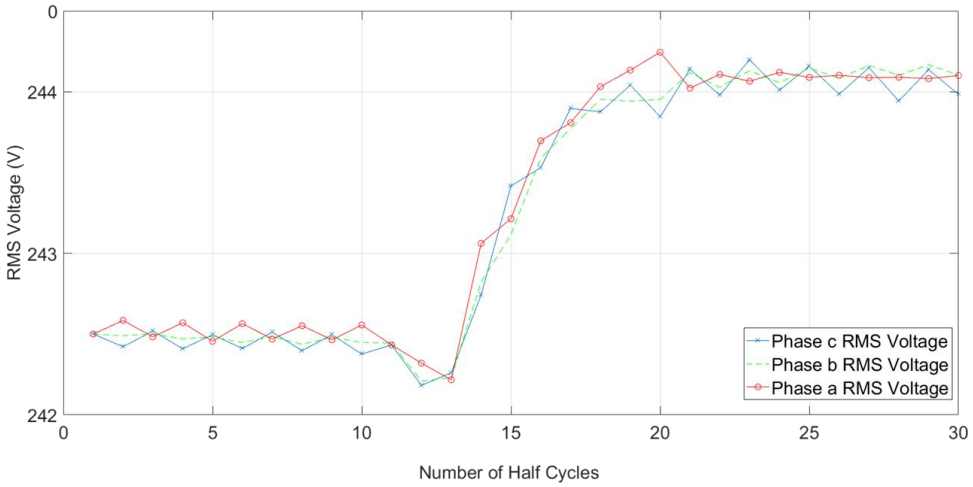

Figure 3.13 Three-phase voltage detected at a feeder in Bath during a tap up change event

3.5.5 Feature selection

Although a tap can complete switching in around 60 milliseconds, no other prior knowledge of the voltage signatures exists other than the range of voltage magnitude change and an approximate transient time. In order to ensure a pattern which includes steady state voltage both at beginning and end, all 30 voltage points in each training data are considered as the feature inputs to the MLP neural network. Each half-cycle RMS voltage is fed into the MLP classifier in a chronological order as an input vector. This approach provides a temporal information for the classifier.

3.5.6 MLP network training

Characterization of the neural network is described in this section. Based on the training data, the neural network has 30 inputs as the feature vector and binary outputs 1 and 0 to indicate the tap change event.

The structure of the MLP neural network is shown in ***Figure 3.14***. It consists of input layer, hidden layer and output layer. In this thesis, input x is the feature derived from the half-cycle RMS voltage signal and output y represents the binary classification of the tap change event (1 for tap change and 0 for non-tap change). The following parameters and functions need to be characterised for the neural network: 1. The transfer function and learning algorithm; 2. Division of training, testing and validation subsets within the training dataset; and 3. Number of hidden neurons.

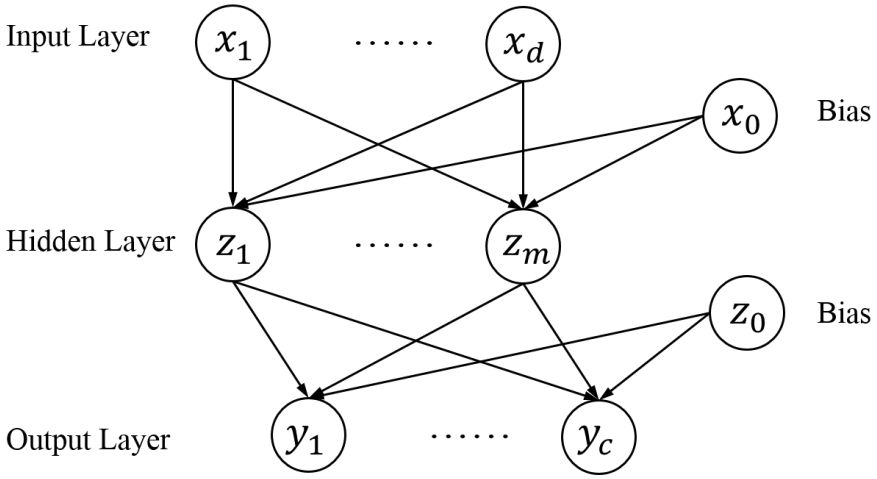

Figure 3.14 Feedforward MLP neural network with two layers of adaptive weights

Transfer function and learning algorithm

The hidden layer of the MLP projects the input data into a new dimension or space through a non-linear transformation, where the classes are more separable from each other

than in the original input data space. A non-linear mathematical relation that maps the input to the output can be written as follows [130]:

$$y_{\mathrm{k}}(x) = f_{\mathrm{output}}\left(\sum_{\mathrm{j}=1}^{m} \omega_{\mathrm{kj}} f_{\mathrm{hidden}}\left(\sum_{\mathrm{i}=1}^{d} \omega_{\mathrm{ji}} x_{\mathrm{i}} + \omega_{\mathrm{j0}}\right) + \omega_{\mathrm{k0}}\right) \qquad \textbf{(3.9)}$$

where ω_{ji} denotes a weight in the first layer, from input i to hidden unit j, and ω_{j0} denotes the bias for the hidden unit j. Similarly, ω_{kj} indicates the weight from hidden unit j to output k, and ω_{k0} indicates the bias for output k. A linear transfer function is used as the output layer transfer function f_{output}. Empirically, the tangent sigmoid function shown in ***equation (3.10)*** is often found to provide faster convergence of training algorithms than logistic functions [131]. Therefore, a tangent sigmoid is used for hidden layer transfer function f_{hidden}:

$$f_{\mathrm{hidden}}(x) = \frac{1-e^{-x}}{1+e^{-x}} = \tanh\left(\frac{x}{2}\right) \qquad \textbf{(3.10)}$$

A learning algorithm needs to be applied to determine the synaptic weights ω in the hidden layer. An effective learning algorithm should be capable of adjusting the synaptic weights based on minimization of an error function. The back-propagation algorithm is a supervised learning technique that propagates the output errors to the hidden neurons by applying a gradient change to it. The scaled conjugate gradient (SCG) back-propagation algorithm [132], developed by Moller, was used in this paper. The SCG algorithm avoids a time-consuming line search for each iteration by using a step size scaling mechanism, allowing it to converge faster than the other back-propagation algorithms.

Training, testing and validation subset

During the training process, the data was divided into three subsets: a training set, a validation set and a test set. The training set was used to compute the gradient and

determine network weights and biases. The validation set was used to determine what the optimum network weights and biases are. The cross-entropy error in the validation set was monitored during the training process. Normally cross-entropy error decreases during the initial phase of training and then begins to rise when the network overfits the data. Network weights and biases are therefore saved at the minimum of the validation set error to ensure that the network is mature and not over-trained. Finally, the test set was used to compare different models. It is useful to plot the test set error during the training process so that, if the error of the test set reaches a minimum at a significantly different iteration number than the validation set error, this might indicate a poor division of the data set.

In this project, the data was randomly divided into training, validation and test sets at a ratio of 60%, 20% and 20% respectively. ***Figure 3.15*** shows that during a tap down training process, the training stops at the 57th epoch when the cross-entropy error reaches the minimum value of 0.07 and the there is no major discrepancy between the test and validation errors. The network weights and biases are therefore taken at that point.

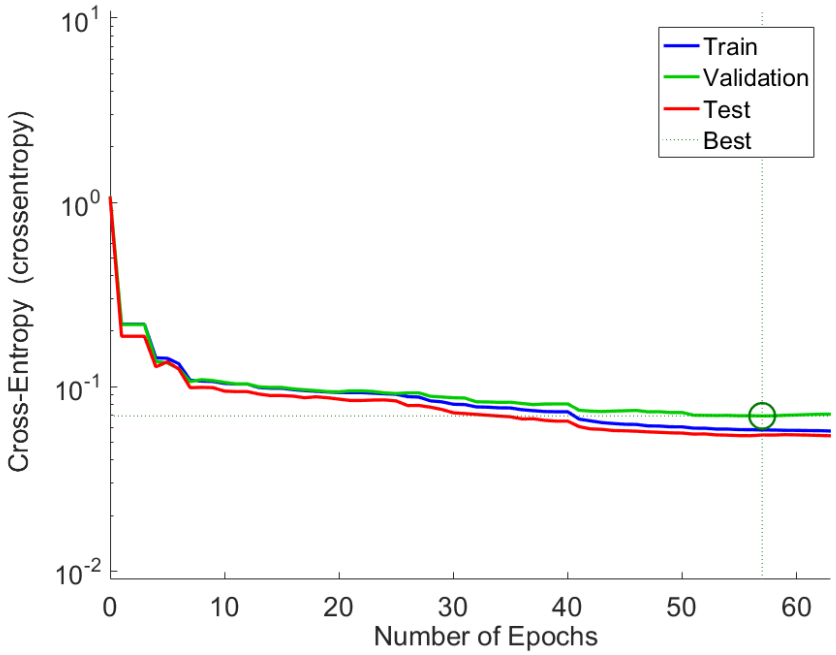

Figure 3.15 MLP training performance with training, testing and validation subsets, indicating that the training stops when cross-entropy performance shows no improvement at the 57th iteration.

Number of hidden neurons

The last feature to characterize is the number of hidden neurons, given that this will significantly affect the classification results of the MLP network. Previous research [131] by Bishop suggests that if the number of hidden neurons is lower than the number of either input or output units (in this case 30 and 2 respectively), then the trained MLP network is possibly not the most general network since information might be lost in the dimensionality reduction in the hidden layer. Therefore, there should be at least 30 hidden neurons in this case for a sufficient MLP network. For the purpose of this thesis, a network growing method is used to determine the optimal number of hidden neurons: the study began with lower number of neurons, which was increased until there was no further error reduction. The error is defined as the percentage of misclassified cases within the total number of all potential cases.

Since the neural network will start each time with different initial values for bias and weights, a network with the same number of hidden neurons may still contain different classification errors. Each network is therefore trained 100 times to ascertain average error in the selection of the optimal number of hidden neurons. The top graph in ***Figure 3.16*** illustrates the error result for tap down classification. It can be observed that 39 is the optimal number of hidden neurons as it has the smallest error, and the networks with more or fewer hidden neurons all tend to have higher classification errors. For tap up events, the minimum classification error was obtained with 36 hidden neurons as shown in the bottom graph in ***Figure 3.16***, where there is an obvious trend towards higher error with 50 hidden neurons or more. This higher level of errors may be attributable to overfitting.

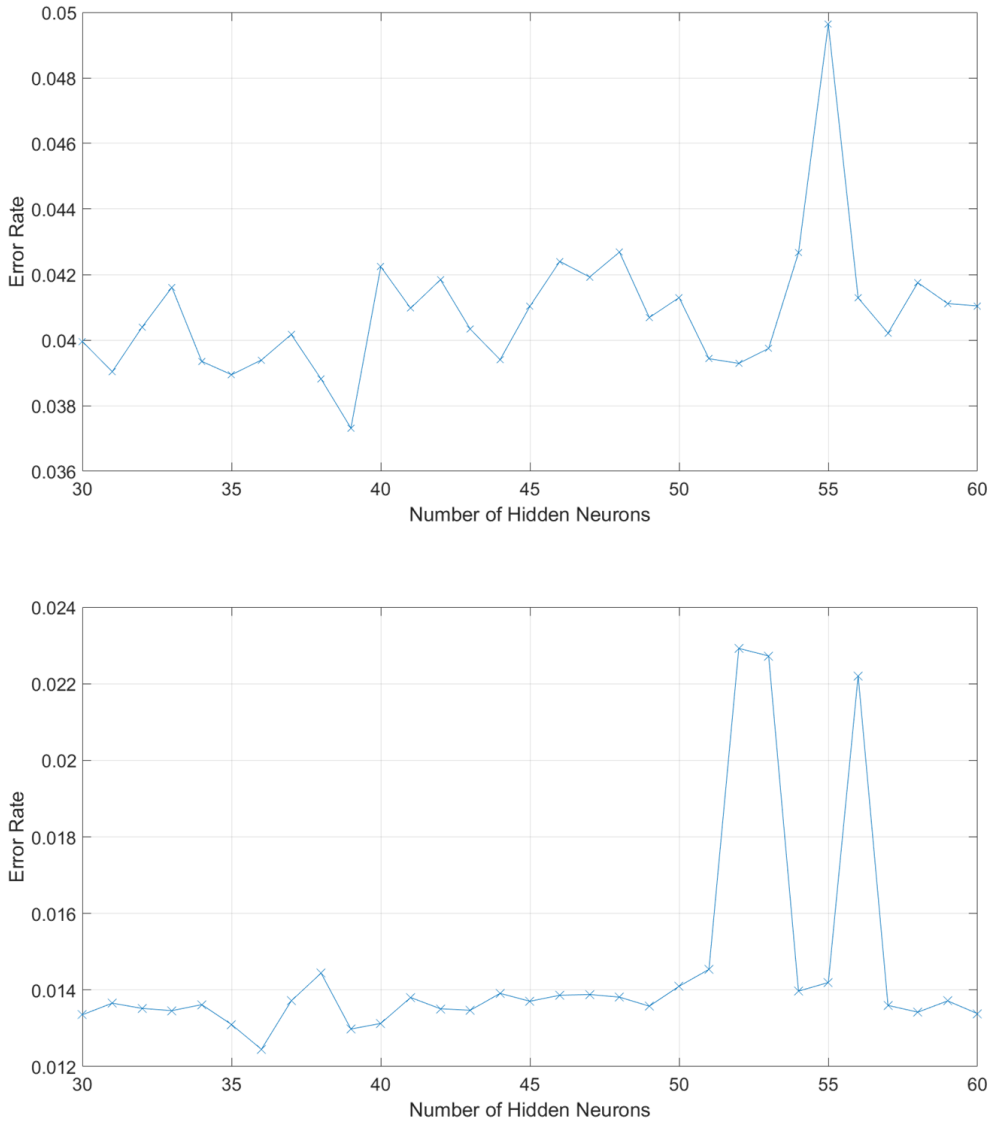

Figure 3.16 Classification errors versus number of hidden neurons for tap down and tap up classification. Top and bottom figures show that optimal number of neurons is 39 and 36 for tap down and tap up classification respectively.

Training results

The steps described above can be used to create an effective neural network based on the training data set. The training data classification results for tap down and tap up events are shown in ***Table 3.3*** and ***Table 3.4*** respectively. The network successfully classified 98.1% (906 out of 924) of the non-tap–down change events and 92.2% (106 out of 115) of the tap down change events, resulting in an overall classification accuracy of 97.4% for tap

down events. The same process was applied to tap up event classification. As shown in ***Table 3.4***, the MLP network successfully classified 98.4% (124 out of 126) of the tap up events, and 99.4% (889 out of 894) of the non-tap–up events, with an overall classification accuracy of 99.3%.

Table 3.3 Classification Result for tap down training data

		Actual	
		Positive (1)	***Negative (0)***
Classifier	***Positive (1)***	106	18
	Negative (0)	9	906
	Total	115	924

Table 3.4 Classification Result for the tap up training data

		Actual	
		Positive (1)	***Negative (0)***
Classifier	***Positive (1)***	124	5
	Negative (0)	2	889
	Total	126	894

3.5.7 Classification validation

In order to evaluate the generalization capability and accuracy of the two neural networks (tap up and tap down) trained in the previous section, it was necessary to test tap change and voltage data from other locations. Voltage data recorded in Bath was used as the validation dataset in this case (note that this is different from the validation subset of

the training data in the previous section, as the previous validation subset is solely used for training purposes).

Using the matured MLP neural networks trained in *Section 3.5.6*, voltage changes associated with tap up and tap down events are detected and plotted in ***Figure 3.17***.

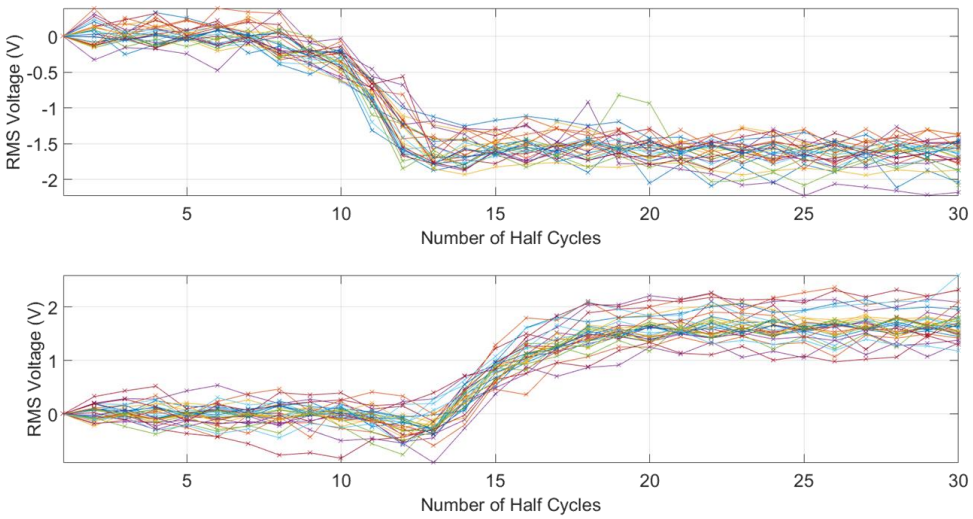

Figure 3.17 Tap down (top) and tap up (bottom) voltage from validation data classified by the neural network

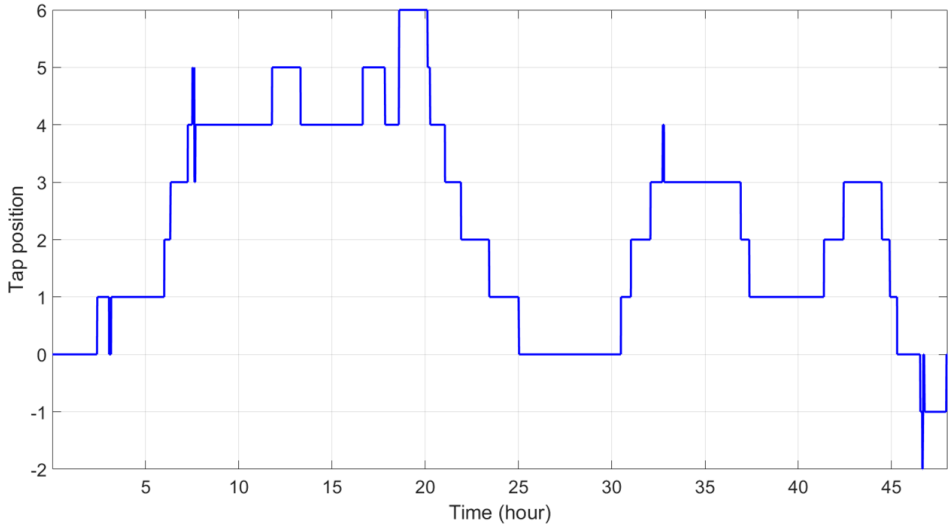

Figure 3.18 Tap position based on the classification results throughout 48 hours

Assuming the initial tap position is at 0 (tap position is set at 0 when the tap is in the middle of all winding positions, i.e. if there are 17 winding positions, the ninth position is 0), a 48 hour tap position based on the temporal information extracted during the classification is plotted in ***Figure 3.18***. It can be estimated from this data that the demand was high throughout the daytime on the first day, and on the second day, load dropped off from noon to late afternoon before picking up again at 6pm.

Sensitivity and specificity tests were carried out in order to evaluate the performance of this binary classification system, and the results are shown in ***Table 3.5***. True positive and true negative indicate the cases when the MLP network successfully classified a tap change and a non-tap change event respectively. The presence of a false negative indicates where the classification system shows a non-tap change event which is actually a tap change event. False positive, also known as a false alarm, is an error case, where the classification system indicates a tap change event when it is actually a non-tap change event.

Table 3.5 Classification Results of the Validation Data

	Tap Up Event	*Tap Down Event*	*Total*
Actual Tap Changes	38	32	70
True Positive	35	28	63
True Negative	1290	2794	4084
False Positive	0	3	3
False Negative	3	4	7
Total Cases	1329	2829	4158
Sensitivity	92%	88%	90%
Specificity	100%	99.9%	99.9%

Sensitivity represents the true positive rate, indicating the ability of the classification system to correctly identify a tap change event. Specificity is the true negative rate, which

shows the classification system's ability to successfully identify a non-tap change event. Sensitivity and specificity can be calculated by ***equation (3.11)*** and ***(3.12)*** respectively.

$$Sensitivity = \frac{true\ positives}{true\ positives + false\ negatives} \quad \textbf{(3.11)}$$

$$Specificity = \frac{true\ negatives}{true\ negatives + false\ positives} \quad \textbf{(3.12)}$$

It can be seen in ***Table 3.5*** that the MLP network trained from Christ Church and Reading's data demonstrates a good generalization capability. In total, this pre-trained system successfully identified 63 tap change events, misidentified 3 non-tap changes ('false alarm'), and missed 7 tap changes. Notably the system never had a false alarm for tap up change events. This data yields a sensitivity of 92% and a specificity of 100% for the classification of tap up events, and a sensitivity of 88% and a specificity of 99.9% for tap down events. Overall, from the validation data set the system correctly identifies 90% of the tap change events and 99.9% of the non-tap change events.

It is worth noting that tap changes could be miscounted due to classification errors, which would result in a deviation between the estimated tap position and its actual value over time. In this study, two standard deviations from daily average tap position were used as a criterion for indicating MV network stress (this is further explained in the following section). A success rate of 90% indicates that on average one out of ten tap change events could be missed, which would not affect the stress indication result on a daily basis. Therefore, this success rate is considered acceptable. To avoid accumulated error, however, the tap position was reset to a default value on a nightly basis, given that the data provided by SSE showed that the tap always tended to return to the same position at midnight (see ***Appendix 3.3***).

During the training process and validation of the network, it was observed that the more training data was provided to the network, the higher was the classification accuracy. This is attributable to the nature of neural networks. With more training data, weights and bias are better defined and estimated to separate the two classes. Therefore, future work should include collecting more training data to improve the classification accuracy.

3.5.8 Indication of MV network stress

Unlike frequency, tap position is not subject to any grid code during operation except the physical limitation of tap windings that an OLTC transformer has. However, as is explained in *Section 3.2*, given that tap position implies the load condition demanded by the network downstream of the OLTC transformer, a boundary on the tap position can be set to indicate the stress within the MV network.

Both absolute and relative values can be used to set the stress level boundaries, and the severity of the stress can also be defined by using different bandwidths of values. In this thesis, a z-score approach was used to normalize original tap position TP_i to an index $z_{\mathrm{tp}(i)}$ by the following ***equations***:

$$z_{\mathrm{tp}(i)} = \frac{(TP_i - \overline{TP})}{\sigma_{\mathrm{tp}}} \quad \textbf{(3.13)}$$

$$\overline{TP} = \frac{1}{m}\sum_1^m TP_i \quad \textbf{(3.14)}$$

$$\sigma_{\mathrm{tp}} = \sqrt{\frac{\sum_1^m (TP_i - \overline{TP})^2}{m}} \quad \textbf{(3.15)}$$

where $z_{\mathrm{tp}(i)}$ represents the distance between the original tap position TP_i and daily average tap position $\overline{TP}$ in the units of standard deviation σ_{tp}, and m is the number of total points available over a day.

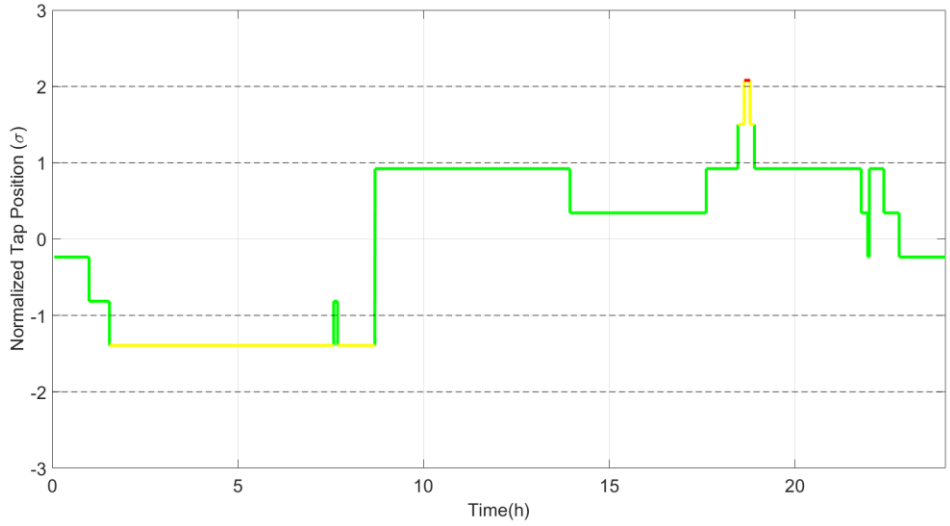

Figure 3.19 Tap position and indication of MV network stress using z-score approach (with 100% successful tap change detection)

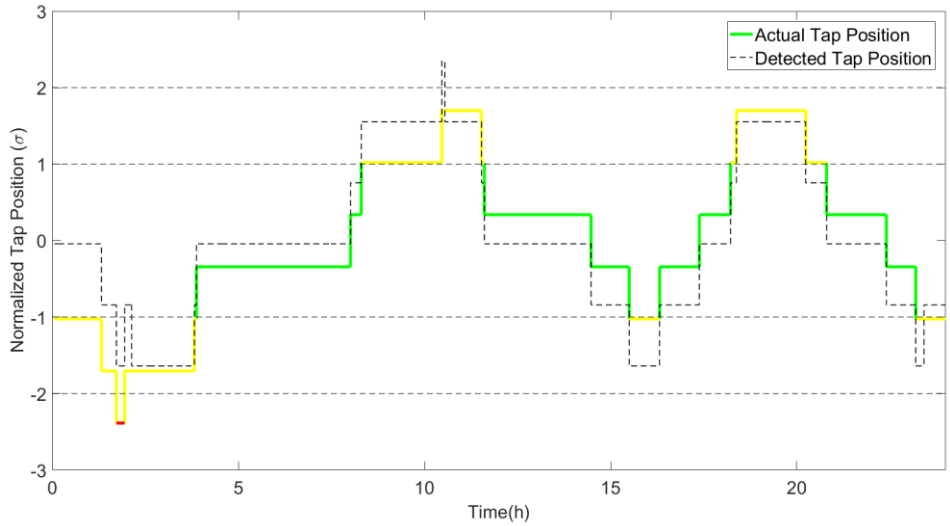

Figure 3.20 Tap position and indication of MV network stress using z-score approach (with three misclassified tap change events)

An example showing the normalized tap position with indicated regional scale (MV level) stress in a domestic distribution network in Bath is illustrated in ***Figure 3.19***. The normalized tap position highlighted in yellow is between one and two standard deviations away from the daily average, whereas red indicates a distance above two standard deviations. The further tap position is away from daily average, the greater stress the network is under. The rising order of the stress condition (either overload or underload) is

therefore green, yellow and red. The figure indicates that the MV network is most overloaded during the period between 6pm to 7pm. This matches the peak demand period for the domestic sectors, when many users come home and start to use appliances for heating, cooking, washing, etc.

To illustrate the impact of tap change classification performance on MV stress indication, another example of the normalized tap position is plotted in ***Figure 3.20***, where the solid line and the dashed line indicate the actual tap position and the tap position detected by the algorithm respectively. Three out of 23 tap change events were detected incorrectly (false positive) at 02:08:11, 10:32:46 and 23:25:00, and consequently, even though there was no significant discrepancy between actual and detected tap positions, the algorithm did miss the short underload stress period around 2am and indicated a short false alarm for an overload period around 10:30am. One of the important future areas of work is therefore to improve the accuracy of the tap change detection algorithm.

3.6 Detecting the Stress in LV networks

So far the approaches in this chapter enable both users and smart appliances to perceive the system-wide (HV) and regional-wide (MV) stress without any external real-time communication. On top of that, stress conditions in the neighbourhood area where the user is based are also critical for turning the smart appliances on and off at the right time. Especially with the growing penetration of intermittent renewable generations, the local supply and demand conditions tend to fluctuate even more. In this section, the voltage impacts associated with tap change events are removed from the measured mains voltage. The result reveals that the processed voltage provides a more indicative relationship with the power consumed at the same location than the original measured mains voltage.

3.6.1 Removal of tap change impacts

Using the tap change detection approach described in *Section 3.5*, voltage change associated with a tap change event can be detected and removed from the original voltage. For instance, ***Figure 3.21*** shows an example of the original voltage and the voltage without the impact of OLTC in the same location. The top figure shows two tap up change events which occurred at around 473.0 and 473.5 seconds and which were detected by the classification system. In the bottom figure, the plot is the compensated mains voltage as if no tap change events had occurred.

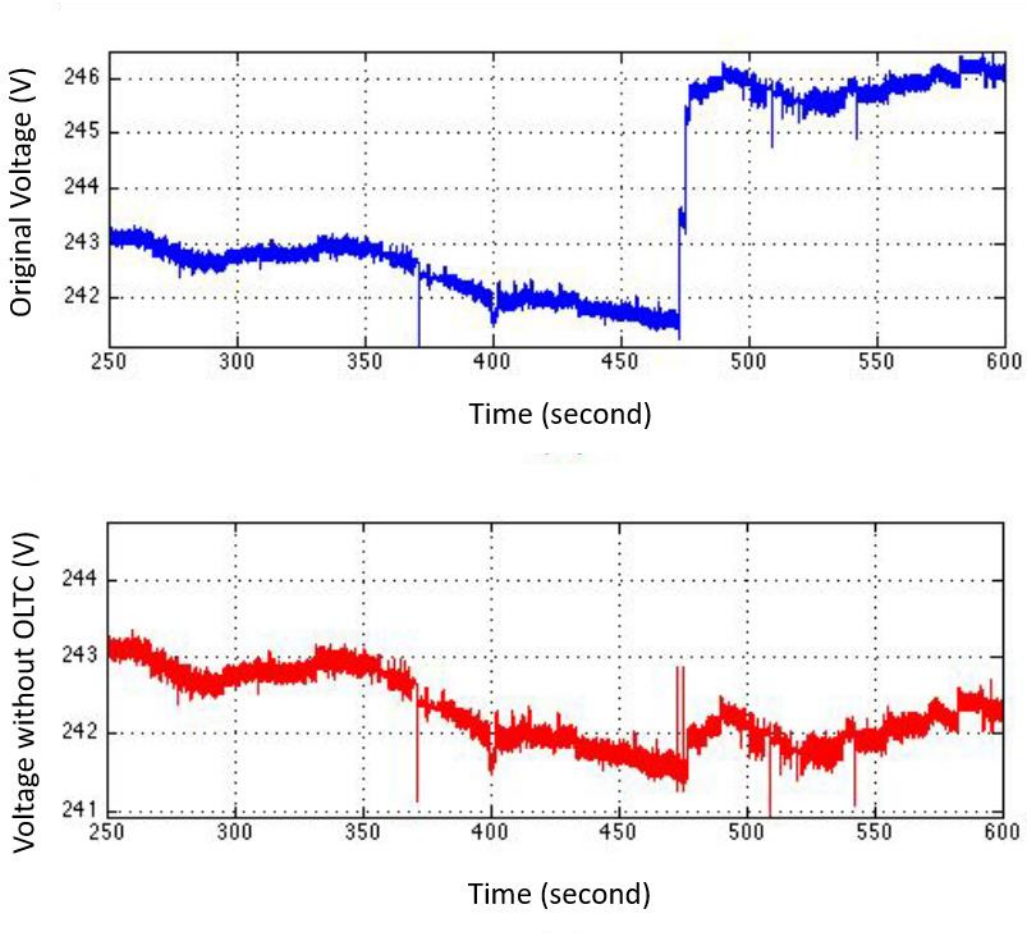

Figure 3.21 Voltage before (top) and after removing the impact associated with tap change events

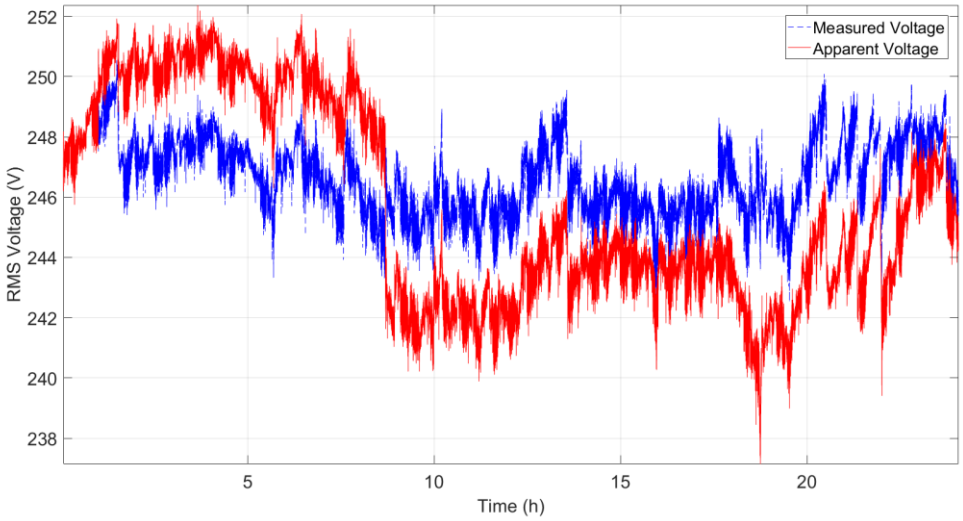

Figure 3.22 Difference between measured voltage and apparent voltage

Figure 3.22 plots the measured mains voltage V_{measured} and the apparent voltage V_{app} which removed the impacts of tap changes during a 24 hour period in Bath. It is clear that the OLTC transformer plays an important role in maintaining mains voltage on the user side, that V_{app} fluctuates much more than V_{measured}. How could V_{app} be used to reflect the local stress is further explained in the following section.

3.6.2 Apparent voltage and active power

Suitable parameters that can be used to refer local stress are the active power and reactive power consumed at that measurement point. Active and reactive power data are available from the location in Bath only, as this was the only place that took both voltage and current measurement.

The power *P* is calculated as an average over a half-cycle in ***equation (3.16)***:

$$P = \sum_1^n V_{\text{i}} \cdot I_{\text{i}} / n \qquad \textbf{(3.16)}$$

where n is the number of sampling points within half-cycle.

Similarly, *Q* is calculated as an average value over a half-cycle in ***equation (3.17)***:

$$Q = \sum_1^n V_{\mathrm{i}} \cdot I_{\mathrm{i+m}} / n \qquad \textbf{(3.17)}$$

where m is the number of sampling points for a quarter of cycle, in which case, $I_{\mathrm{i+m}}$ is 90 degrees away from I_{i}.

As the focus of this study is to investigate the general trends between the voltage and power, the original data resolution at 100 Hz (updated 100 times per second) is too high, and would contain unnecessary transient noise. A moving average for every 100 points (resolution of 1 second) was thus applied to the data to smooth out the curve and the first 100 data points were ignored for all parameters.

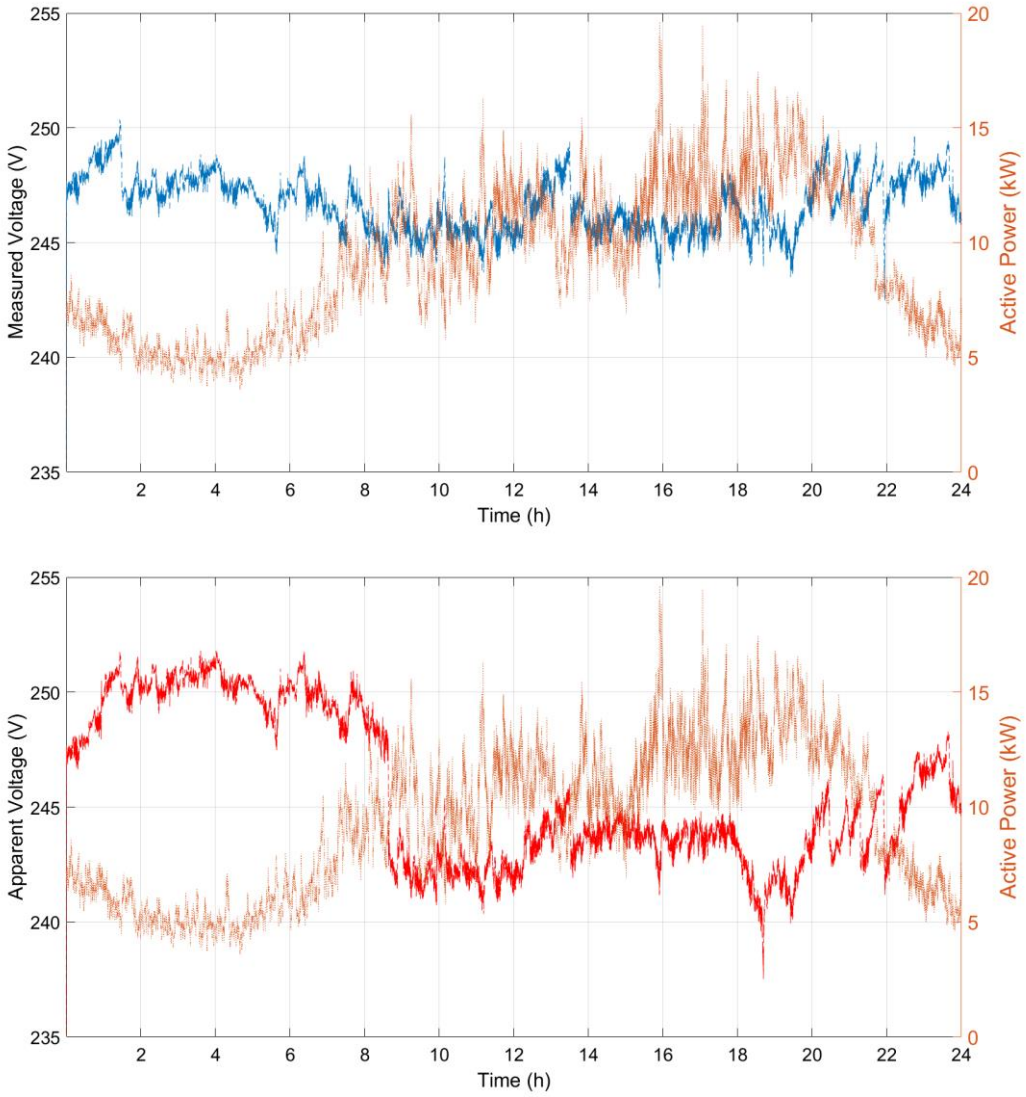

Figure 3.23 Measured (top) and Apparent (bottom) voltage compared to active power *P* in the same location

Figure 3.23 shows the measured V_{measured} and apparent voltage V_{app} compared with the active power P demanded at the same location on 27th March, 2011. As both figures are in the same range, it seems clear that the two parameters in the bottom figure represents a more obvious inverse relationship than those in the top figure. A similar conclusion can be drawn from ***Figure 3.24*** that V_{app} is more inversely proportional to the reactive power Q than V_{measure}.

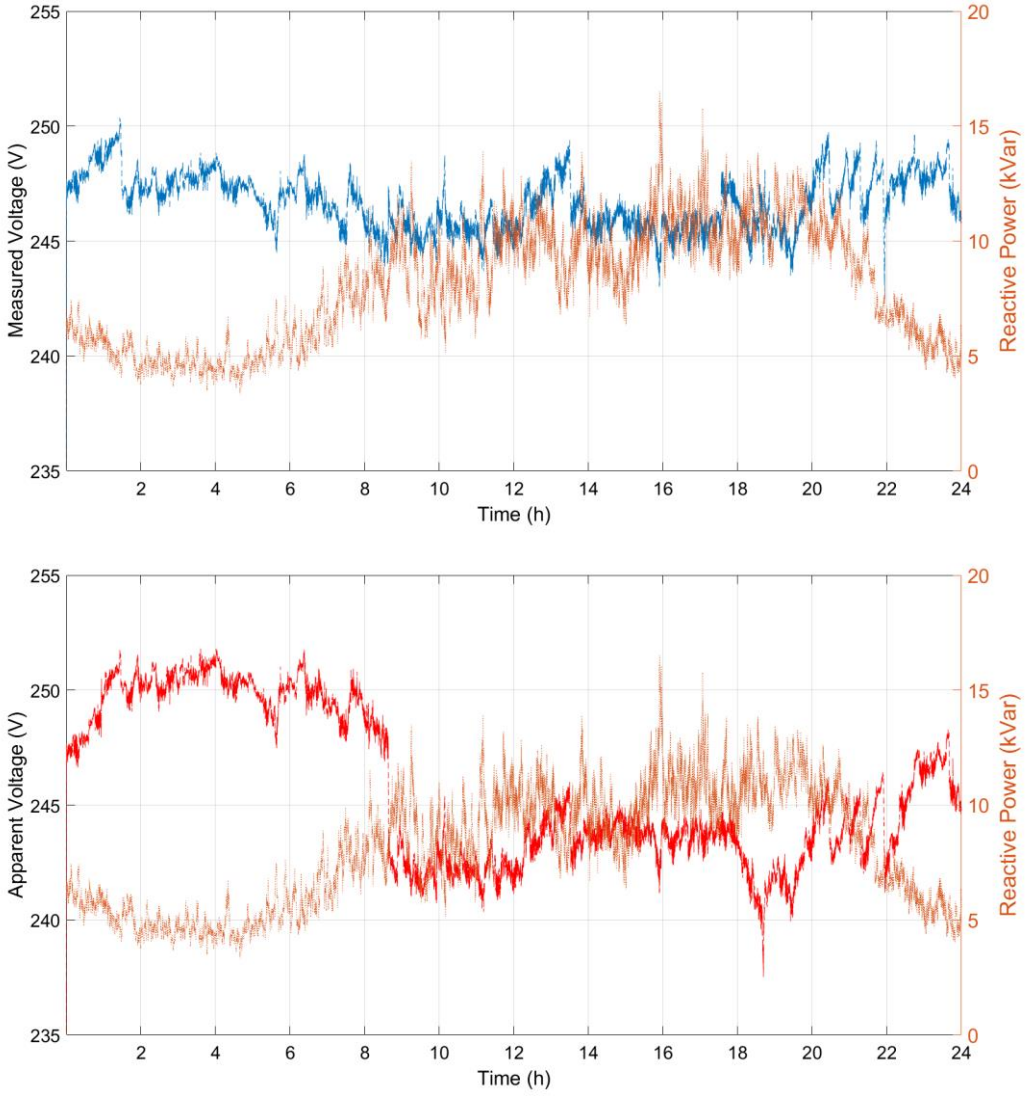

Figure 3.24 Measured (top) and Apparent (bottom) voltage compared to reactive power Q in the same location

To further quantify this relationship, the scatter plots of the measured and apparent voltage with active power are illustrated in ***Figure 3.25***. It can be seen that whilst having the same range of active power, V_{measure} in the right figure is in a much narrower band than the V_{app} on the left. Since both figures show a decreasing trend in terms of active power with measured and apparent voltage, first order linear regression models could be sufficient to fit the data to determine the quantitative relationship between the different voltages and power.

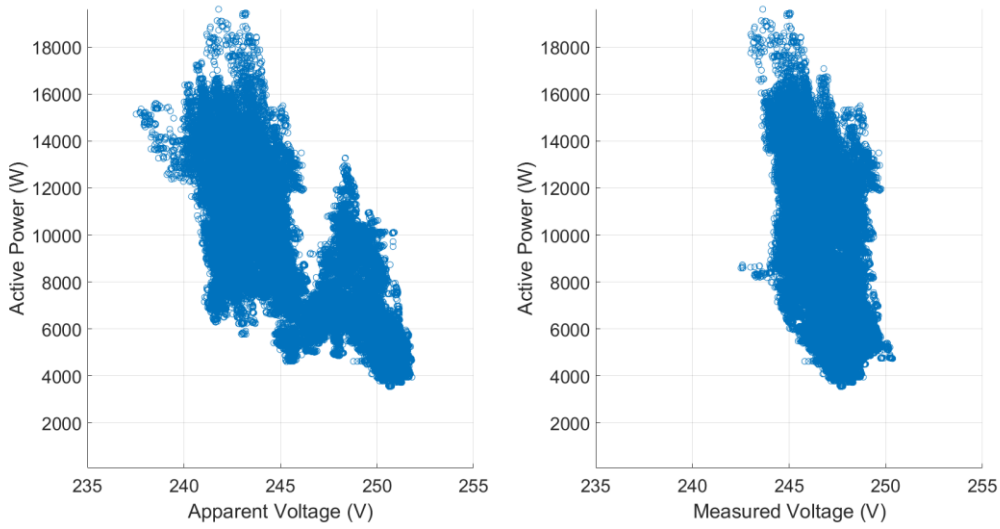

Figure 3.25 Scatter plot of measured and apparent voltage versus active power

Table 3.6 shows the linear regression models derived from the data in ***Figure 3.25***. While both models have 0 P-values, the R^2 value of the model with apparent voltage is more than double the one with measured voltage. In addition, the root mean square error (RMSE) for the model with apparent voltage is one third less than that with measured voltage. Although there is a degree of inaccuracy in both models, V_{app} was proven to be a better indicator of the power than V_{measure} due to its better data fitting and lower level of prediction error. It would be useful if further investigation on using apparent voltage to

infer other local stress indicators such as line voltage drops could be carried out in the future.

Table 3.6 Regression model for different voltages and active power

Voltage	*Regression Model*	*P-value*	R^2	*RMSE*
Measured	$P = -1446 \cdot V_{\text{measure}} + 3.7\times10^5$	0	0.3	2.64×10^3
Apparent	$P = -773 \cdot V_{\text{app}} + 1.99\times10^5$	0	0.654	1.86×10^3

RMSE is root mean square error for the regression model

3.6.3 Indication of LV network stress

Unlike frequency and tap position of the OLTC transformer, apparent voltage is derived from other network parameters such as mains voltage and tap changes so that it cannot be directly measured. It is therefore not subject to any grid code as for frequency nor physical constraints as in the case of tap position. Due to the inversely proportional relationship of apparent voltage and the power, it is however, possible to infer the level of demand around the measurement point based on the apparent voltage value.

Similar boundary conditions to those used for MV network stress in *Section 3.5.8* were used in this case; that the stress indication boundary is set as $\overline{\text{V}} \pm \sigma_{\text{v}}$ and $2 \cdot \sigma_{\text{v}}$, where $\overline{\text{V}}$ and σ_{v} are the daily average and standard deviation of the apparent voltage respectively. Any apparent voltage below the lower limits is indicated as the overload condition, and vice versa. ***Figure 3.26*** shows an example of apparent voltage with indicated LV level stress in a distribution network in Bath, where the system is most overloaded at around 7pm and registers the lowest demand between mid-night to 8am.

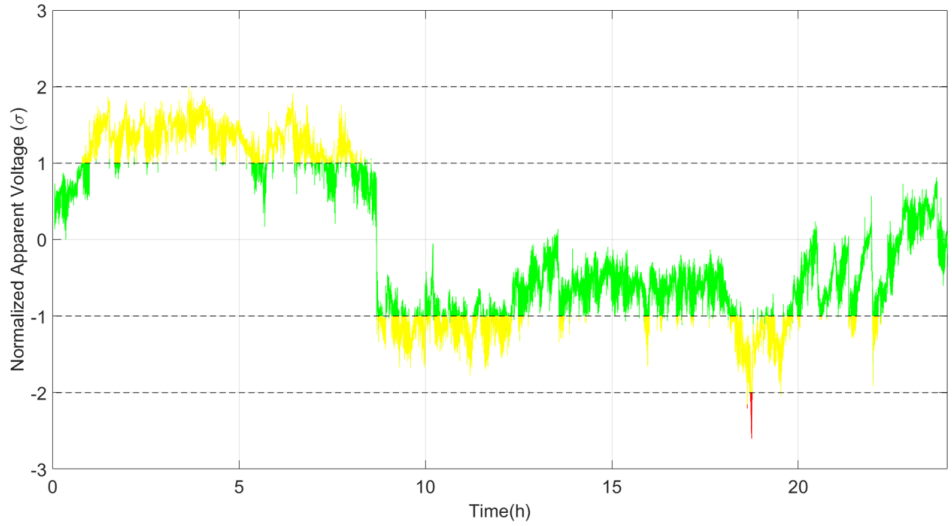

Figure 3.26 Apparent voltage and indication of LV network stress using z-score approach (with 100% successful tap change detection)

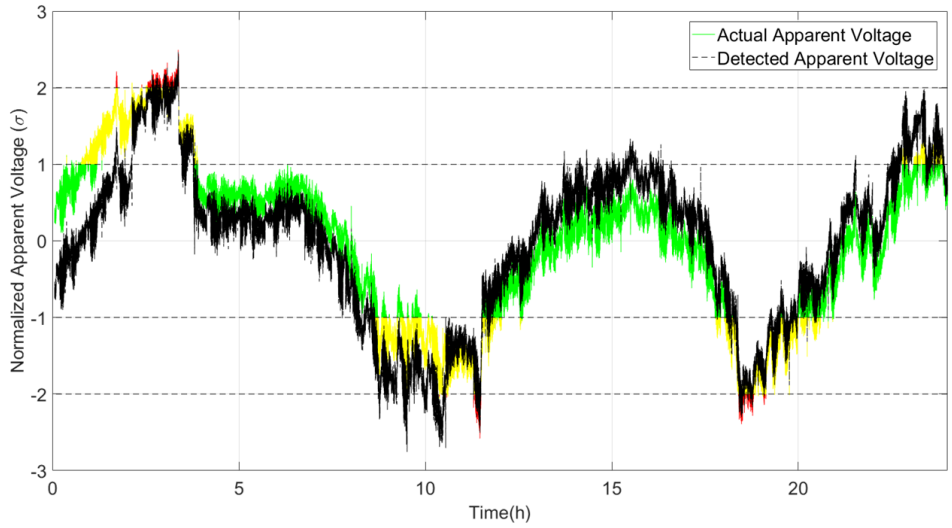

Figure 3.27 Apparent voltage and indication of LV network stress using z-score approach (with three misclassified tap change events)

To demonstrate the impact of tap change detection performance on LV network stress indication, the actual and the detected apparent voltage, within the same period shown in ***Figure 3.20***, were plotted in ***Figure 3.27***. With three false positive tap change detections, the detected apparent voltage did not deviate too far from the actual apparent voltage, and

both curves indicated similar stress periods. It can be seen that misclassified tap changes would have a bigger impact on stress indication in the MV network than in the LV network.

3.7 Significance to the DSM Strategy

With the function of load shifting, domestic-level DSM strategy faces a number of questions and challenges, such as, what is the best time to turn on or off the devices, or how to relieve local stress without exacerbating the stress in the upstream network. One scenario could be that when a LV network is experiencing excessive PV generation, with only local stress intelligence, the smart appliances would be turned on to absorb surplus generation. However, other LV networks supplied by the same OLTC transformer could be over-loaded at the same time that the transformer is actually under stress. Turning on the appliances in that particular LV network could solve the voltage problem locally, but would worsen the overload problem for the OLTC transformer which supplies to the whole MV network.

Another scenario could happen with the existing DSM scheme, ripple control. Devices under ripple control scheme may react based on the frequency measurement, which represents the system-wide stress. If frequency goes high, devices will be turned on, and vice versa. However, this ignores the stress across both MV and LV networks. Local demand can be very different from overall generation and load condition, and turning a device on or off to relieve system-wide stress could counteract the load control for the local network.

Given these different scenarios, all three levels of stress should be considered in the DSM operation. The rules used to solve the problems related to the first and second scenario described above are: 1. The device will not take an action if the MV and LV

network are in the opposite stress condition (i.e. the device will only be turned on when either or both networks are underloaded and neither is in overload condition); 2. If the MV and LV network are in the opposite stress condition from the HV network, the device should not be turned on or off (i.e. when the HV network is underloaded, both the MV and LV network need to be either underloaded or in normal condition for them to turn on).

If the stress condition (above two standard deviations away from the daily average) is defined as follows: -1 for underload, 1 for overload, 0 for normal, the following lookup table can be used for the DSM action:

Table 3.7 Lookup table for DSM control based on stress indication

Scenarios	*HV Stress*	*MV Stress*	*LV Stress*	*Device action*
I	$\bar{1}$	-1	-1	
	$\bar{1}$	-1	0	Turn On
	$\bar{1}$	0	-1	
	$\overline{-1}$	1	1	
	$\overline{-1}$	1	0	Turn Off
	$\overline{-1}$	0	1	
II	1	$\overline{-1}$	$\overline{-1}$	Turn Off
	-1	$\bar{1}$	$\bar{1}$	Turn On

$\overline{-1}$ stands for 0 or 1 stress condition and $\bar{1}$ stands for 0 or -1 stress condition

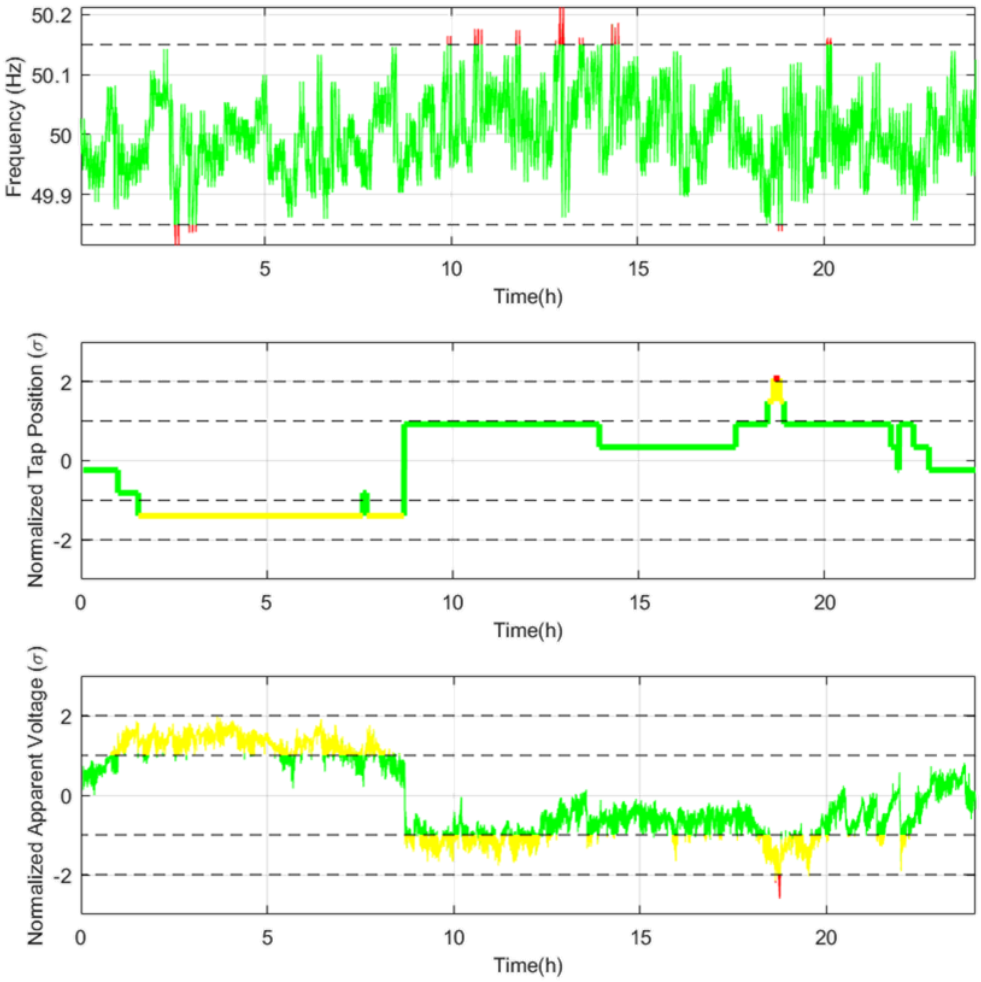

Figure 3.28 Stress indicator at three levels plotted on the same time scale

An example of the stress identification from a location in Bath is shown in ***Figure 3.28***, suggesting that the following load controls to be implemented:

1. From 1am to 8am, devices could turn on to alleviate the MV and LV underload stress. However, this action should avoid the period between 2am and 3am when the HV network is overloaded.
2. Between 10am to 3pm, when the HV network is underloaded and the MV and LV networks are in normal condition, devices can be turned on.

3. All three levels of the network are overloaded for a short period between 6pm to 7pm. Load shedding should be considered at this time.

So far the DSM strategy in this thesis considered bang-bang (on or off) control. More complex rules can be defined, such as considering degrees of stress for proportional load control rather than employing a discrete band. This chapter has focused on the techniques used to detect such stress, and it would be beneficial if there could be further investigation of the definition of DSM rules in the future.

3.8 Summary

This chapter has addressed the question: *"Without further investment into the communication infrastructure, is there a technique that can enable domestic devices to perceive the stress across the network in real time?".* Two types of stress across three different levels of network are first explained, and this is followed by a proposal of an approach to identify the stress at three levels, namely, system-wide (HV level), MV and LV level through mains voltage measurement at the connection point of a domestic DSM asset.

At the system-wide, HV level, the disparity between supply and demand can be represented by the deviation of frequency from its nominal value. *Section 3.4* proposed a frequency estimation approach using zero crossing detection and Butterworth low pass filtering based on measured voltage data. The validation results demonstrated a close proximity between the estimated data and the frequency data provided by the National Grid.

At the MV level, network stress is reflected by the tap position of the OLTC transformer. A novel classification system incorporating a MLP neural network was proposed and validated in *Section 3.5* to classify voltage changes associated with the tap change events. The results demonstrate a high degree of accuracy and good generalization

capability using a MLP network. It was validated to have a 90% success rate in classifying tap change events (sensitivity) and a 99.9% success rate in classifying non-tap change events (specificity).

At the LV level, the network stress is revealed by compensating the influence of the OLTC transformer's tap changes. Compensated voltage, defined as apparent voltage, showed an inverse relationship with both active and reactive power consumed at the same measurement point. Statistical analysis showed that apparent voltage provided a better indication of the LV stress than the measured voltage.

The outcome of this chapter could be incorporated in a decentralized control scheme which does not require the overheads associated with a large, centralised communication system. It would therefore be practical to exploit this method in the smart appliances or energy storage systems installed in domestic households.

Chapter 4. Sizing Design of Domestic Hot Water Tanks

4.1 Introduction

Chapter 3 introduced a technique which enables domestic appliances to perceive stresses across the power network without real-time communication, allowing them to be used as decentralised DSM assets. The next step, then, is to consider which appliances might be suitable for such a scheme.

As discussed in *Section 2.4*, compared to other domestic appliances such as home batteries, EVs and fridges, electric hot water tanks (EHWTs) present a better economic opportunity for DSM on the basis of cost and existing presence in the residential sector in the UK. There is, however, no standard set of tank sizes in the UK market and often households do not have the correct size of tank for their needs. In order to explore the potential of EHWTs as DSM assets, an understanding of the performance of the tank and the user's hot water usage pattern is essential. This chapter therefore sets out to answer the following questions: *"1. Is there a way to determine the optimal tank size to provide customers with greater economic benefits, given the pattern of their hot water usage? 2. What are the typical patterns of hot water usage and the most common optimal tank size for UK consumers?"*.

We begin with *Section 4.2*, where an energy node model is used to simulate domestic energy storage systems. This model is then characterized specifically for EWHTs. In *Section 4.3*, a sizing optimization problem is formulated to determine the optimal size of tank required to achieve the minimum household energy cost per kWh used.

In *Section 4.4*, this size optimization strategy is applied to a data set consisting of 112 hot water usage profiles from an Energy Saving Trust (EST) study in order to determine the most common optimal tank size in the UK. Finally, in *Section 4.5*, the user profiles are

clustered into different groups, indicating different hot water usage behaviours. A correlation study covering different occupancy features and usage patterns is carried out, with a view to investigating whether there is any linkage between the household models and optimal tank size.

In the next chapter, we will seek to understand the potential demand response capability and benefits of a fleet of EHWTs in real UK LV distribution networks. This requires proper selection of tank size for different household models. The outcome of this chapter therefore determines the optimal tank size for UK households and establishes a fundamental tank model for bottom-up LV distribution network simulation for the following chapter.

4.2 Energy Node Modelling

Before formulating an EHWT sizing optimization problem, the fundamental step is the construction of an energy model, given that different models lead to different results. This section begins by introducing the generic energy storage model adapted from a single power node model as proposed by Huseen et al. [133], [134]. This model is then characterized specifically for EHWTs in *Section 4.2.2*.

4.2.1 A generic domestic energy node model

The domestic energy storage system acts an intermediary between the grid and the individual household, providing or absorbing energy from both sides. There are three components in the structure of an energy node: grid, energy storage and demand side, and energy can flow bidirectionally between each of these. ***Figure 4.1*** presents a generic energy storage model which integrates electricity grid and household, where arrows indicate the

flow of energies. If we lump sum the energy in each direction into one value, along with three energy characters within the energy storage system, there will be seven parameters in the scheme:

- E_{dsin} is the renewable energy feed-in such as roof-top PV generation.
- E_{dsout} is the energy demand from the household including services that can be supplied in the form of energy (e.g. hot water services).
- E_{egin} is the energy supplied from the grid.
- E_{egout} is the energy exported from the storage system to the grid.
- C is the energy capacity of the storage system (including thermal storage in terms of energy).
- S is the state of charge of the energy storage system where $S \in [0\ 1]$.
- E_{sl} is the energy storage loss.

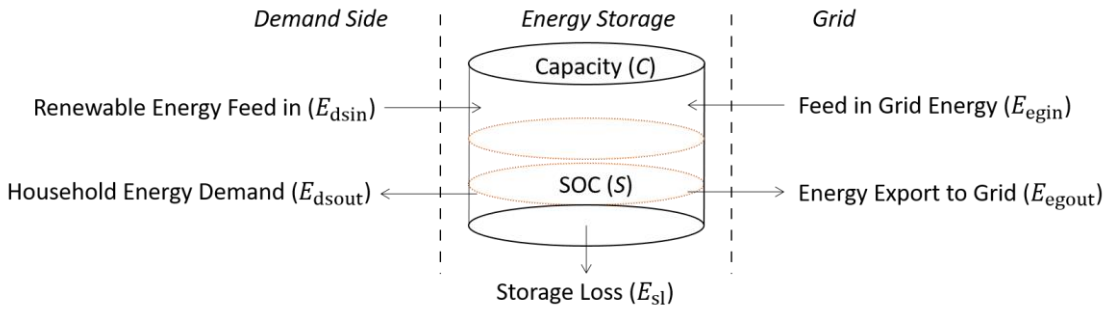

Figure 4.1 Adapted energy node model from Huseen et al. [133]

The dynamics of the energy node model can be described in the following equation:

$$C \cdot \dot{S(i)} = E_{\mathrm{egin}}(i) - E_{\mathrm{egout}}(i) + E_{\mathrm{dsin}}(i) - E_{\mathrm{dsout}}(i) - E_{\mathrm{sl}}(i) \qquad \textbf{(4.1)}$$

where i indicates the iteration of the modelling. As the hourly data may not be sufficient to provide the dynamics shown in the model, the resolution of the data in this chapter is set at

six minutes (1/10 of an hour) so that i ranges from 0 to 240. The model is further subject to the following constraints:

$$0 \leq S(i) \leq 1 \quad \textbf{(4.2)}$$

$$0 \leq E_{\mathrm{egin}}(i) \leq E_{\mathrm{egin}_{\max}} \quad \textbf{(4.3)}$$

$$0 \leq E_{\mathrm{egout}}(i) \leq E_{\mathrm{egout}_{\max}} \quad \textbf{(4.4)}$$

$$0 \leq E_{\mathrm{dsin}}(i) \leq E_{\mathrm{dsin}_{\max}} \quad \textbf{(4.5)}$$

$$0 \leq E_{\mathrm{dsout}}(i) \leq E_{\mathrm{dsout}_{\max}} \quad \textbf{(4.6)}$$

$$0 \leq E_{\mathrm{sl}}(i) \quad \textbf{(4.7)}$$

where $E_{\mathrm{egin}_{\max}}$, $E_{\mathrm{egout}_{\max}}$, $E_{\mathrm{dsin}_{\max}}$ and $E_{\mathrm{dsout}_{\max}}$ represent the maximum energy flow during each iteration. ***equation (4.3) - (4.6)*** represent non-negative and bounded energy for each flow direction. ***equation (4.7)*** defines energy loss as always positive.

Depending on the specific case represented by the energy node model, the observability and controllability of parameters in the e***quation (4.1) - (4.7)*** may vary. The next section goes on to characterise all of these parameters specifically for EHWT study.

4.2.2 Energy Storage Model for the EHWT

This section introduces a new EHWT topology [135] which can be represented by a simple, battery alike model.

A conventional EHWT heats up water via the immersion heater at the bottom of the tank, mixing the water above the immersion element to an approximately unified temperature. Given that the outlet water will only be usable above a certain temperature (43 °C defined in [90]), it would take a long time to heat up a tank of water to a usable temperature (for example, it would take over an hour to heat up a 150-litre tank from 20 °C to 43 °C with a 3kW heating element). The new "*instant*" topology shown in ***Figure 4.2***

resolves this problem by taking the cold water from the bottom, heating it up through an inline heater and pumping the hot water to the top of the tank, so that thermocline is pushed from top to bottom. The arrows in the figure indicate the direction of the flow. Coupled with a thermocline sensor which can be used to infer the SOC of the tank (i.e. the available hot water left), the user will be able to control how much water is to be heated and consequently shorten the waiting time required for hot water to become available. With a diffuser at the bottom of the tank to improve thermal stratification, the instant topology is considerably more straightforward to model since there is no need to consider the effects of thermal mixing during the heating and drawing event.

In the new EWHT model, the following assumptions are made:

- Hot and cold water are well stratified.
- The inlet water temperature is 20 ℃.
- The thermostatic of the immersion heater is set to 60 ℃ in accordance with British standards [136]. If $S(i) > 0$, the outlet water temperature will always be 60 ℃.
- The power consumption of the circulation pump is not considered in the model.

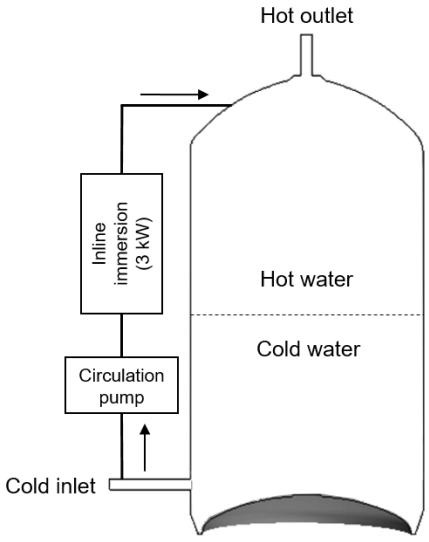

Figure 4.2 '*Instant*' heating topology patented in [135]

Given these assumptions, the energy behaviour of EHWT could be considered similar to battery storage system, in that the draw event and the heating of the tank are equivalent to discharging and charging the battery respectively. The only difference is that the battery energy storage system has bidirectional energy flow to both grid and household, whereas EHWT does not feed energy back to the grid and the energy provided to the household is in the form of hot water. Translating these features into the energy modelling parameters used in *Section 4.2.1*, this means that $E_{\mathrm{egout}}(i) = 0$ under all circumstances, and the hot water service can be represented in units of kWh energy by:

$$E_{\mathrm{dsout}}(i) = mC_{\mathrm{p}}(T_{\mathrm{out}} - T_{\mathrm{in}}) \quad \textbf{(4.8)}$$

According to this assumption, T_{out} and T_{in} represent the outlet and inlet temperature at 60 ℃ and 20 ℃ respectively. This EHWT topology is incorporated as energy storage in the energy node model in ***Figure 4.1***, and the sizing optimization approach based on this scheme is introduced in the next section.

4.3 Sizing Optimization of EHWTs

The sizing design for the EHWT consists of two stages of optimization: operation and sizing optimization. The structure (flow chart) of the design process is shown in ***Figure 4.3***, where the two stages of the optimization can be described as follows:

1. Operation optimization is used to determine the optimal charging profile with minimum operating cost based on a given usage profile and a fixed tank size.
2. Given the minimum operation cost associated with each size, a brute-force approach is applied to all sizes, and the one with overall minimum operating costs is defined as the optimal tank size. The reasons for using the brute-force approach is further explained in *Section 4.3.6*.

This section begins with an introduction of the background of the problem in *Section 4.3.1*, which defines hot water usage profile and optimal tank size as the overall input and output. It then continues with the formulation of the operation optimization problem, which consists of the following components: an objective (cost) function with decision variables, a collection of constraints, and an optimization solver. The cost function (with decision variables) and constraints are defined in *Section 4.3.2* and *4.3.3* respectively, followed by the introduction of a Matlab based solver in *Section 4.3.4*. Finally, examples of two stages of optimization are presented, along with the reasons why these optimization solvers were used.

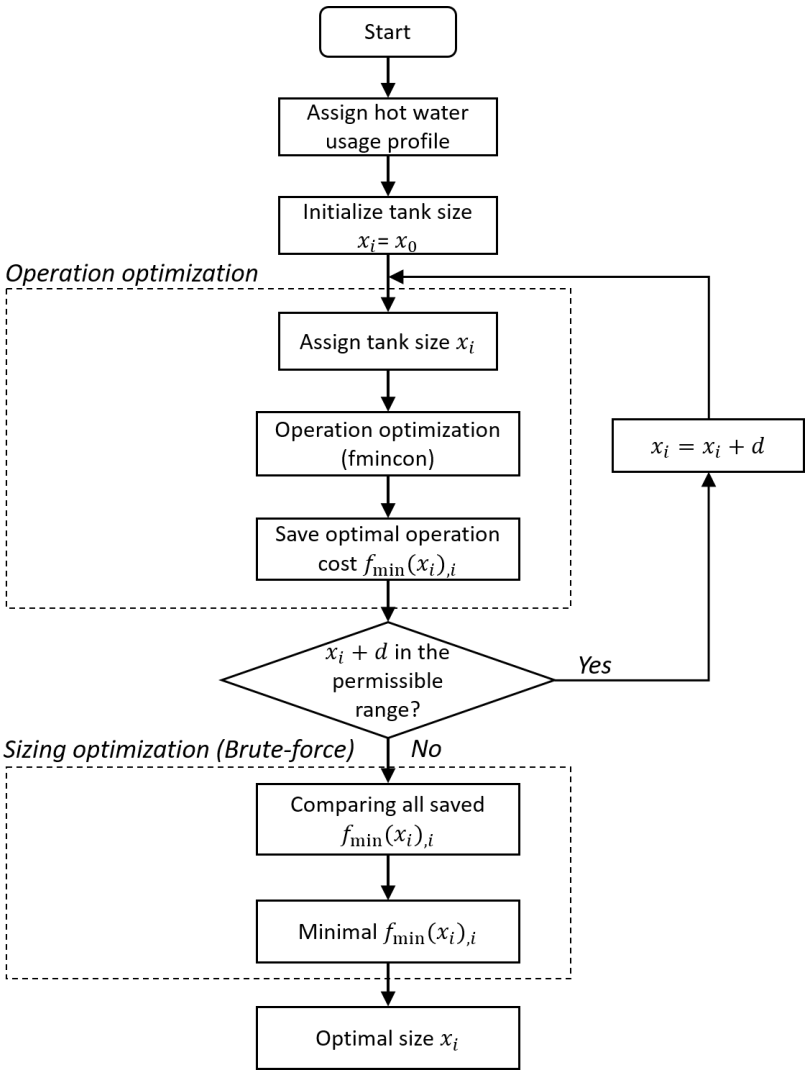

Figure 4.3 Flow chart for two-stage optimization: brute-force approach embedded with operation optimization

In summary, the sizing optimization problem is formulated in such a way that there will be one optimal tank size which can provide a minimal cost of energy with a given hot water usage profile. *Section 4.3.7* will discuss the results and logic behind the sizing optimization approach.

4.3.1 Scenario

This section is to investigate the optimal tank size to maximize the benefit for most of the users from price arbitrage with a given usage. This section will therefore define the most common EHWT scenario that occurs to the UK households.

The first thing to exam is the opportunities for price arbitrage. With flat energy prices, there is no incentive to have a storage system because the cheapest way would be to heat up the right amount of water instantly, thus saving the capital cost of the tank. However, with the increasing adoption of tariff schemes which offer different prices at different times of day, the cost of energy can be reduced significantly by turning on the EWHT at the right time. While there are different tariff schemes on the market, such as Economy 10 [137] or the sunshine tariff [138] (still on trial), Economy 7 is the most widely-adopted electricity tariff scheme [139], charging two different prices for electricity usage at day and night. In 2014, the off-peak price was charged at 7-10 p/kWh between midnight and 7 am (the actual time may vary depending on different utility suppliers), whereas the peak price was between 13 and 17 p/kWh for the rest of the time [140]. This price arbitrage provides a major incentive to users with thermal storage systems such as EHWTs or storage heaters because the cheap, night-time energy can be used to store heat which would be needed later on during the day, when the electricity is expensive. It is worth noting that the Distribution Use of System (DUoS) charges were not taken into account because it would not impact

on the determination of the optimal size. It can be seen in *Section 4.3.6* that the tank would not operate during DUoS charge period (normally 4 to7 pm) at its optimal size.

The second element to consider is inbound renewable generation. According to the report by DECC in 2014 [141], 369,700 (1.6%) out of 23.4 million households in England and Wales had installed rooftop PV panels. While nearly 50% of households used an electric immersion heater as either a primary or a secondary source of heat for hot water production within tanks [20], households with both EHWT and renewable generation accounted for only a small proportion (< 3%) of the group.

Given the facts above, the majority of the EHWT scenarios in UK households involve a tank with Economy 7 circuitry and no inbound renewable generation ($E_{\mathrm{dsin}} = 0$).

4.3.2 Cost function for operation optimization

Cost function defines the function to be optimized to either its minimum or maximum value depending on the objective. It should therefore be characterized in terms of definition of the objective and of decision variables.

The objective of seeking maximum benefits for EHWT users translates into searching for the minimum cost of energy per kWh paid by the user to heat water. This cost should include both utility cost and the capital cost of the tank.

In terms of decision variables, there are two stages of optimization with one decision variable for each stage. For the operation optimization, with a given usage profile and a fixed tank size, the tank charging profile is the decision variable to be optimized. In the brute-force sizing optimization, tank size is the decision variable which determines the overall minimum operating cost.

Overall, the optimization problem is formulated in such a way that with a given hot water usage profile, there will be an optimal tank size which provides the minimum energy cost per kWh. This can be achieved by the following cost function:

$$f(EGin) = (\sum(C_{\mathrm{pi}}(i) \cdot E_{\mathrm{egin}}(i) - C_{\mathrm{pe}}(i) \cdot E_{\mathrm{egout}}(i)) + C_{\mathrm{rn}} + C_{\mathrm{es}}) / \sum E_{\mathrm{dsout}}(i) \quad \textbf{(4.9)}$$

where i is the time of day, C_{pi} is the electricity price, C_{pe} is the export tariff, and C_{rn} and C_{es} are the normalized daily capital cost of the renewable generation unit (such as solar PV panels) and the energy storage system (such as EHWTs or home batteries) respectively.

Since there is no inbound renewable generation based on the scenario described in the previous section, ***equation (4.9)*** can be simplified to:

$$f(E_{\mathrm{egin}}) = (\sum C_{\mathrm{pi}} \cdot E_{\mathrm{egin}}(i) + C_{\mathrm{es}}) / \sum E_{\mathrm{dsout}}(i) \quad \textbf{(4.10)}$$

As stated in the previous section, C_{pi} is the Economy 7 tariff, it is set at 7.5 p/kWh between midnight and 7 am and 15 p/kWh for the rest of the time. In many cases, EHWT comes as part of the home, and its cost may already be included in the cost of the property. The same mortgage equation used for the purchase of the home is therefore used to calculate the normalized daily capital cost of the energy storage system C_{es} (£/day) based on different tank size m:

$$C_{\mathrm{es}}(M) = C_{\mathrm{t}}(M) \frac{\mu(1+\mu)^n}{(1+\mu)^n - 1} \quad \textbf{(4.11)}$$

where μ is the daily interest rate (0.081% assuming a 3.0% annual interest rate), M is the mass of water in the tank, and n is the number of days of service life of the EHWT (assumed to be 7300 days, or 20 years). $\mathrm{C_t}(M)$ is the value of the new EHWT determined by interpolating the existing market price available online in 2015 [142]. The available vented tank size and its corresponding price are listed in ***Table 4.1***.

Table 4.1 Vented hot water cylinder size and price

Tank size (Litres)	100	120	150	180	250
Price (£)	516.27	878.32	915.34	1271.94	1421.23

The linear regression model shown in ***equation (4.12)*** was used to extrapolate the data. This model demonstrates a good fitness ($R^2 = 0.87$) and its root-mean-square error is £147. The original data and the regression model are plotted in ***Figure 4.4***.

$$C_t(m) = 5.66m + 95.26 \quad \textbf{(4.12)}$$

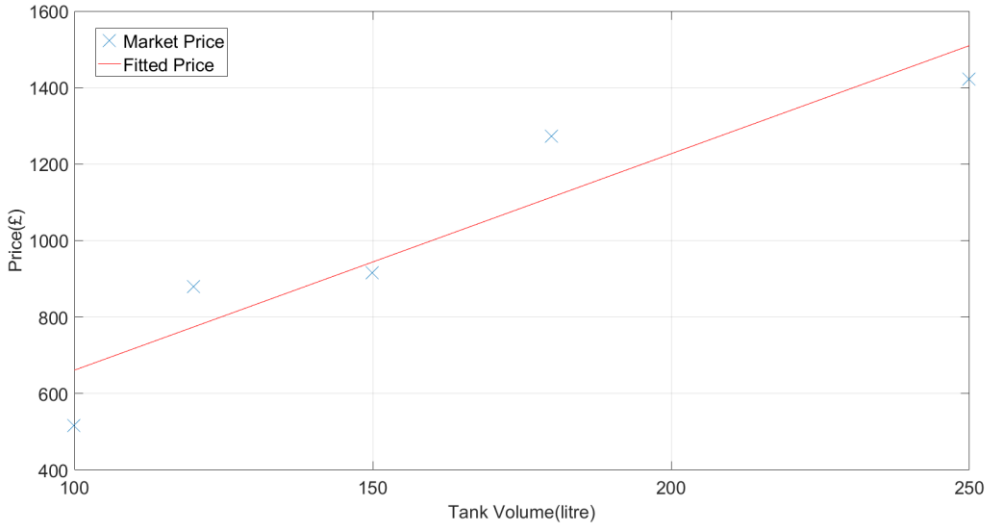

Figure 4.4 The original tank size with market prices and its linear regression fit

In summary, the objective function is ***Equation (4.10)*** and the decision variables are charging profile (Stage 1) and tank sizes (Stage 2).

4.3.3 Constraints for operation optimization

The constraints define the range of possible values of the decision variables and other parameters. As the ***equation (4.1)*** to ***(4.7)*** in *Section 4.2.1* have already defined the

constraints in a general model, this section extends to characterizing these constraints specifically for the operation optimization under the scenario described in *Section 4.3.1*.

Tank energy model

Equation (4.1) defines the tank energy model, without inbound renewable generations and export tariff. This model can be simplified to:

$$C \cdot \dot{S(\imath)} = E_{\text{egin}}(i) - E_{\text{dsout}}(i) - E_{\text{sl}}(i) \quad \textbf{(4.13)}$$

The thermal energy E_c stored in the water tank can be calculated as:

$$E_{\text{c}} = MC_{\text{p}}(T_{\text{t}} - T_{\text{a}}) \quad \textbf{(4.14)}$$

where C_{p} is the specific heat capacity for water at $4186\ \text{J}/(\text{kg} \cdot \text{K})$, T_{t} is the hot water temperature in the tank (which is the same as outlet water temperature T_{out} at 60 °C), and T_{a} is the ambient temperature (which is the same as inlet water temperature T_{in} at 20 °C).

The energy storage loss $E_{\text{sl}}(i)$ is proportional to the surface area of the hot water and the temperature difference between the water and ambient temperature. However, as tank sizes in the market vary significantly, it is difficult to infer surface area by tank size alone. In addition, heat loss coefficients vary with different tank and insulation materials. In this thesis, therefore, the energy (heat) loss is simplified as a proportion of total thermal energy in the tank. Based on experimental heat loss data provided by a British tank manufacturer (Newark Copper Cylinder Ltd), a 120-litre tank (with 5.35 kWh heat storage Q_{total}) would lose 1.31 kWh heat Q_{loss} within 24 hours. It may therefore be calculated that the heat storage loss is 0.15% of full tank energy for every 6 minutes by the following equation:

$$Q_{\text{total}}(1 - E_{\text{sl}}(i))^{240} = Q_{\text{total}} - Q_{\text{loss}} \quad \textbf{(4.15)}$$

State of charge

The state of charge represents the percentage of hot water in the tank, and is defined in ***Equation (4.2)*** where 0 indicates no hot water and 1 indicates a full tank. To avoid situations where the user might run out of hot water, the minimum state of charge is set at 20% so that:

$$0.2 \leq S(i) \leq 1 \quad \textbf{(4.16)}$$

Charging Energy

The energy charged into the tank is limited by the immersion heater. According to British standards, the power of the immersion heater is rated at 3kW [136]. As the model iteration is set at six minutes (1/10 of an hour), the maximum energy a tank can take from the grid is 0. 3 kWh (1/10 of 3 kWh). ***Equation (4.3)*** is therefore explicitly defined as:

$$0 \leq E_{\text{egin}}(i) \leq 0.3 \quad \textbf{(4.17)}$$

Overall, ***Equations (4.13), (4.16)*** and ***(4.17)*** are defined as the constraints condition for the EHWT scenario, and they will be used to formulate the Stage 1 operation optimization problem. There are no further constraints for Stage 2 sizing optimization, except for the assumed limit of tank size available on the market (50 – 400 litres) [142].

4.3.4 Solver for operation optimization

With the given constraints and cost function, the last step in the optimization process is to determine the solver. Since the number of points to be optimized is not large (240 points) in our case, the fmincon solver provided by the Optimization Toolbox in Matlab is used. The fmincon solver is used in many small to medium optimization cases to ascertain

the minimum of constrained nonlinear multivariable function, and it is specified as follows [143]:

$$\min_{x} f(x) \ such\ that \begin{cases} c(x) \leq 0 \\ ceq(x) = 0 \\ A \cdot x \leq b \\ Aeq \cdot x = beq \\ lb \leq x \leq ub \end{cases} \quad \textbf{(4.18)}$$

Based on the definition in our case, x is the charging profile, which is E_{egin}. Accordingly, ***equation (4.10)*** is used as the nonlinear cost function $f(x)$:

$$f(x) = (\sum_{i=1}^{240} C_{\text{pi}} \cdot x(i) + C_{es}) \,/\, \sum_{i=1}^{240} \sum E_{\text{dsout}}(i) \quad \textbf{(4.19)}$$

Equation (4.16) and ***(4.17)*** are used to setup nonlinear inequality constraint $c(x) \leq 0$ and upper and lower boundaries $lb \leq x \leq ub$ respectively:

$$c = [0.2 - S \quad S - 1] \quad \textbf{(4.20)}$$

$$lb = 0 \quad \textbf{(4.21)}$$

$$ub = 0.3 \quad \textbf{(4.22)}$$

where S is the state variable defined by the following equation:

$$C \cdot \dot{S(\imath)} = x(i) - E_{\text{dsout}}(i) - E_{\text{sl}}(i) \quad \textbf{(4.23)}$$

Before the solver can be used for solving the optimization problem, several features are specified, including the optimization algorithm, "MaxFunctionEvaluations" and initial point x_0. The 'Interior point' optimization algorithm handles anything from large, sparse problems to small, dense ones. It satisfies bounds at all iterations and is recommended as the 'first try' algorithm by the developers of Optimization Toolbox [144]. This algorithm has been proven to be effective (further explained in the next section) and was therefore chosen for our study.

"MaxFunctionEvaluations" defines the maximum number of function evaluations allowed before the optimization meets its criterion and stops. The default number is 3000, which was proven to be too small, given that the optimization stops before the result converges to its optimal value. The number of evaluations was therefore increased to 60000 so that the optimization did not stop prematurely.

Finally, since it has been established that the optimal charging profile would make the best possible use of price arbitrage (in our case, the off-peak tariff before 7am), the tank should be charged before 7am under optimal operation condition. In order to enable a faster convergence to the optimal state and to avoid being stuck at local minima, an initial value x_0 is set to be "on" for two hours before 7am and "off" for the rest of the time. Two hours' charging can provide 6kWh, which is just above the 5.6 kWh average total hot water energy usage (as suggested in the EST study described later).

The remaining features are set at default values provided by the solver and they are proven to demonstrate a satisfactory result in the following sections.

4.3.5 Operation optimization results (fmincon)

This section presents the optimization output E_{egin} based on the inputs of different tank sizes M and one hot water usage profile E_{dsout}. The results demonstrate how different tank sizes may affect the operation of the charging profile for the minimum operating cost.

Two tank sizes, 100 and 300-litre have been used as examples. In addition, a typical domestic hot water usage profile shown in ***Figure 4.5*** from an EST study [145] was used as the input. The original hourly data was linearly interpolated to change the resolution to six minutes in order to meet optimization requirements.

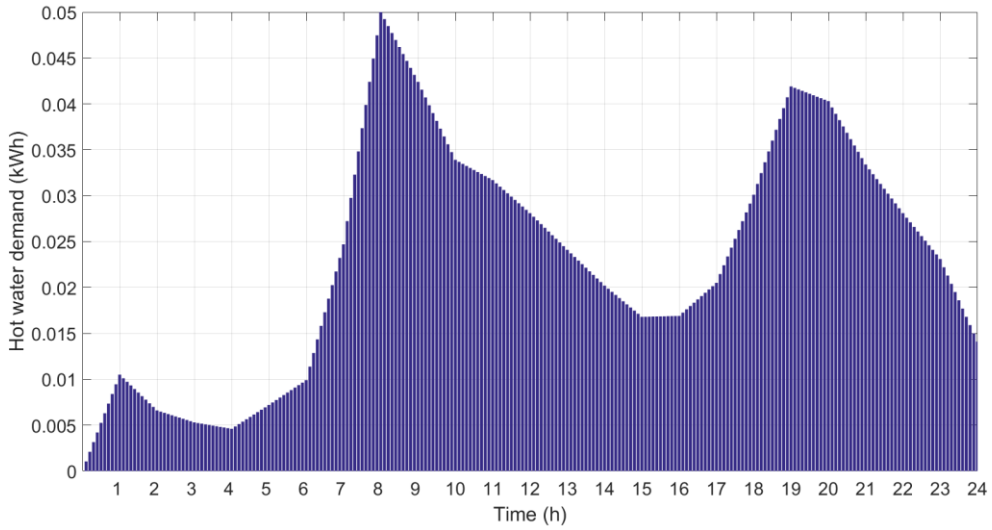

Figure 4.5 A hot water usage profile in EST study (represented in kWh units) [145]

100-litre tank simulation results

Assuming a 100-litre tank and the hot water usage profile provided in ***Figure 4.5***, an optimal charging profile and corresponding state of charge of the tank can be determined from the operation optimization. The results are shown in ***Figure 4.6*** and ***Figure 4.7***, yielding a minimum energy cost of £0.1289/kWh. The tank was charged to its full SOC at 7 am and charged further at night to maintain SOC above its lower limit.

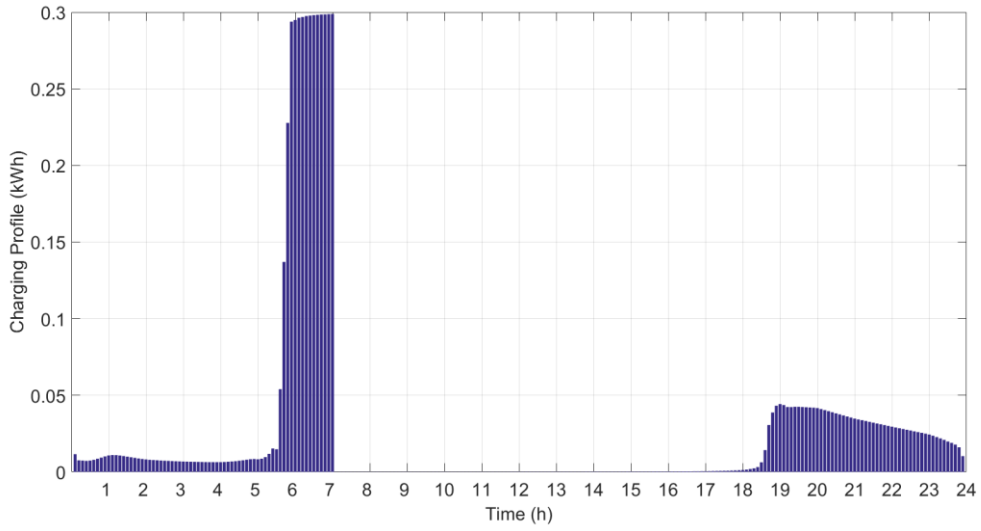

Figure 4.6 Optimal charging profile of 100-litre tank

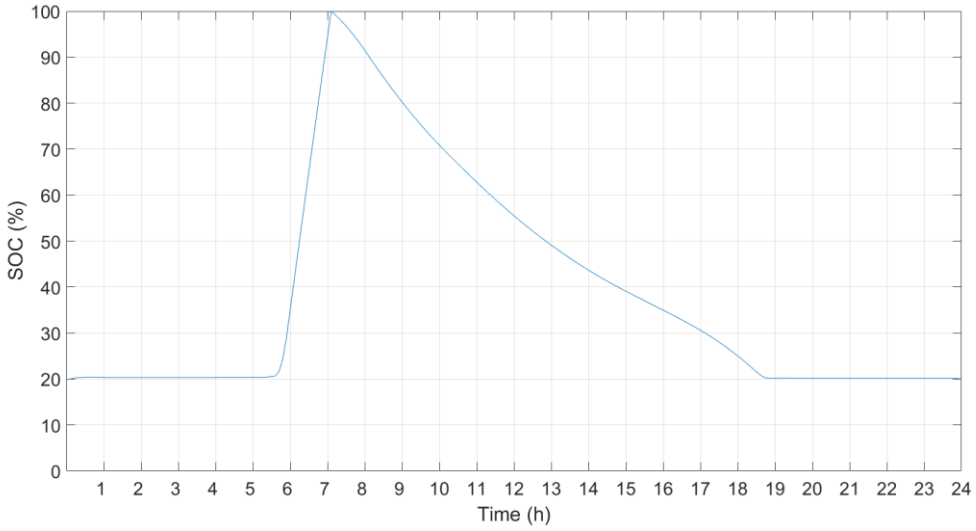

Figure 4.7 Optimal state of charge of the 100-litre tank

300-litre tank simulation results:

Using the same approach, the optimal charging profile and state of charge results are shown in ***Figure 4.8*** and ***Figure 4.9***, yielding a minimal energy cost of £0.1583/kWh. The tank was charged only once to 65% of SOC at 7 am, and this provided all the hot water required throughout the rest of the day.

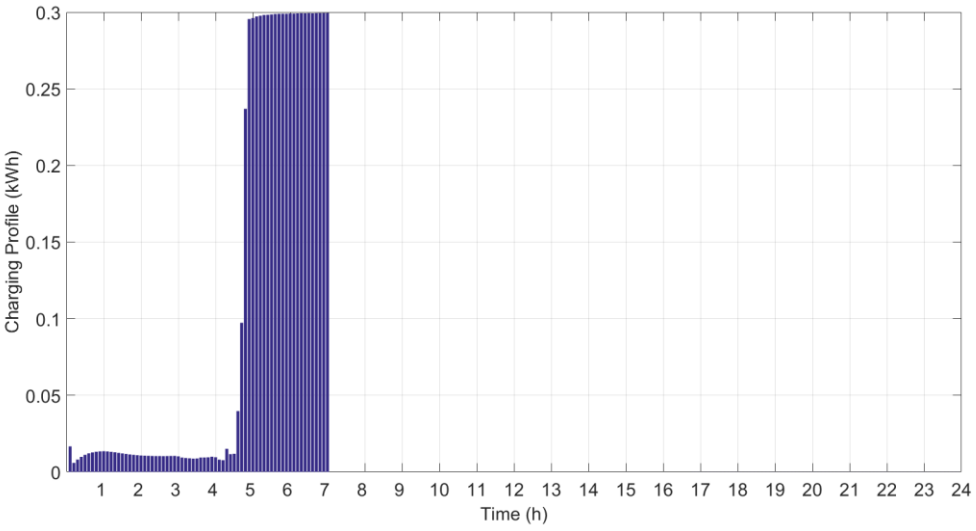

Figure 4.8 Optimal charging profile of 300-litre tank

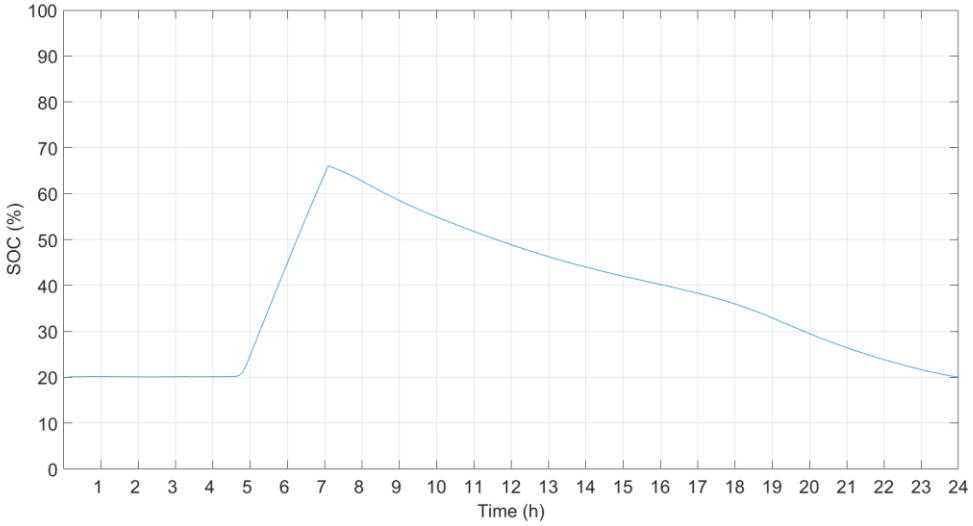

Figure 4.9 Optimal State of charge of the 300-litre tank

Analysis

Both results demonstrated similar charging strategies: starting from midnight, only charge the amount of energy to compensate heat loss to maintain a minimal SOC at 20%. Before 7 am, when the tariff changes, the tank charges at its maximum rate so that it has just enough hot water for the rest of the day (including standing heat loss). If the tank is small in comparison to the hot water demand (100-litre in this case), the tank will be fully charged at 7 am and will later only be charged to match demand. This ensures a maximum use of the cheap night-time tariff and minimizes the operating costs associated with heat loss (because the SOC of the tank has been kept at its minimal value most of the time).

The difference between the minimum operating costs associated with different tank sizes indicates that there is a trade-off between the size of the tank and its corresponding optimal charging profile. Therefore, further optimization is carried out in the next section to determine the size that provides overall minimum operating costs.

4.3.6 Sizing optimization (Brute-force)

With a fixed hot water usage profile, operation optimization produces different optimal operating costs for different tank sizes. In this section, a brute-force optimization approach is used to analyse all tank sizes to determine the global minimum for the overall optimization problem. The results will produce a minimum cost associated with the optimal charging profile (output) based on a given hot water usage profile (input).

Brute-force, also known as exhaustive search, is a straight-forward optimization method which systematically enumerates all possible costs associated with different decision variables values, and then decides which is the optimal solution. Brute-force is a simple algorithm which guarantees to find the minima if it exists. Whilst it suffers from the drawback of long computational time, in this thesis this represents a relatively small problem, as the sizing optimization is only required once for each usage profile. The computational time is therefore not a concern. It is worth mentioning that in the following *section*, an approach is proposed for the estimation of optimal size, so that the range of sizes subject to brute-force searches can be significantly reduced. Alternatively, a gradient descent algorithm, which could potentially reduce the computational time, can be used.

In this brute-force approach, tank size M is the decision variable which is assumed to be limited between 50 and 400-litre. Whilst the size of the domestic hot water tanks available on the market could be very sporadic, in this thesis we define a 5-litre interval of tank sizes to ensure that the resolution is high enough to determine the best possible optimal result. The pseudo code for such optimization can be expressed as follows:

for $M = 50\ to\ 400\ at\ every\ 5$

$calculate\ \min f(EGin)|_M\ using\ fmincon$

end

find the optimal M with minimal value of all $f(EGin)_M$

The sizing optimization results are shown in ***Figure 4.10***. It can be observed that it is a convex cost function where the optimal tank size is 160-litre with an overall minimum operating cost of just over £0.1262/kWh. The corresponding charging profile and SOC with an optimal sized tank are plotted in ***Figure 4.11*** and ***Figure 4.12*** respectively.

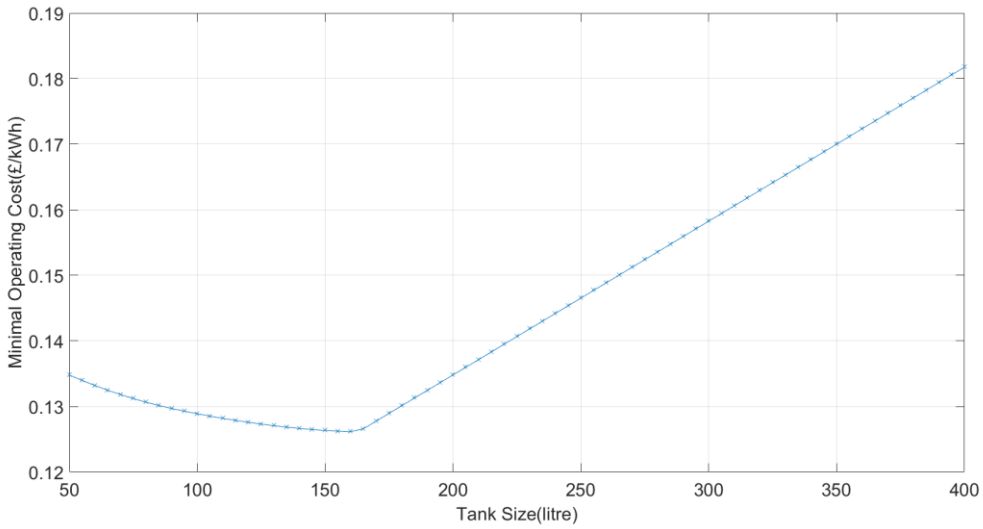

Figure 4.10 Sizing optimization results for a given hot water usage profile

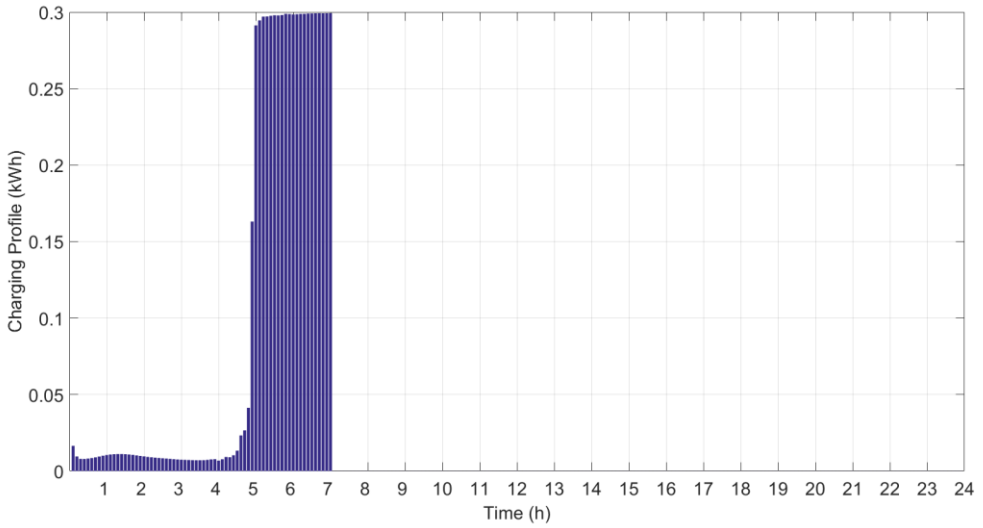

Figure 4.11 Charging profile of the tank with optimal size (160-litre)

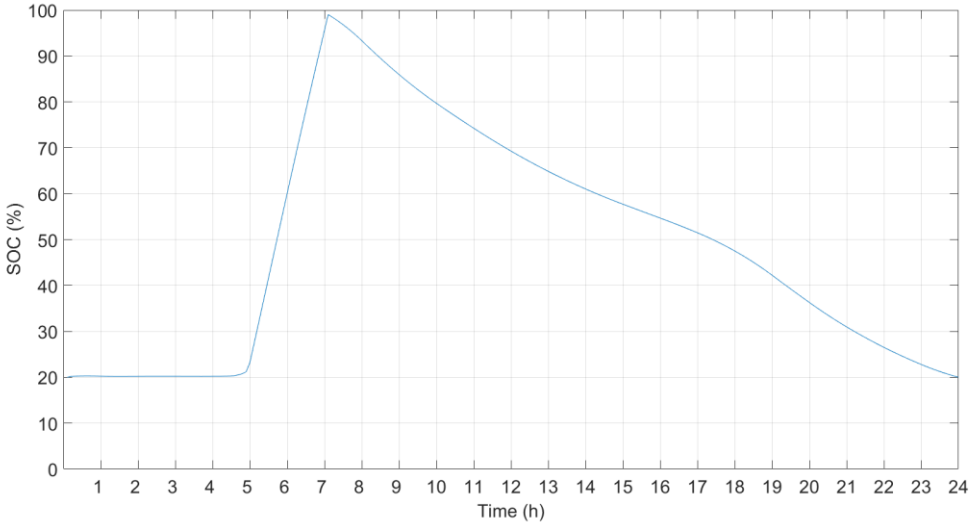

Figure 4.12 State of charge of the tank with optimal size (160-litre)

4.3.7 Discussion of results

The optimal results in the previous section suggest the following scenario: when the tank is sized optimally (160-litre in our case), its SOC reaches 100% just before the tariff increases (7 am in case of the Economy 7 tariff). The tank stores just enough hot water for usage (including heat loss) for the rest of the day so that SOC of the tank reaches 20% by midnight.

If the tank is too small, not enough hot water will be stored for daily use in a single charge before 7 am, and the tank will have to be recharged during the daytime as shown in ***Figure 4.6***. This introduces the extra cost of using the expensive peak tariff (potentially including other additional peak use surcharges such as the DUoS charge). On the other hand, if the tank is too big, the capital cost of the tank and the heat loss associated with the 20% of tank capacity will rise, consequently increasing the daily operating costs.

Given the fact that an optimally sized tank could store enough hot water for the demand after 7 am, including the heat loss, it is possible to work out in reverse an approximate

optimal tank size M_{opt} based on a given hot water demand profile, using the following ***equation***:

$$0.8 \cdot M_{\mathrm{est}} C_{\mathrm{p}} (T_{\mathrm{t}} - T_{\mathrm{a}}) = \sum_{70}^{240} E_{\mathrm{dsout}}(i) + \sum_{70}^{240} E_{\mathrm{sl}}(i) \qquad (4.24)$$

Assuming that the state of charge decreases arithmetically from 100% at 7 am to 20% at midnight, and heat loss is 0.15% of the total thermal storage within the tank for every six minutes, the total heat loss can be calculated as follows:

$$\sum_{70}^{240} E_{\mathrm{sl}}(i) \approx 0.154 \cdot M_{\mathrm{est}} C_{\mathrm{p}} (T_{\mathrm{t}} - T_{\mathrm{a}}) \qquad (4.25)$$

In our case, $\sum_{70}^{240} E_{\mathrm{dsout}}(i)$ is 5.0037 kWh and the estimated optimal tank size M_{est} is 166-litre, which is very close to the optimization result (160-litre). As this is based on arithmetical decrease of the SOC, the actual optimal size could deviate from the estimated size. Therefore, it remains necessary to implement the sizing optimization method. This estimate may, however, narrow down the range of tank size to be searched in the brute-force optimization. Adopting such an approach will prove beneficial in the following section, where a large number of usage profiles must be handled.

It is worth noting that using the heuristic rule described above we can only determine a tank size close to optimum value, and the optimization problem still need to be formulated and solved in order to determine the exact optimal tank size. Furthermore, one of this chapter's objectives is to establish a framework for tank size design, which would consider more constraints and variables in future, such as nonlinear heat loss or time varying tariffs. The formulation of the optimization problem has the capability to handle those uncertainties and variable and is therefore more robust than the heuristic approach.

4.3.8 Sensitivity analysis for heat loss

One uncertainty in this study is the heat loss in the tank model, defined as 0.15% of the total energy stored in the tank for every six minutes (0.1 hour). This section reproduces the sizing optimization results with two different heat loss ratios, 0.1% and 0.2% (±33% of the original value) to show the result's sensitivities to the uncertainties regarding heat loss.

Figure 4.1 shows the 160-litre tank SOC profiles under the same charging profile, but with different heat loss ratios. In 24 hours, three SOCs reach approximately 25, 20 and 15%, with 0.1, 0.15 and 0.2% heat loss ratio respectively.

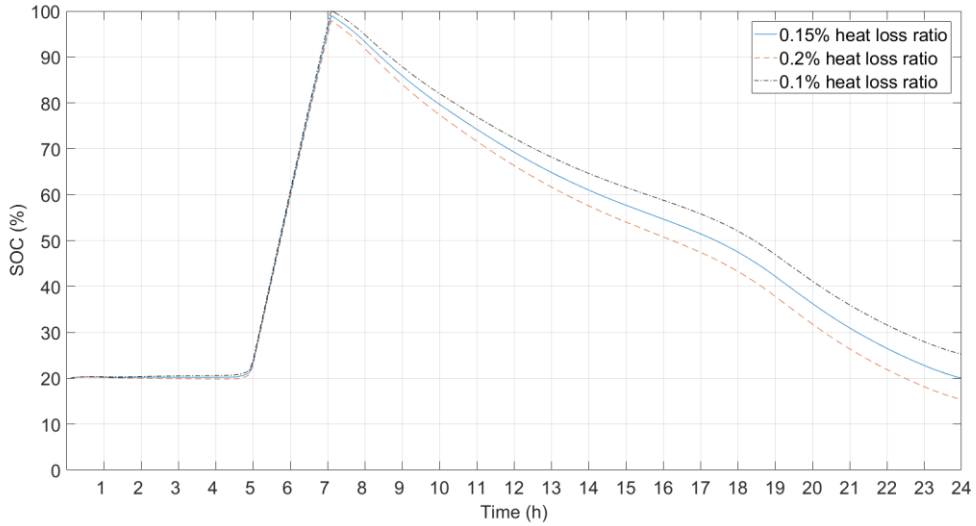

Figure 4.13 160-litre tank SOC profiles with different heat loss ratios

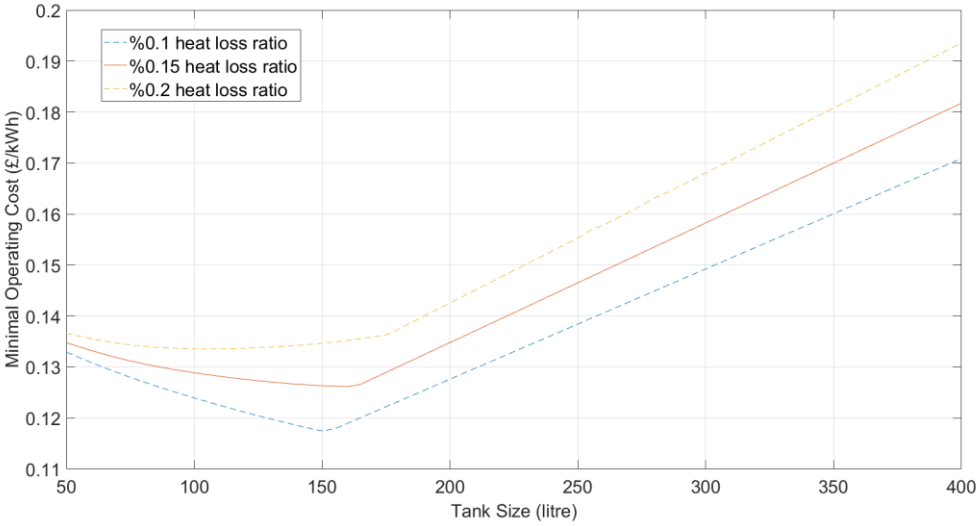

Figure 4.14 Optimal size and operation cost results with different heat loss ratios

Figure 4.14 plots the results of optimal size and operation cost under different heat loss ratios. The figure suggests that the higher the heat loss ratio, the higher optimal tank size and operation costs will be, owing to the reduction in efficiency caused by the extra heat loss. It can be seen from the figure that a 33% change in heat loss ratio will result in a approximately £0.01/kWh change in minimal operation costs. As optimal results are to some extent dependent on the heat loss ratio, future studies would include seeking more precise heat loss models for the optimization problem.

4.4 Case Study with EST Data

The previous section proposed an optimization approach which determines the optimal size of tank with a given hot water usage profile. In this section, a set of real-world data covering a wide range of UK demographics was applied to the optimization problem to provide a more realistic sizing proposal.

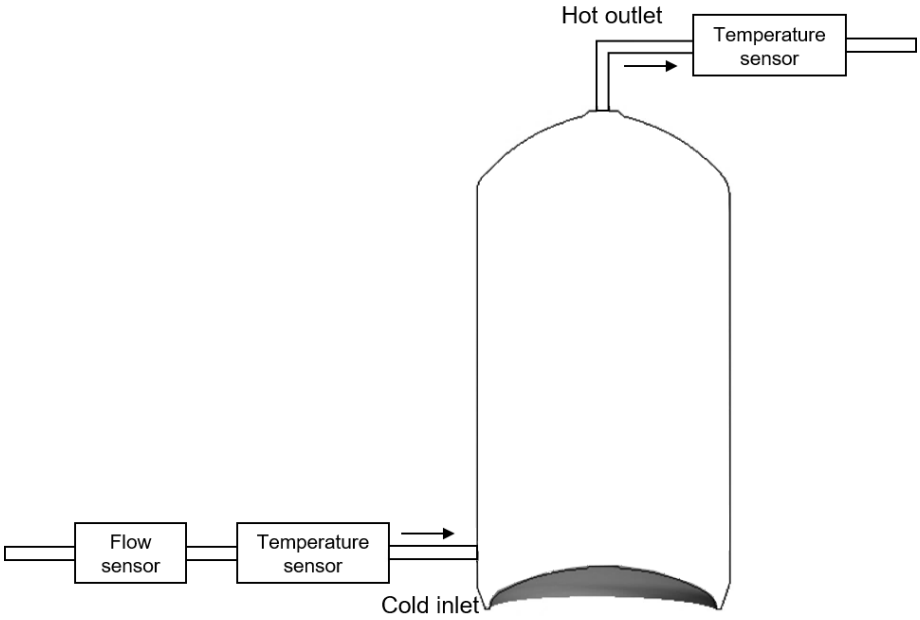

Figure 4.15 Monitoring device installation for boilers in the EST study [145]

4.4.1 EST data

In 2009, the Energy and Saving Trust (EST) conducted a survey of hot water usage in the domestic dwellings across the UK [145]. The researchers installed flow meters and temperature sensors in boilers' inlet and outlet pipes (as shown in ***Figure 4.15***) to monitor volumetric hot water usage as well as the equivalent energy consumption. ***Equation (4.8)*** was used to calculate such hot water energy consumption, where inlet, outlet temperature and flow data were obtained during the experiment.

There were in total 112 households' usage data available from the study, which covered a variety of occupancy features shown in ***Table 4.2***:

Table 4.2 Features and sample size of EST data

House Type					
Flat	Bungalow	Terrace	Semi-detached	Detached	
7 (6%)	11 (10%)	33 (29.5%)	33 (29.5%)	28 (25%)	
Boiler Type					
Regular	Combi-	Unidentified			
68 (61%)	39 (35%)	5 (4%)			
Region					
Scotland	Midlands	North England	South England		
19 (17%)	17 (15%)	31 (28%)	45 (40%)		
Number of adults					
One	Two	Three	Four	Five	
14 (12.5%)	68 (61%)	18 (16%)	9 (8%)	3 (2.5%)	
Number of children					
None	One	Two	Three		
67 (60%)	14 (12%)	21 (19%)	10 (9%)		
Number of residents					
One	Two	Three	Four	Five	Six and more
11 (10%)	38 (34%)	18 (16%)	29 (26%)	13 (11%)	3 (3%)
Number of bedrooms					
Zero	One	Two	Three	Four	Five
36 (32%)	5 (4.5%)	15 (13.5%)	46 (41%)	9 (8%)	1 (1%)

For each household, the study provided a 24-hour hot water usage profile at one-hour resolution, where the hourly consumption was represented by the average value during that hour throughout the logging period (12 months). All 112 profiles were linearly interpolated into tenth-of-an-hour resolution as shown in ***Figure 4.16***, and these figures could then by applied as input for the sizing optimization method formulated in the previous section.

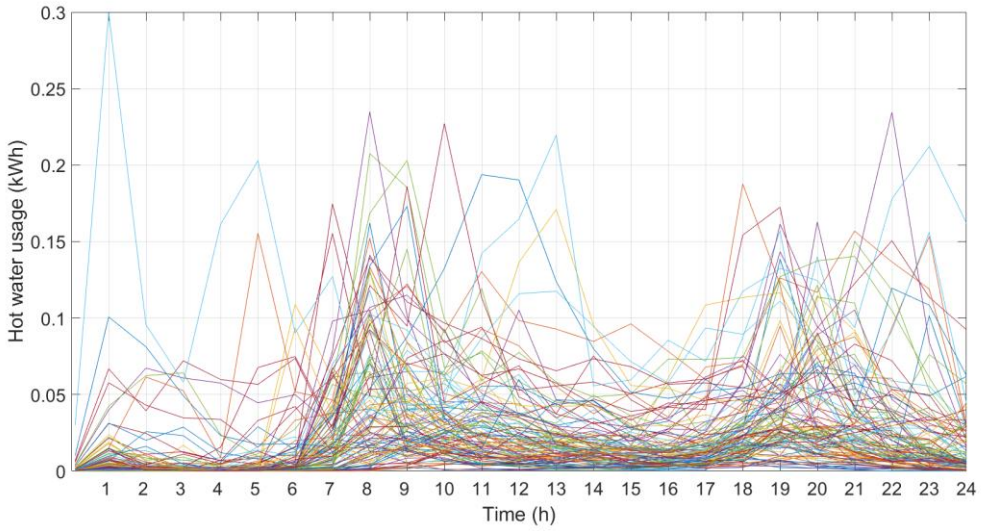

Figure 4.16 112 hot water usage profiles in the EST study

It is worth noting that the purpose of sizing the tank is to explore the economic benefits over the course of the tank's servicing period (normally over 20 years). These profiles, which are the average values over a 12-months' period, should therefore be appropriate for use as input, even though they may not reflect instantaneous hot water demand in real-time. A similar approach was used to by Granado et al. [146] to evaluate the benefit of domestic battery storage systems, with only hourly average electricity consumption data in each season used as input.

4.4.2 Optimal size based on EST data

In this subsection, the hot water usage profiles described in the previous section are applied to the sizing optimization approach proposed in S*ection 4.3* in order to determine the most beneficial tank size for users in the UK.

As described in *Section 4.3.8*, optimal size could be roughly estimated before running the sizing optimization program, thus avoiding the need to "brute-force" search all sizes. The following pseudo-code describes the search method for the EST profiles:

for each usage profile

estimate the approximate optimal size

round it to the nearest multiple of 5 (M_{est})

for $M = M_{\mathrm{est}} - 25\ to\ M_{\mathrm{est}} + 25\ at\ every\ 5$

calculate $min\ f(EGin)|_M$ *from the operation optimization*

end

end

find the optimal M *with minimal value of all* $f(EGin)_M$

Instead of searching all sizes, the code above only searches sizes surround (±25 litres) the estimated sizes, and yet still guarantees to find global minima (given that the cost function is convex). The distribution of the optimal sizes and operation costs associated with the EST profiles are illustrated in the histogram plots in ***Figure 4.17*** and ***Figure 4.18*** respectively. It should be noted that the size of tank on the market may be highly variable. It is therefore assumed that tank size is available between 50 and 400-litre at intervals of 50 litres, with the calculated optimal size rounded to the nearest available size. Similarly,

calculated optimal costs are rounded to the nearest multiple of £0.005 so as to show a more representable distribution.

The histogram in ***Figure 4.17*** indicates that the most beneficial tank size in the UK, based on the usage profiles provided by the EST study, is 100-litre. The majority of optimal tank sizes are between 50 and 200-litre (82 out of 112). Similarly, it can be seen from ***Figure 4.18*** that most optimal costs are £0.13/kWh.

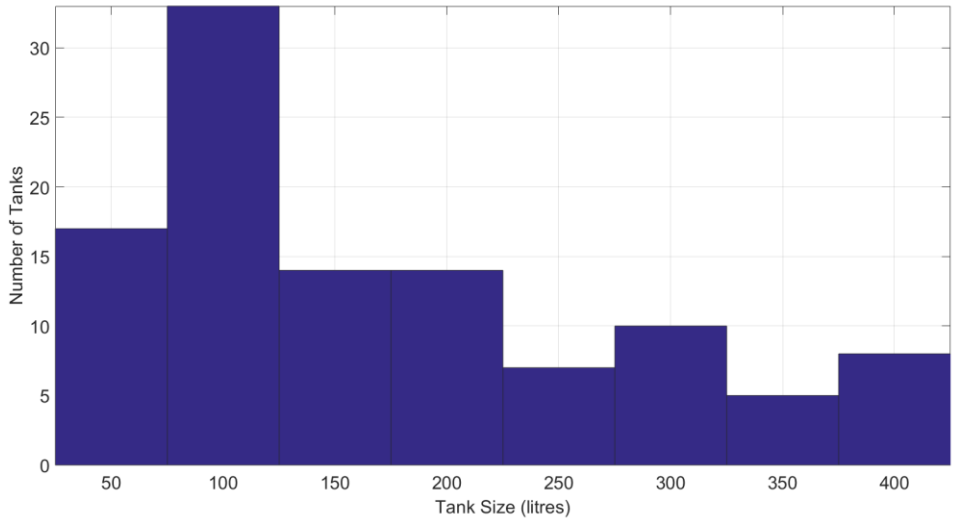

Figure 4.17 Distribution of optimal sizes based on EST profiles

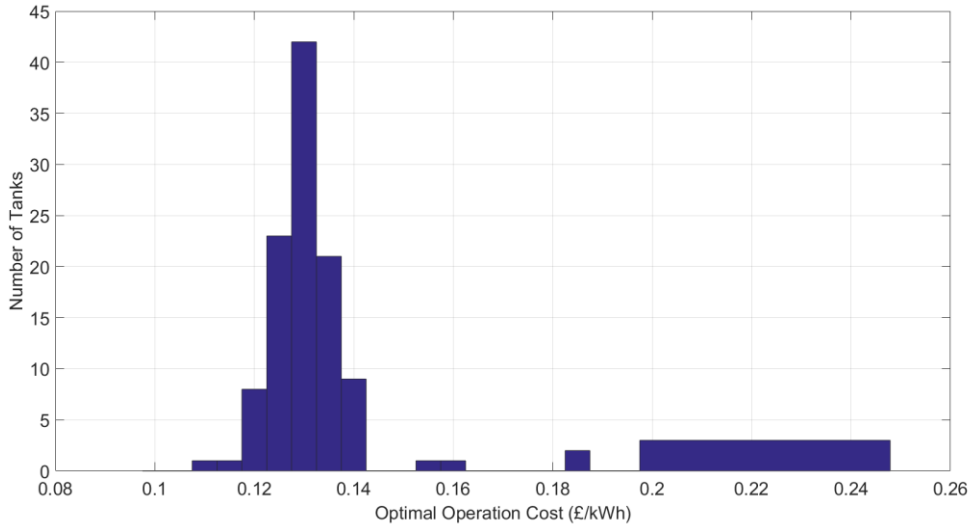

Figure 4.18 Distribution of optimal costs associated with EST profiles

Based on the hot water usage from the EST study, this section determined the tank size that would bring the greatest economic benefit to dwellings in the UK. The following section extends the research further to explore the patterns of hot water usage in the UK and investigate whether there is any correlation between these patterns and household features such as the number of occupants. The results will help to further identify the appropriate household consumption model to be used in the distribution network simulation in the next chapter.

4.5 Hot water usage patterns

This section identifies four hot water usage patterns from the 112 profiles in the EST data. In *Section 4.5.1,* a clustering approach using the Dirichlet Process Mixture Model (DPMM) is introduced. This method is then used in *Section 4.5.2* to cluster the 112 profiles into four different groups, each representing a hot water usage pattern. Finally, the correlation between each usage pattern and house features is investigated in *Section 4.5.3*.

4.5.1 Selection of the clustering technique

A clustering technique usually involves the use of unsupervised machine learning algorithms that can divide a data set into sub-groups without a priori information such as pre-defined classes or annotated examples. The objective is to group elements that are similar and to ensure that the elements of each cluster are different from the ones in other clusters. In this case, the clustering algorithm should be able to detect similar hot water usage profiles in the EST data and group them together.

The core techniques used in the clustering algorithms are the approaches used to model the data. The literature provides a number of different types of models, including distance-

based, centroid models (K-means), distribution models (such as Gaussian Mixture Model) which assumes a probabilistic distribution of the model, and connectivity models (hierarchical clustering) which is based on distance connectivity.

Most of the clustering algorithms mentioned above must declare the total number of clusters before performing analysis. In reality, though, the number of clusters is difficult to ascertain, given the lack of prior knowledge of hot water usage patterns. An alternative approach is therefore to use Dirichlet Process Mixture Models (DPMM), which do not require the declaration of number of clusters prior to computation.

DPMM is a non-parametric Bayesian model with potentially infinite number of parameters. Using such a model provides great flexibility and the robustness that is required to handle the uncertainty presented by the data. Furthermore, DPMM allows us to dynamically estimate the number of clusters and then to adapt this estimate if further data are analysed. Previous research has used DPMM to solve a variety of clustering tasks. In [147], Granell et al. used DPMM to cluster electricity load profiles in both residential and commercial sectors. Given the similar nature of the electricity load and hot water usage profiles, the same method presented in [147] was used in this chapter to identify hot water usage patterns in the UK.

4.5.2 Clustering results

The clustering of hot water usage profiles using the DPMM approach was carried out with the collaboration of Ramon Granell, a colleague at the Energy and Power Group who had previously conducted similar clustering tasks on electricity load profiles in [147]. Ramon implemented the algorithm and the contribution of this thesis is in the field of pre- and post-data analysis.

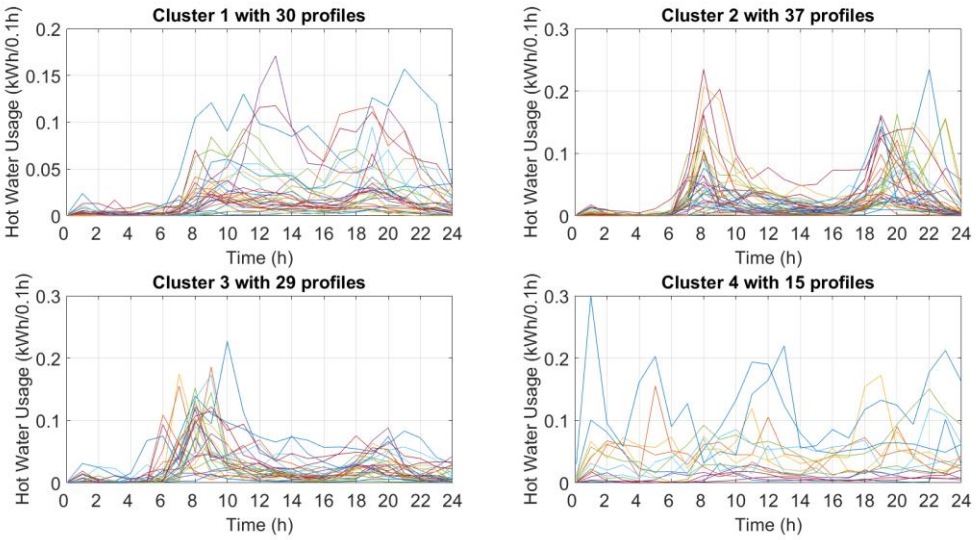

Figure 4.19 Clustering results of hot water usage profiles from the EST study

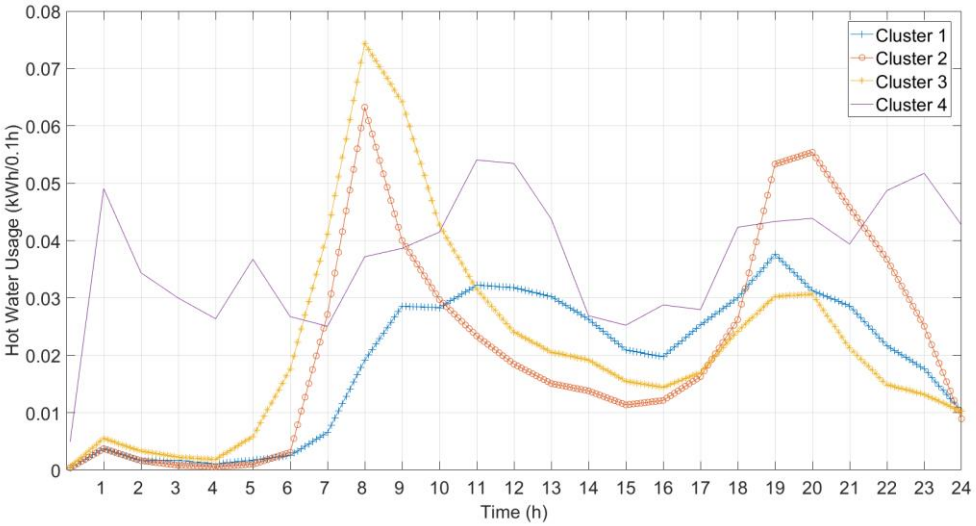

Figure 4.20 Centroids of hot water usage clusters

There were a total four clusters determined from the DPMM algorithm, with 30, 37, 29 and 15 profiles in Cluster 1, 2,3 and 4 respectively. It should be noted that one profile was identified as an outlier (as itself was identified as a single profile cluster) and was therefore excluded from the sample pool. ***Figure 4.19*** plots all the profiles by clusters, and it can be observed with a degree of consistency among the profiles in each cluster. To

further illustrate the difference among the various patterns, ***Figure 4.20*** shows the centroid (average value) profiles for each cluster, capturing the following features:

- The centroid in Cluster 1, 2 and 3 show limited hot water usage until 5am, after which the usage increases.
- The centroid in Cluster 1 has a relatively flat hot water usage profile during the day.
- The centroid in Cluster 2 shows two usage peaks during the day; one at around 8 am, and the other between 7 and 8 pm. The night-time peak is slightly lower than the one in the morning, but with a longer duration.
- The centroid in Cluster 3 also shows two usage peaks at same time as those in Cluster 2. However, night-time peak is significantly lower than the morning one.
- The centroid in Cluster 4 can be considered as an outlier group, given that the total number of the profiles is only a small fraction of the overall sampling pool and usage behaviour varies significantly among the different profiles within the cluster.

Analysis therefore leads us to conclude that each hot water demand pattern displays different features. The next task is to determine whether there are any linkages between hot water usage patterns and other user features (such as daily hot water use and number of residents).

4.5.3 Indication and correlation

Based on the clustering results and occupancy information in ***Table 4.2***, this section performs a correlation study by analysing feature distributions within each cluster. The features presented in this section are daily hot water energy consumption, number of

residents and number of bedrooms. The distributions of the remaining features in ***Table 4.2*** are provided in ***Appendix 4.1***.

The correlation of daily hot water consumption was first analysed because it is directly related to optimal tank size as indicated in *Section 4.3.8*. It is desirable to explore whether optimal tank size distributes differently in each usage pattern (cluster). ***Figure 4.21*** shows the boxplot of daily hot water energy consumption for each cluster, where the central red line indicates the median, the box represents 25th and 75th percentiles, the top and bottom whiskers represent a +1.5 and -1.5 interquartile range respectively, and the red '+' indicates an outlier.

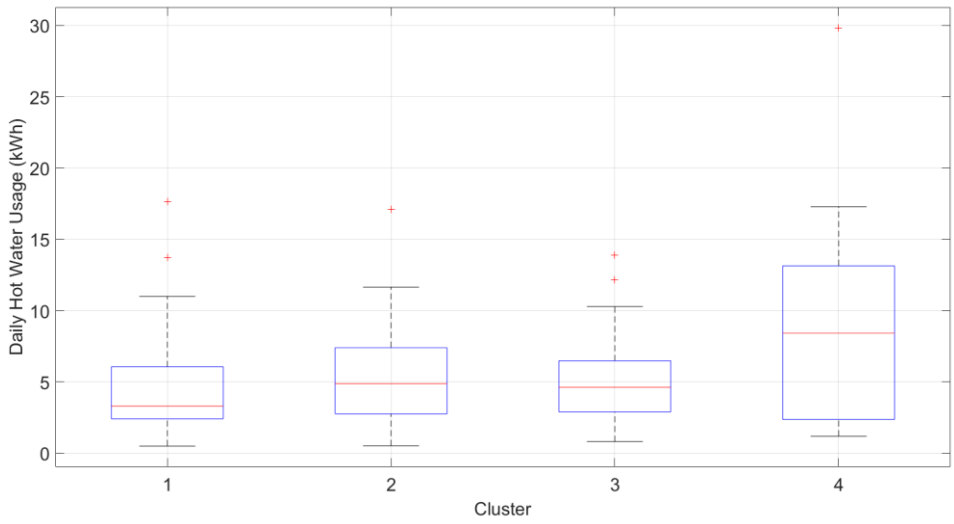

Figure 4.21 Box plot of total daily hot water usage (in kWh) for each cluster

It can be seen from the boxplot that Cluster 1, 2 and 3 have a very similar distribution of daily hot water usage (with majority of usage slightly under 5 kWh). Although Cluster 4 shows a higher value for consumption distribution, it can be excluded from the analysis because it is an outlier group, as indicated in the previous section. The distributions of optimal tank size for each cluster are plotted in ***Figure 4.22***. The results suggest that the most beneficial tank size for each hot water usage pattern are the same as for the whole

sampling pool (100-litre) as shown in *Section 4.4* (except for Cluster 3, where the number of 100-litre tank is lower than 150-litre by 1).

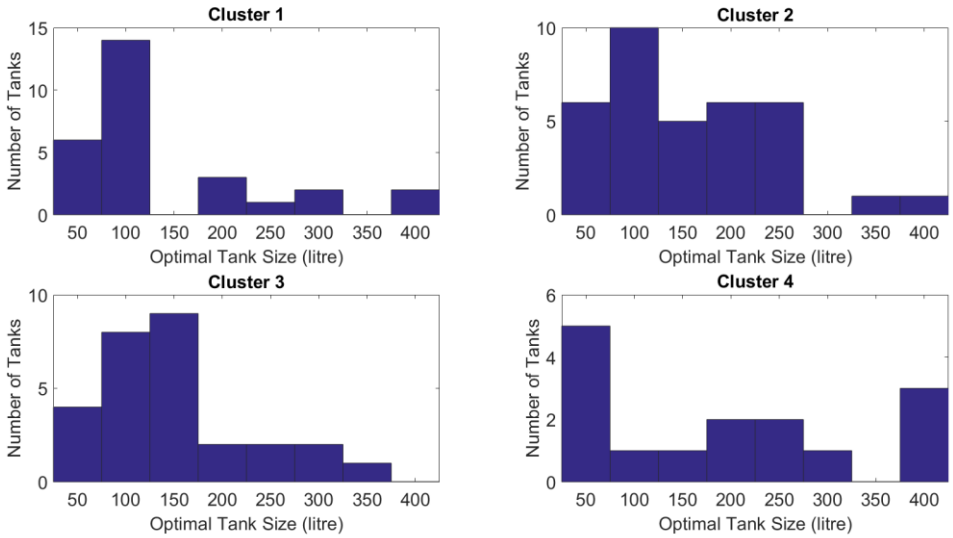

Figure 4.22 Distributions of optimal tank sizes for each cluster

Unlike daily water usage, which is a continuous variable, the number of residents and bedrooms are categorical parameters. The normalized (to percentage) distributions of these two parameters are therefore represented by the stacked histograms in ***Figure 4.23*** and ***Figure 4.24***. One observation from the two figures is that houses of 4 to 5 bedrooms and a corresponding number of residents form a slightly higher proportion (56% and 62% respectively) in Cluster 2, which shows two equal usage peaks in the morning and at night. At the same time, though, a higher proportion of houses of 5 to 7 bedrooms (and a corresponding number of residents) are observed in Cluster 1 and 3 in comparison to Cluster 1. It is therefore difficult to draw any conclusion regarding a direct link between the number of bedrooms and residents and different hot water usage patterns (clusters).

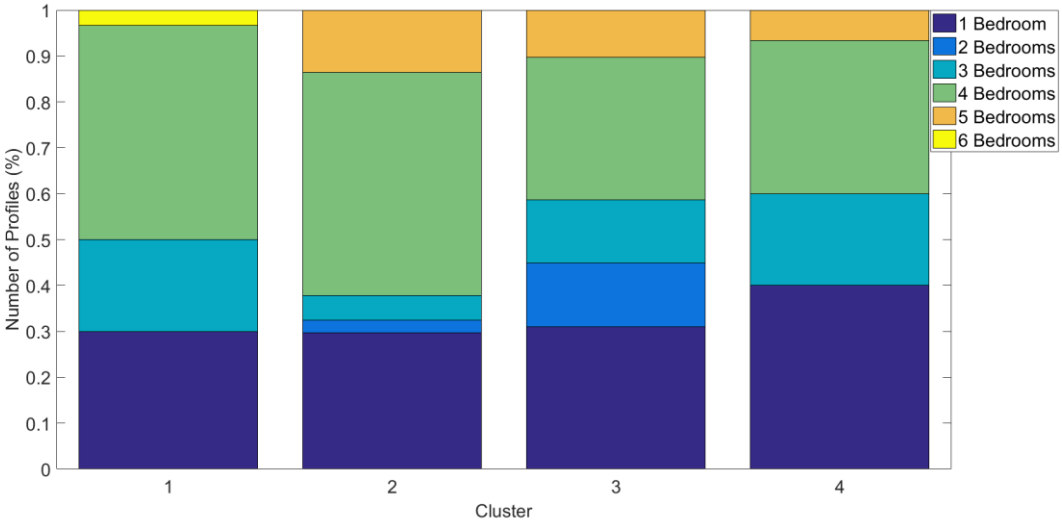

Figure 4.23 Distributions of number of residents in each cluster

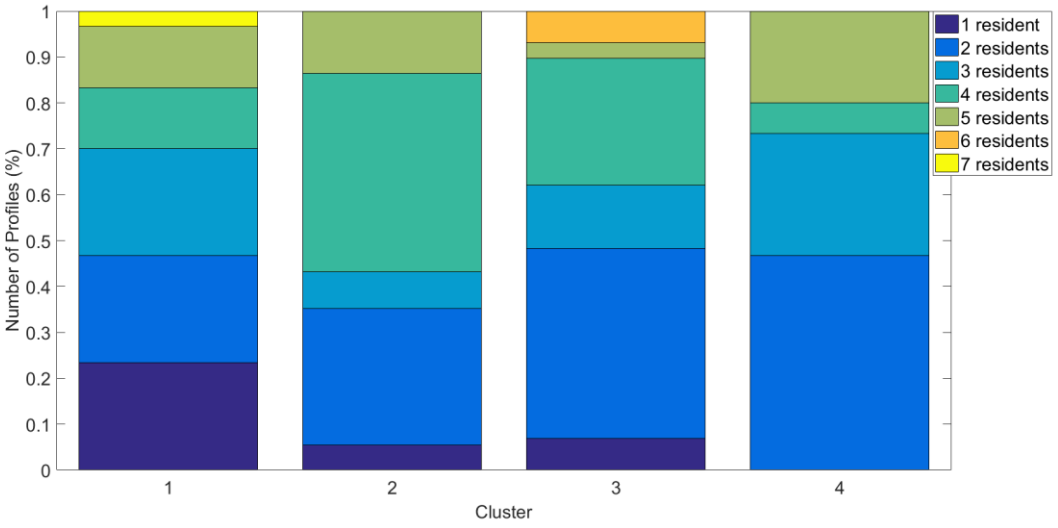

Figure 4.24 Distributions of number of bedrooms in each cluster

From the results above, it can be concluded that regardless of hot water usage patterns, the most advantageous tank size is 100-litre. Furthermore, occupancy features (i.e. number of residents or bedrooms) do not show a significant correlation with the pattern of hot water usages.

4.6 Summary

This chapter addressed the following questions: *"1. Is there a way to determine the optimal tank size to provide customers with greater economic benefits, given the pattern of their hot water usage? 2. What are the typical patterns of hot water usage and the most common optimal tank size for UK consumers?"*. The first questions were answered by formulating and solving a sizing optimization problem based on real-world hot water usage data from a EST study, whereas the second questions were answered by analysing the DPMM clustering results of the EST data.

This Chapter began by proposing an adapted energy node model which can be used for modelling different energy storage systems in various scenarios. This model was further characterized specifically for EHWT studies so that it could be used to formulate the constraints in the sizing optimization problem, which consists of two-stage optimizations; operation optimization and size optimization. The problem was formulated in such a way that, given a hot water usage profile (in kWh unit) under the Economy 7 tariff scheme, the optimization will determine optimal tank size to ensure minimum energy costs per kWh of hot water service. It was discovered that the optimal tank size would store just enough energy for hot water consumption (including heat loss) after 7 am. In such a case, the tank will not operate during the day, using expensive electricity and will not be subject to additional capital costs due to oversizing.

To provide more realistic sizing results, real-world hot water usage data from a EST study which covers wide range of occupancy features was used for the case study for sizing optimization. The results revealed that 100-litre is the most common optimal tank size.

This chapter also investigated whether there is any link between optimal tank size and different hot water usage patterns. By applying a DPMM clustering technique, four usage group were discovered from the profile pool. However, data analysis showed that 100-litre

is the prevailing optimal tank size for all groups (with the exception of the fourth group which is considered as an outlier group). Furthermore, there is no strong indication of any correlation between different usage patterns and occupancy features.

In the next chapter, we shall explore the potential DSM capacity of the EHWT in the LV network by means of networking simulation. The outcome of this chapter thus provides guidelines on the modelling of network components such as tank size and hot water usage profile.

Chapter 5. Impact of Electric Hot Water Tanks on LV Distribution Network

5.1 Introduction

The previous two chapters have investigated how individual electric hot water tank can be optimally sized and how the algorithms operating within it can perceive network stress without an external communication network. This chapter builds on these steps by endowing the tanks with the ability to decide when best to switch on, thus allowing us to address the question: "*To what extent can intelligent EHWTs be used to alleviate voltage and thermal (current) problems caused by excessive PV generation?*".

To represent realistic scenarios for the purpose of the study, two real UK LV distribution networks [148] were used for impact assessment. In *Section 5.2*, the physical network layout was built up in a power flow simulation platform, OpenDSS. It is, however, designed specifically for power flow calculation and is not flexible enough to implement complex algorithms or handle data processing. MATLAB was therefore used for the remaining part of the assessment, including the implementation of the EHWT control algorithm, the profile generation, and the pre- and post-simulation data processing. *Section 5.3* explains how the different demand and PV generation profiles are generated in MATLAB and used as input to for the power flow simulation, and finally the control strategy within each EHWT is discussed in *Section 5.4*.

Owing to variations and uncertainties that surround user demand and PV generation profiles, one-off simulation results alone are insufficient to reach any solid conclusions. A Monte-Carlo simulation was therefore carried out in *Section 5.5* to assess the impact of different EHWT control scenarios including: no EHWT at all, Economy 7 control of the EWHT, instant heating control and intelligent control. In the last section, it is shown that

implementing an intelligent control strategy within EHWTs allowed for a 50% increase in PV penetration before distribution network voltage limits were breached.

5.2 Framework of Impact Analysis

To understand the impact of EHWTs on the LV network under the penetration of residential PV systems, it is essential to stablish frameworks to serve as a basis for simulation and analysis. This section establishes such structures for both the simulation platform and the subsequent analytical processes.

5.2.1 Framework for simulation platform

In *Section 2.6*, the bottom-up approach was proposed for network simulation for impact analysis. The framework of such an approach consists of two key components: 1) the household demand model and 2) the LV network model (which aggregates all households).

At the network level, the power flow software, OpenDSS, is used to build the physical structure of the LV distribution network, including feeder transformers, distribution cables and connection points for households. OpenDSS is a script-based simulation tool designed primarily for power distribution systems, and it can be used for the RMS steady-state analysis commonly performed for utility distribution systems [149]. Although OpenDSS is not flexible for either data processing or handling complex control algorithms, it does have a server which provides a communication interface with other software tools such as Matlab or Python. Therefore, at a household level, given the variable occupancy features and demand profiles, Matlab was used for the following tasks: creation of EHWT models, generations of hot water and household energy demand profiles, implementation of control algorithms and analysis of pre- and post-simulation data.

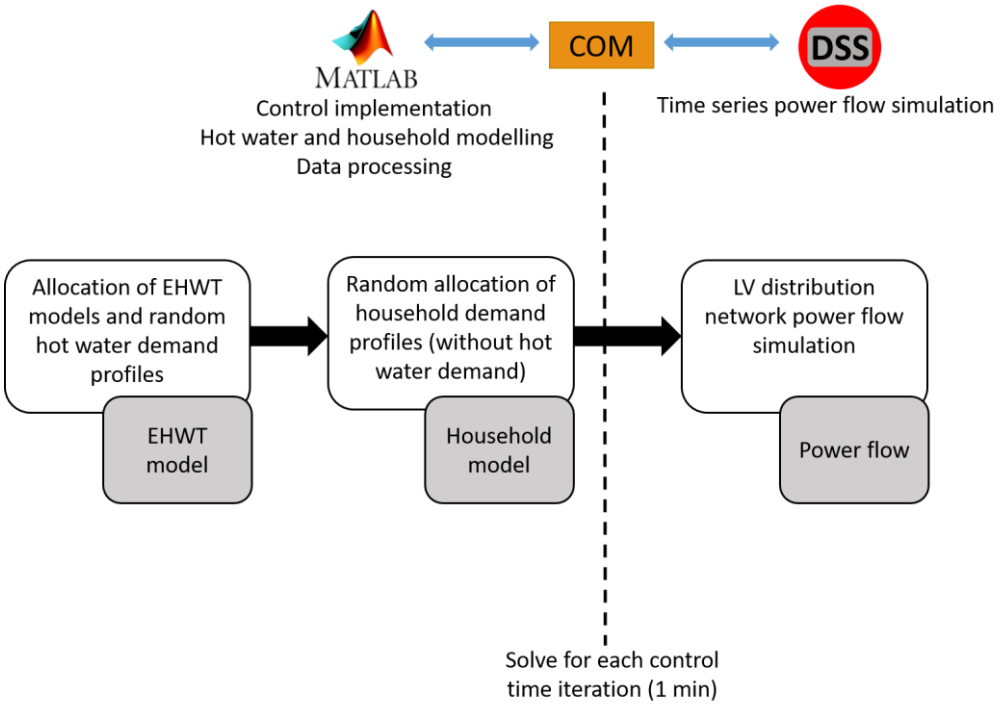

Figure 5.1 Framework for the simulation using Matlab and OpenDSS

The framework for the simulation package is illustrated in ***Figure 5.1***, with the tasks undertaken by Matlab and OpenDSS described above. The selection of load profiles and implementation of control strategies are further explained in detail in *Sections 5.3* and *5.4* respectively.

5.2.2 Methodology for probabilistic analysis

The Monte-Carlo method is a computational algorithm which uses repeated random sampling inputs to obtain numerical results, with the core idea of using randomness to produce a more robust conclusion. This method is commonly used in the field of power system research to tackle uncertainties within parameters [102], [105], [150]. In our case, there is a need to account for uncertainties related to different occupancy features (which affect demand profiles), household locations and panel sizes. For this reason, the Monte-Carlo simulation needs to repeatedly change these inputs to produce more conclusive results.

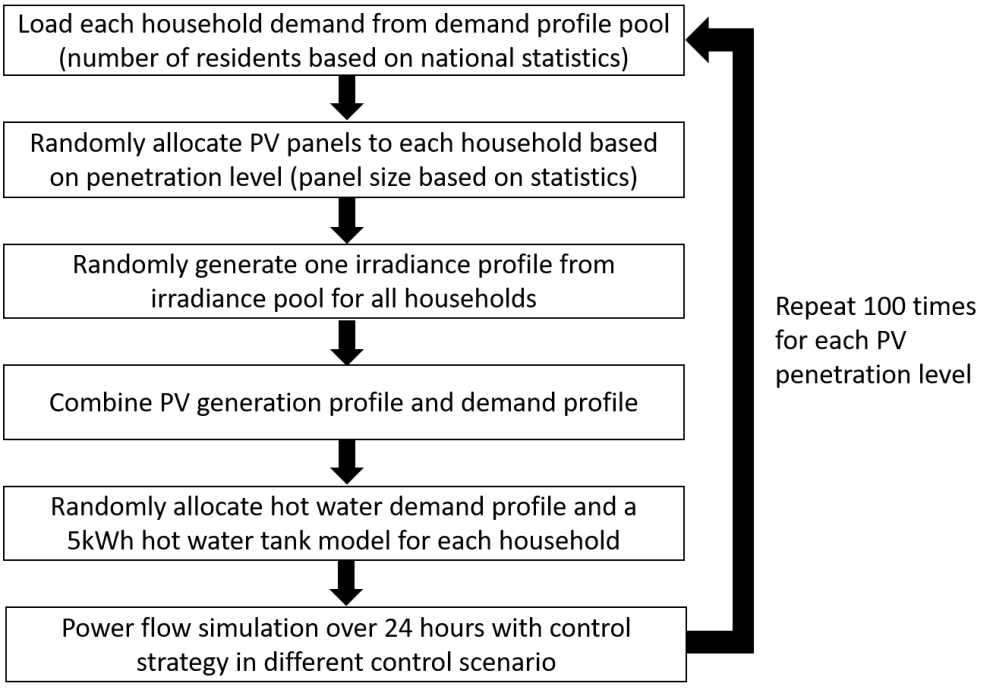

Figure 5.2 Flow chart for the Monte-Carlo process for network simulation

The flow chart for the Monte-Carlo simulation is shown in Figure 5.2 and the main steps are described in further detail, as follows:

1. Each household is randomly allocated a demand profile from a sampling pool. It should be noted that the demand profile pool has already taken into account a realistic distribution of the number of residents according to the data provided by the Office for National Statistics in 2015 [151]. The selection of the sample pool is further described in *Section 5.3.1*.
2. A PV panel is randomly allocated to each household, given the probability of PV penetration level set by the scenario and the realistic distribution of panel size according to the data provided by Ofgem in 2015 [152] (if there is no PV in the household, then the size is 0 m^2). In addition to a irradiance profile which

was randomly generated from a sampling pool, a PV generation profile can be calculated for each household. This part is further explained in *Section 5.3.2*.

3. The profiles generated in Step 1 and 2 are added up to produce an overall household demand profile.
4. Hot water demand profiles and EHWT model were considered separately from the household demand profiles and model. The hot water demand profile is drawn from a sample pool, whereas an EHWT energy model (as described in *Section 4.2.2*) is connected to the network through the same point of common connection as the household model. These steps are further explained in *Sections 5.3.4 and 5.3.5*.
5. Once all the profiles were allocated, household and EHWT models were connected to the network through nodes, and a 24-hour time series power flow with one-minute resolution was performed in OpenDSS using the proposed control strategy (introduced in *Section 5.4*). The results are then exported to Matlab for data analysis.
6. Steps 1 to 5 are repeated 100 times at each level of PV penetration, and PV penetrations are simulated from 0 to 100%, with a 10% interval.

Following the Steps 1 to 6, a Monte-Carlo simulation can be carried out to study the impact of different EHWT control strategies at different levels of PV penetration. All the power data, including active power, voltage and current across the LV network is exported to Matlab for results analysis. The following section introduces the parameters used for impact assessment.

5.2.3 Metrics for impact assessment

There are two operating limits that impact the operation of the LV distribution network: voltage and thermal (current) limits. These are used as the basis for the metrics to assess the performance of the controller. Similar metrics have been used in various researches [102], [105], [148], [150] to evaluate the benefits of low carbon technologies such as electric vehicles, heat pumps and solar PV panels. In addition, a cost metric is applied to evaluate the economic benefits of EHWTs.

Percentage of households with voltage problems: In this metric, RMS voltages at the household connection points are recorded and evaluated against the power quality requirements set out by European Standard EN 50160 [153]. The ratio of number of households with voltage breaching this standard to the total number of household is defined as the metric.

EN 50160 specifies that customer's voltage must be between 0.9 and 1.1 p.u. (230 V nominal voltage in the UK) for more than 95% of the time, and never below 0.85 or above 1.1 p.u. [153]. To make it even more compliant with UK regulations [41], the permissible voltage range was narrowed down to between 0.94 and 1.1 p.u. Furthermore, the resolution of the sampling time of the voltage data must be 10-minute, and so data provided in other formats must be converted to a 10-minute average value for the purpose of evaluation.

Loading level: This metric is defined as the ratio of the maximum current delivered by the first segment of the feeder network (where it connects to the upstream network) to the rated current of the cable (ampacity). Since a three-phase network is modelled, the average value of three individual phase loading levels is used to calculate the final metric. This provides information on network capacity of the devices studies (EHWT and PV panels, in our case).

Cost of energy for heating the tank: This metric is calculated as the total electricity price paid by the user divided by the total energy used to heat up the tank, assuming it is under Economy 7 tariff scheme, which is £0.075/kWh between midnight to 7 am and £0.15/kWh from 7 am to midnight (see *Section 4.3.1* for details). If the energy comes from surplus PV generation which would otherwise be spilled, it will be treated as 'free' electricity. This metric provides an insight into the economic benefits provided by the devices under study.

5.3 Household Level Profiles

This section introduces the methodology for modelling and validation of the household level profiles needed for network simulation, including household demand (without electric heating), PV generation and hot water demand profiles. It is worth noting that all profiles are simulated with 1-minute resolution so that the thermal time-scale of the network response can be fully understood.

5.3.1 Household demand profiles

Elexon electricity load profiles [154] have been widely adopted in the past for modelling domestic household demand. They are, however, only provided in a half-hourly resolution, which is not sufficient to investigate the dynamics of the network. For this study, demand profiles with one-minute resolution were created using a modified CREST tool developed by researchers at Loughborough University [155].

CREST tool is an open-source, VBA based application that creates computational profiles for residential load based on the realistic behaviour of British domestic electricity consumers [156]. This tool uses the stochastic method to model domestic occupancy and

usage of appliances to produce 24-hour household demand profiles. The results were validated and showed consistency with real-world data.

The model requires number of residents, month and day of week (weekday or weekend) as inputs. To ensure that a realistic demand profile is selected for network simulation, the following specifications were determined to create the sample pool made up of 1000 demand profiles:

Number of residents

The number of residents is an important feature to specify because it determines the number of active residents throughout the day and consequently affects electricity consumption.

To mimic the real distribution of the number of residents in the UK, 1000 demand profiles were created with a proportional number of residents based on the official report by the Office for National Statistics (UK) in 2015 [157]: 29% (290), 35% (350), 16% (160) and 20% (200) for households with one, two, three and four or more residents, respectively, as shown in ***Figure 5.3***. This approach ensures that the profile represents real-world distribution if it is randomly drawn from the sample pool.

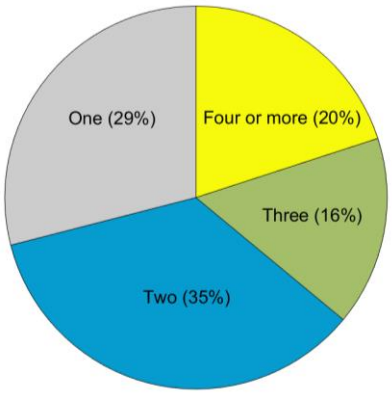

Figure 5.3 Percentage of UK households by household size (2015) [157]

Day and month

Household electricity demand is affected by season as well as the day of week (weekday or weekend). The CREST tool took these two factors into consideration, ensuring that the month and day of the week were specified before simulation. In this chapter, given that our main focus lies in investigating voltage problem associated with solar PV generation, July was chosen for simulation, as it has the longest solar irradiance time and strongest irradiance. As regards day of the week, weekday is chosen because it has lower daytime power consumption for domestic household compared to weekday [158]. In this case the network would be more stressed for not being able to absorb surplus generation.

Appliances

The last factor to specify before generating demand profiles is the appliances to be included in simulation. The original CREST tool covers models based on UK statistics on appliance ownership, where resistive load is considered with unity power factor, and electronic and cold appliances are assigned with 0.9 and 0.8 lagging power factor respectively. The range of appliances, however, includes electrical appliances (EHWTs and electric shower devices) associated with water heating. The EHWT model and the household model are two separate objects in the framework described in *Section 5.2.1*, EHWT and electric shower models are therefore removed from appliance ownership data to produce a demand profile which excludes hot water heating demand. A method to provide hot water demand profiles is introduced later in *Section 5.3.4*.

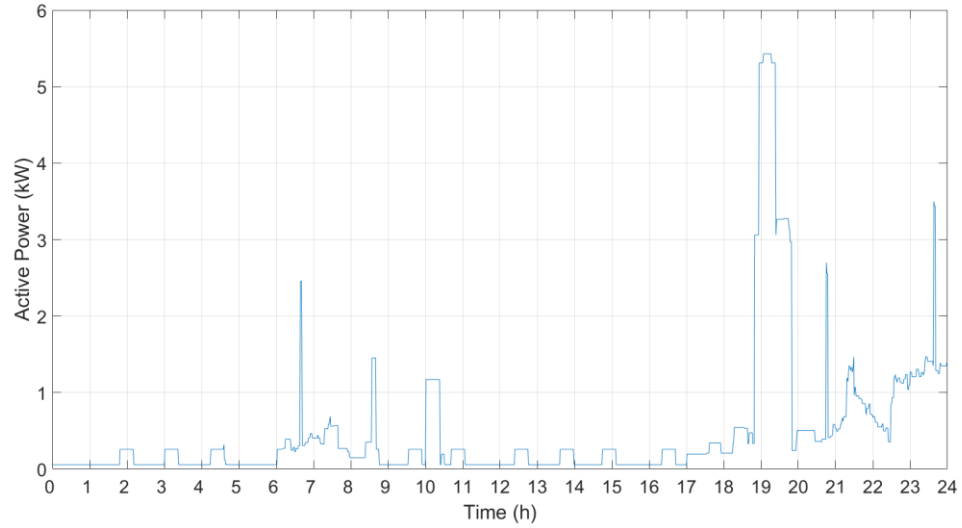

Figure 5.4 An example of load profile (without water heating devices) produced by CREST tool

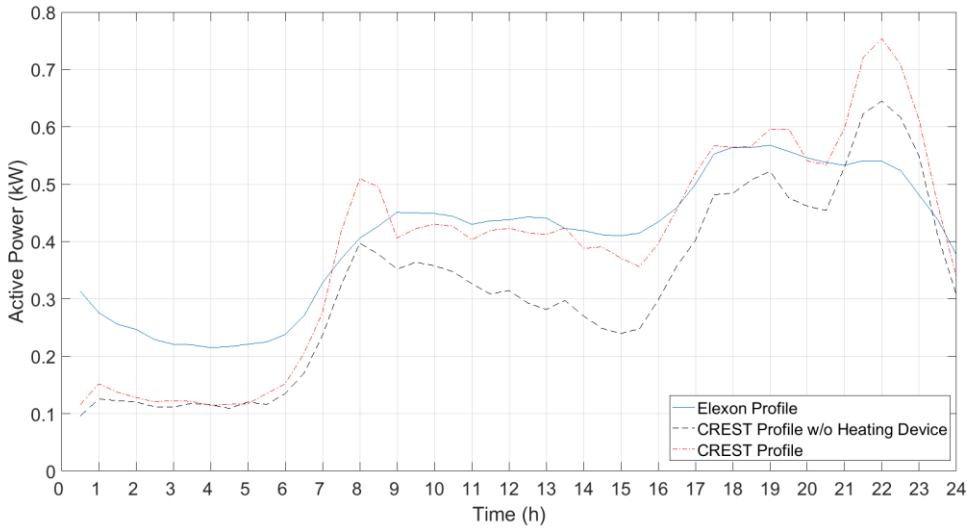

Figure 5.5 A comparison of averaged CREST profile and Elexon profile

Following the specifications above, it is possible to provide realistic load profiles, with an example showing in ***Figure 5.4***. The average values of the 1000 CREST profiles each with and without heating devices are plotted in ***Figure 5.5***, along with an Elexon Class 1 summer weekday profile. It is worth noting that CREST profile is slightly lower than the Elexon profile owing to the absence of water heating devices in the appliance ownership

model. In the power flow simulation, the overall power factor for each demand profile was set at 0.93, which represents the average value across all appliances.

5.3.2 PV generation profiles

PV generation is determined by ***Equation (5.1)***, where A is the panel size in kWp, H is the irradiance on the panel in kW/m^2 and η is the scaling factor. This section explains how to produce realistic PV generation profiles based on these parameters.

$$P = A \cdot H/\eta \quad \textbf{(5.1)}$$

Panel size

A recent report [159] from Ofgem gives a breakdown of accredited installations (PV, wind and other types of renewable energy) in the UK under the Feed-in Tariff scheme in 2016. Data related to domestic PV installations (≤ 4 kWp) was retrieved from the report in order to infer a realistic distribution of PV panel sizes. Panel size was rounded to the nearest 0.5 kWp, and the following distribution shown in ***Figure 5.6***.

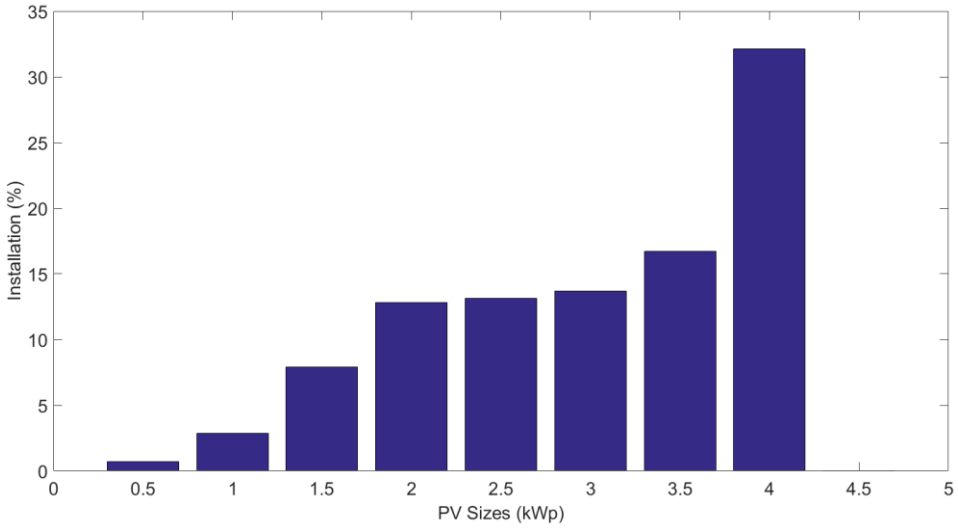

Figure 5.6 Distribution of the domestic PV sizes in the UK [159]

Based on the penetration level of PV installations in the LV network, a fixed number of PV panels will be randomly assigned to households within the network, and the size of each panel will be determined based on the probabilistic distribution provided above. For instance, the panel has a 32% chance to be 4 kWp.

Irradiance and efficiency

The CREST tool described in the previous section also includes an integrated model of domestic photovoltaic system output, capable of producing realistic solar irradiance profiles. This tool can generate data on clear sky beam radiation at surface (horizontal) and total radiation on panel based on information about geographical location, month of the year and panel installation (such as angle) specification. The model also simulates a random sky clearness index so that final net radiation on the panel takes cloud transient into account.

A number of features were specified for the simulation: Coordinates were set to Manchester (50.48° N, 2.24° W), where the LV networks are located (the LV networks used in this study are further explained in *Section 5.5.1*). July was selected as the month of the year to ensure consistency with the month used to generate household demand profiles. Furthermore, the panel angle is set at 45° (the common roof pitch in the UK is between 40° and 50° [160]), facing south. An example of irradiance profiles is shown in ***Figure 5.7***. The final parameter to determine is scaling factor η, which is 1000 kW/m^2 [161].

In accordance with the steps described above, a sample pool with 100 irradiance profiles (in W/m^2) was created. As all households involved in the simulation are within the same LV network and their geographical locations are close to each other, the same irradiance profile should be applied to all PV panels in each simulation. One irradiance profile was therefore randomly drawn from the sample pool and multiplied by the allocated panel size and scaling factor to determine PV generation profiles for each household.

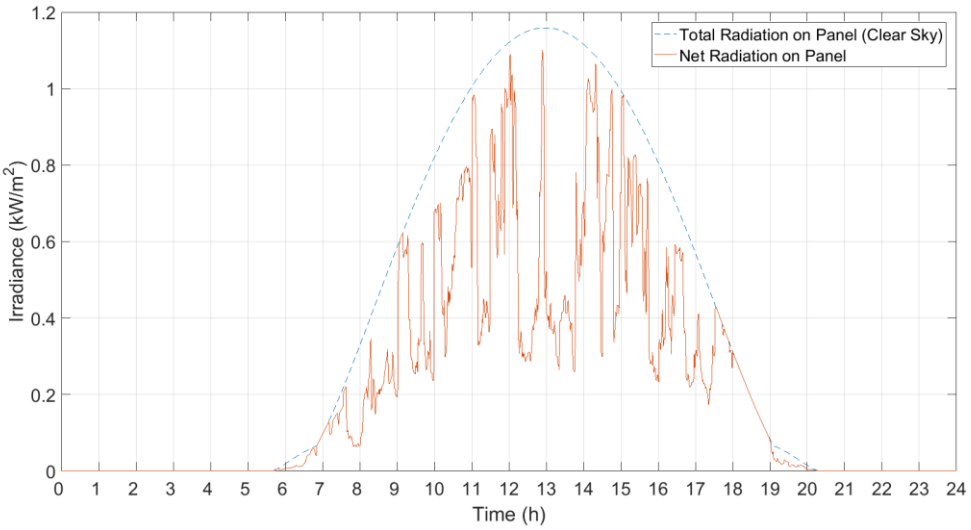

Figure 5.7 Irradiance profiles (W/m^2) generated by CREST Tool

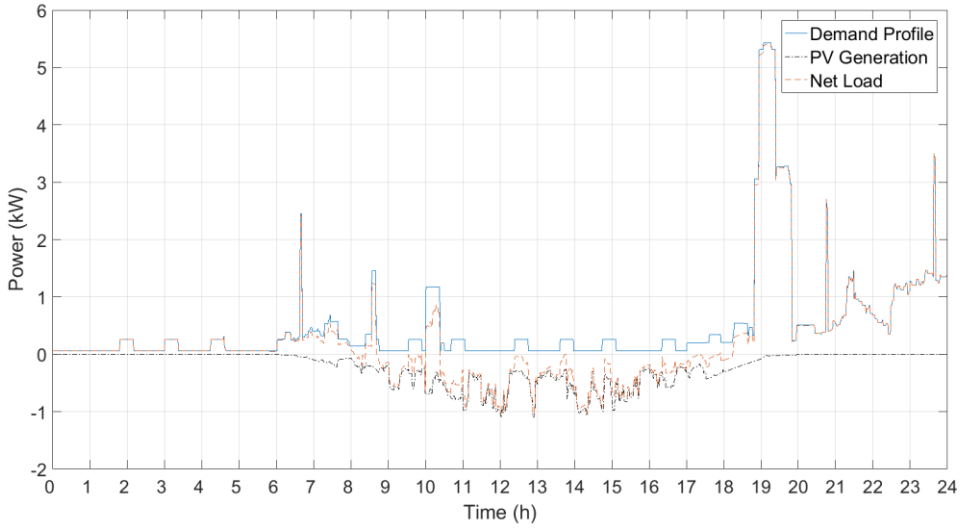

Figure 5.8 An example of household's demand, net load and PV profiles

5.3.3 Overall household demand profiles

Once household demand and PV generation profiles are allocated to a household, they are added up to show a net load profile for the household, given that only one power consumption profile is required at the household's point of connection to the grid. As regards signs of the profile, given that household demand is considered to be a load in power flow calculation, the original demand profile should be positive and PV generation

should be considered as a load in negative value. An example showing a household's original demand, PV generation and net load profiles are illustrated in ***Figure 5.8***.

5.3.4 Hot water demand profiles

The demand profile of a household was excluded hot water demand. This section shows how to create and allocate hot water demand profiles to each household and integrate these profiles into the network model.

Similar to other profiles, in order to provide real insight into network dynamics, the hot water demand profile should have a 1-minute resolution. The EST data used in the previous chapter does not meet this requirement, as it was in hourly format, and so it was necessary to employ another model or source of data.

A report by the International Energy Agency [162] proposed a domestic hot water usage model for European and Canadian residential customers. This model uses a probability based approach with monitored consumption data to model residential DHW demand at 1-, 6- and 60-minute intervals. The model can be used to provide one year of data with daily DHW consumption of 100, 200 and 300 litres.

In the previous chapter, it was suggested that, regardless of the type of customers or their water usage patterns, the most common daily water consumption was slightly under 107 litres (based on 5 kWh hot water energy consumption, given $T_{\text{out}} = 60$ ℃ and $T_{\text{in}} = 20$ ℃). The closest available hot water consumption model from [162], 100 litres at 1-minute resolution, was therefore chosen to provide the hot water demand profiles for this study. Since the model only provides volumetric profiles (in litre), same assumptions and equation used in the previous chapter, ***Equation (4.8)*** with assumptions of $T_{\text{out}} = 60$ ℃ and $T_{\text{in}} = 20$ ℃, were used here to convert unit from litre to kWh. An example of a DHW profile in July is shown in ***Figure 5.9***.

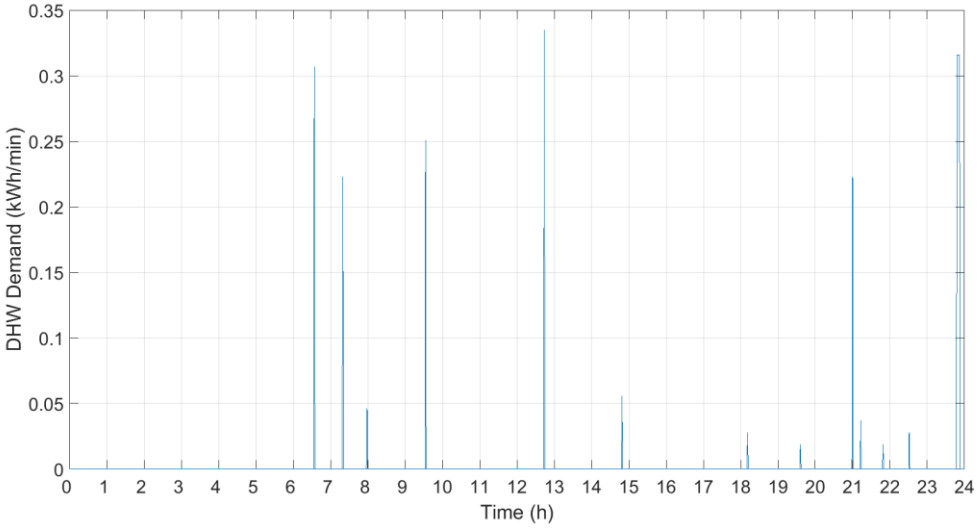

Figure 5.9 An example of DHW demand profile IEA model

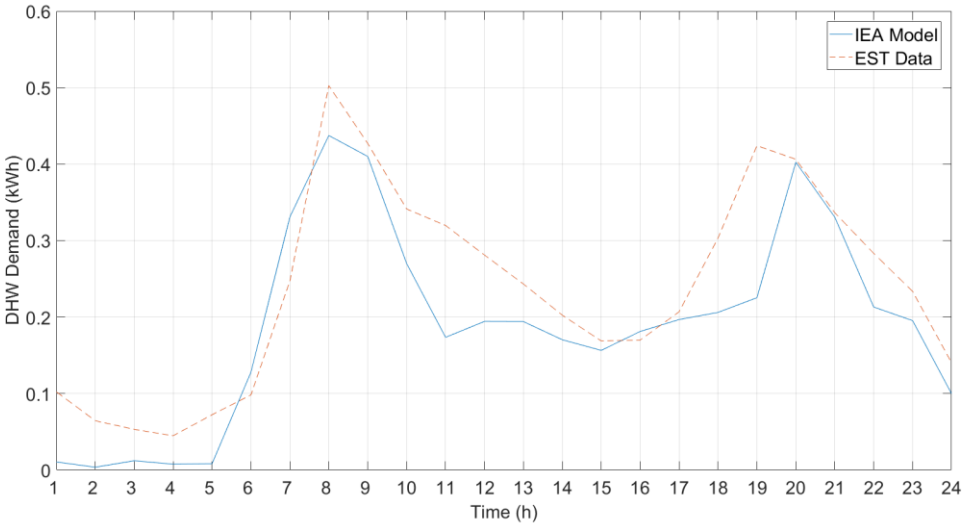

Figure 5.10 Average profiles generated by IEA model and EST data

In total, 31 DHW profiles (one for each day in July) provided in the IEA report were used to create the sample pool. In order to ensure these profiles represented realistic UK customer behaviour, the average of the IEA profiles was plotted against the average of 112 measured profiles in the EST study in ***Figure 5.10***. It can be seen from the figure that the IEA profile shows a close proximity to the real-world profiles measured in the EST study.

Since the previous chapter suggested that there is no direct link between usage pattern and user features (such as number of residents or number of bedrooms), DHW demand profiles were randomly drawn from the sample pool and allocated to each household.

5.3.5 Hot water tank models

Once all the profiles were allocated, the final element to integrate into the LV network was the EHWT model. The same model introduced in *Section 4.2.2* was adopted for the simulation. A modelling diagram showing how to integrate the EHWT model into the network is illustrated in ***Figure 5.11***. For each household, EHWT was modelled separately and connected to the network via the same point of connection as the household demand model. Unlike the household model, which has bidirectional power flow to the network due to potential surplus PV generation, the EHWT only draws power from the network to heat water. From the point of view of power flow simulation (OpenDSS), the charging profile is therefore treated as an additional load to the demand profile.

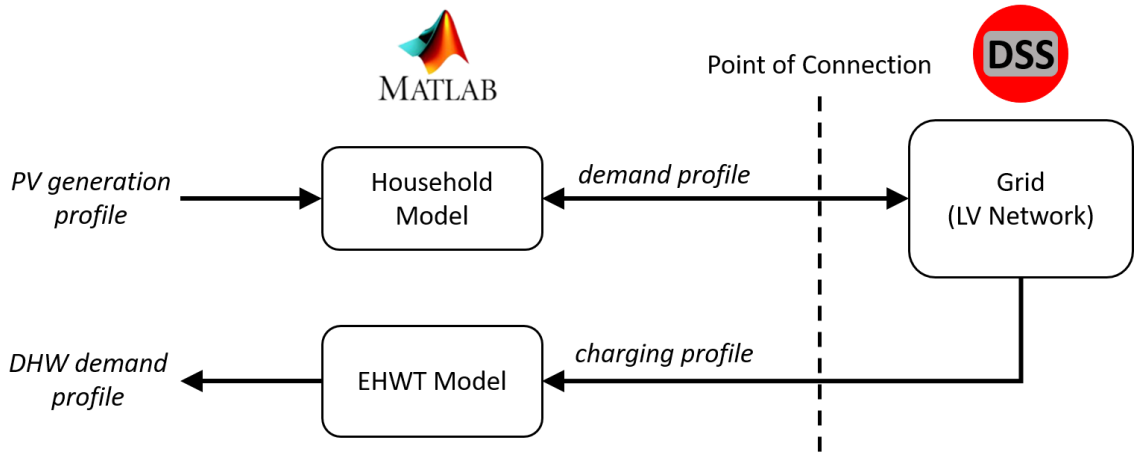

Figure 5.11 Modelling diagram for single household

From the previous chapter, based on the results of the EST study, it could be inferred that the 100-litre tank would be the most economical for consumers in the UK, assuming that they are under Economy 7 tariff scheme. Since this chapter is based on the same tariff scheme and similar DHW usage profiles, the capacity of the EWHTs for all households was specified as 100-litre, or 4.7 kWh in terms of energy capacity.

5.4 EHWT Control Strategy and Scenarios

Once the physical layout of the network was established, the next step was to determine EHWT control strategies. This section introduces four scenarios, each implemented with a different EHWT control strategy, for the purpose of impact analysis.

5.4.1 Scenario 1: No EHWTs

This is considered to be the baseline scenario (control group) for the evaluation of the performance of other EHWT control strategies. In this scenario, hot water demand is met by energy produced from sources other than electricity, such as natural gas, coal, or bio-energy. Given this assumption, the charging profile, along with the EHWT model, can effectively be removed from ***Figure 5.11***. The simulation results therefore reflect the impact of PV generations and household energy demand (without impact of hot water demand).

5.4.2 Scenario 2: Instant electric heating

In this scenario, there are no energy storage systems in the network, and consumers' hot water demands are provided by instant electric water heating. This could be achieved by having electric showers or direct electric heating devices. An example of instant power

is shown in ***Figure 5.12***, where it is used to meet the hot water demand shown in ***Figure 5.9***. Note that the power rating in this scenario has been capped at 12kW, which can be commonly found in the market as the power rating for instantaneous water heating device [163]. The on time for the device is calculated by dividing the service required by 12 kW, where the last minute uses the proportional power that equals to the remainder after the division. It can be seen from the figure that the drawback of this approach is high instantaneous power consumption, which could result in large fluctuations of network's voltage and current.

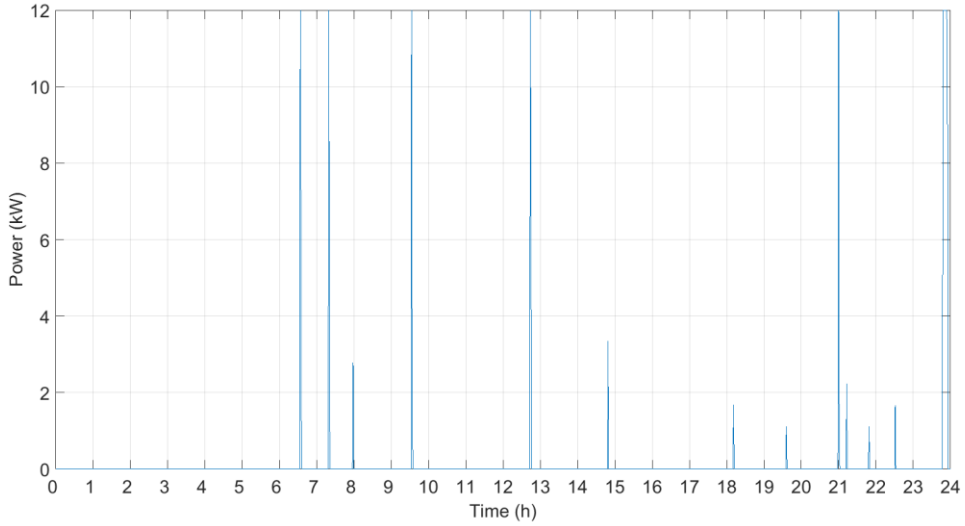

Figure 5.12 Instant power delivery for hot water demand

5.4.3 Scenario 3: EWHTs with adapted Economy 7 control

Economy 7 is a common water heating scheme which could be implemented via an electro-mechanical controller. There are two immersion heaters in the tank, controlled by two separate switches; an overnight off-peak switch which turns the heater on during a pre-set night-time period when the tariff is cheap, and a 'boost' switch which can be turned on if extra hot water is needed during the day.

Assuming that the immersion heater is rated at 3 kW, it takes approximately one and half hours to heat the tank to 100% SOC. To ensure that a tank is fully charged before 7 am (when the tariff changes to peak rate), the latest ON time should be set at 5 am to give a two-hour headroom. In the simulation, the off-peak immersion was therefore set to turn on at a random time between midnight to 5 am and turn off when tank is fully charged. Furthermore, to ensure that the user does not run out of hot water, the 'boost' immersion is turned on when the SOC of the tank drops below 20% and turned off when it reaches 100%. It is worth noting that the immersion heater operates with bang-bang control, under which the heater's power is either 3 kW in ON mode or 0 kW at OFF mode. A control flow chart of this scheme is further illustrated in ***Figure 5.13***.

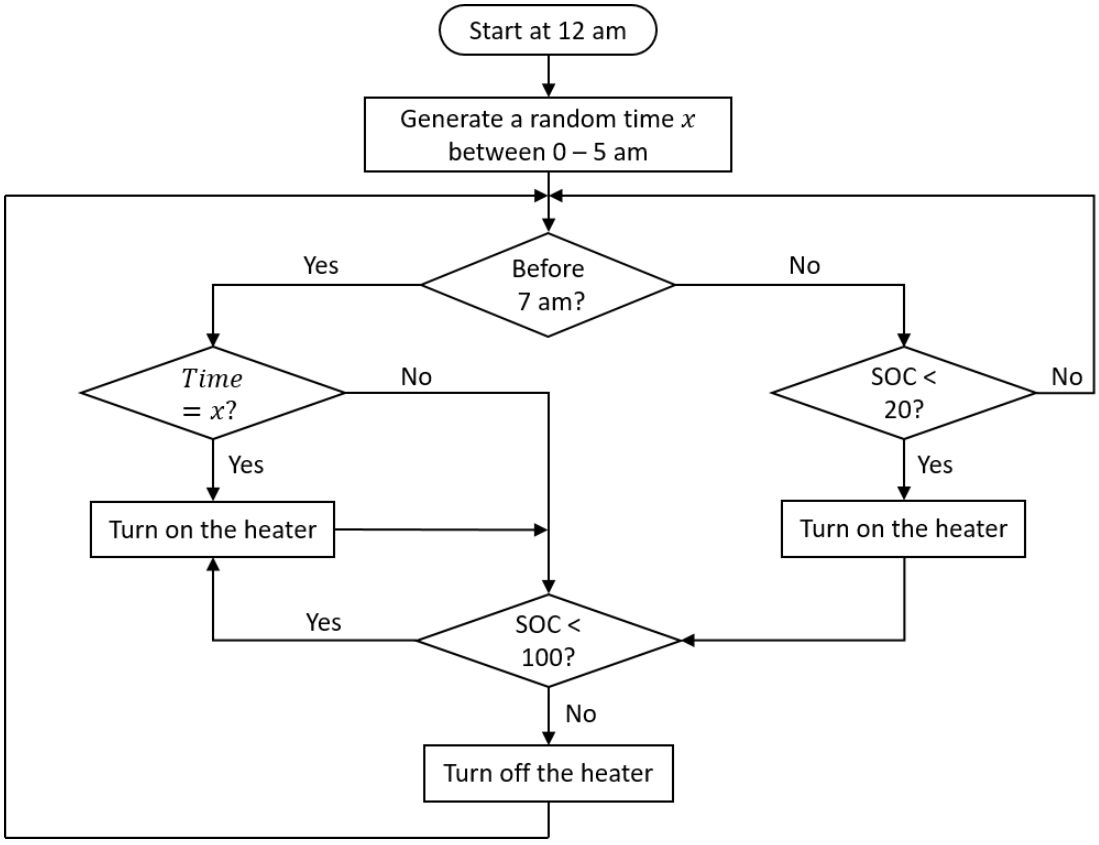

Figure 5.13 Flow chart of adapted Economy 7 control

5.4.4 Scenario 4: EWHTs with intelligent control

In the last scenario, we adopted a rule-based control algorithm. This intelligent control includes the same Economy 7 control features described in the previous section. In addition, measures to prevent over-voltage and under-voltage were also incorporated in the control algorithm, with the aim of mitigating the voltage issues created by surplus PV generation and overload condition respectively.

UK regulations [41] mandate that household voltage supplies V_{hs} across a LV network must be between +10% (253 V) and -6% (216 V) of 230 V. Excessive PV generation will result in a voltage rise, surpassing the upper limit of the permissible voltage range. The control algorithm therefore set a voltage threshold V_{UT}, that $V_{\mathrm{hs}} > V_{\mathrm{ut}}$ enables the immersion to be turned on to absorb surplus PV generation. It is, however, important to consider the following scenario: if significant number of V_{hs} reach V_{ut} at the same time, this would enable all these immersion heaters to be turned on simultaneously, causing V_{hs} to drop significantly across the network and resulting in an under-voltage issue. To avoid this scenario, the following random delay scheme was adopted: when $V_{\mathrm{hs}} > V_{\mathrm{ut}}$, turned on the immersion with a random delay x minutes ($0 \leq x \leq 10$). If V_{hs} dropped below V_{ut} within x minutes, immersion heater would not be turned on. Furthermore, the immersion heater would only remain on for 10 minutes before checking again whether $V_{\mathrm{hs}} > V_{\mathrm{ut}}$ with immersion heater being turned off. This was done to ensure that tank was not absorbing energy when PV generation reduces from higher to a lower level, for instance if there are clouds.

A flow chart of the over-voltage mitigation algorithm is illustrated in ***Figure 5.14***, where t is simulation iteration. V_{ut} was set at 248 V (230 V + 8%) to ensure an overhead for the immersion heater to be turned on before $V_{\mathrm{hs}} > 253$ V (230 V + 10%) during the random delayed period. It should be noted that the heater's power was modulated to match

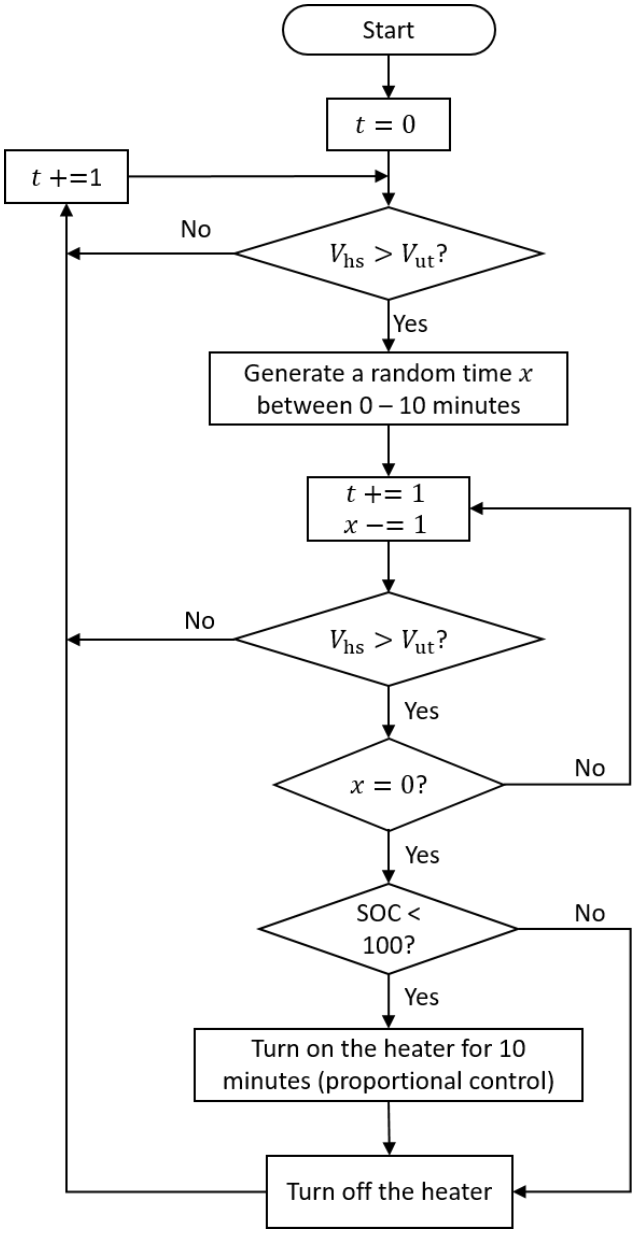

Figure 5.14 Flow chart for over-voltage control

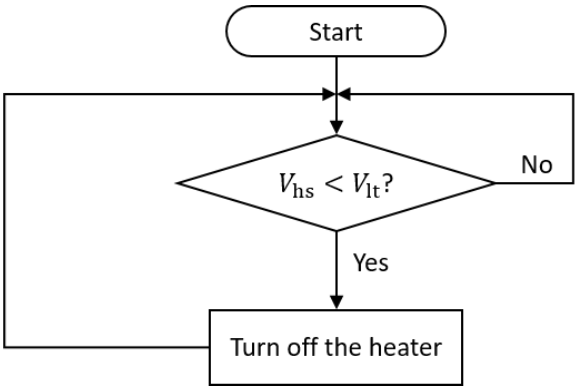

Figure 5.15 Flow chart for under-voltage control

surplus PV generation during over-voltage mode to ensure that no extra energy would be drawn from the grid. This proportional power control can be achieved through IGBT or thyristor devices which are commercially available.

Unlike battery storage systems, EHWTs can only take energy from the grid but not feed it back. Therefore, for the under-voltage algorithm, the only possible mitigation measure it is to turn off the immersion heater if $V_{\mathrm{hs}} < V_{\mathrm{lt}}$, where V_{lt} is the lower voltage threshold set at 216 V. The flow chart for the under-voltage algorithm is shown in ***Figure 5.15***.

5.5 Monte-Carlo Assessment of Intelligent EHWTs

This section applies the profiles and control strategies in the previous sections in real UK networks to study the impact of intelligent EHWTs. It begins by introducing all available LV networks and shows how two representative networks were chosen for the case study. The metrics introduced in *Section 5.2.3* were used to evaluate each network separately, and results were then analysed.

5.5.1 LV networks for case study

A Low Carbon Network project [148] carried out by Electricity North West Limited and the University of Manchester open-sourced 25 LV networks in the Manchester area, corresponding in total to 128 feeder networks, 7539 customers and approximately 200 km of cables.

Due to the time constraint of the project, it was impossible to analyse all 128 feeder networks. Representative networks, therefore, had to be selected for impact analysis. Since the more households in the network, the more voltage and thermal problems related to PV

generation and load consumption were likely to occur, the focus of this chapter was on the networks with large number of households.

As shown in ***Figure 5.16***, the number of households in each feeder network ranged from 2 to 302, with 46 as the median and 142 as the 75th percentile plus 1.5 times the interquartile range (99.3% data coverage if normally distributed and any network beyond that number is identified as an outlier). Given these reasons, two representatively sized networks were selected; the first one the median network, with 46 households, and the second one the large network, with 142 households. The features of each feeder network are described in ***Table 5.1***. It can be seen that both networks are relatively balanced in three phases in terms of number of users, and the cable length of the median network is also consistent with the average cable length (1.5 km) of all feeder networks. The physical layouts of the corresponding networks are shown in ***Figure 5.17***, where the triangle indicates the location of the feeder.

The physical structure of these LV feeder networks was built in OpenDSS, which was then interfaced with Matlab to implement Monte-Carlo simulation to perform analysis on the impact of EHWTs on the LV network.

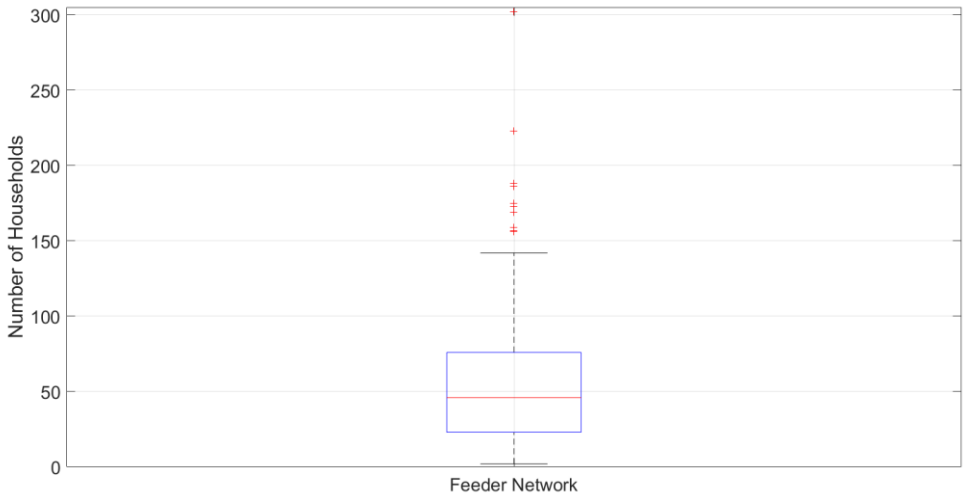

Figure 5.16 Distribution of number of households in all feeder networks

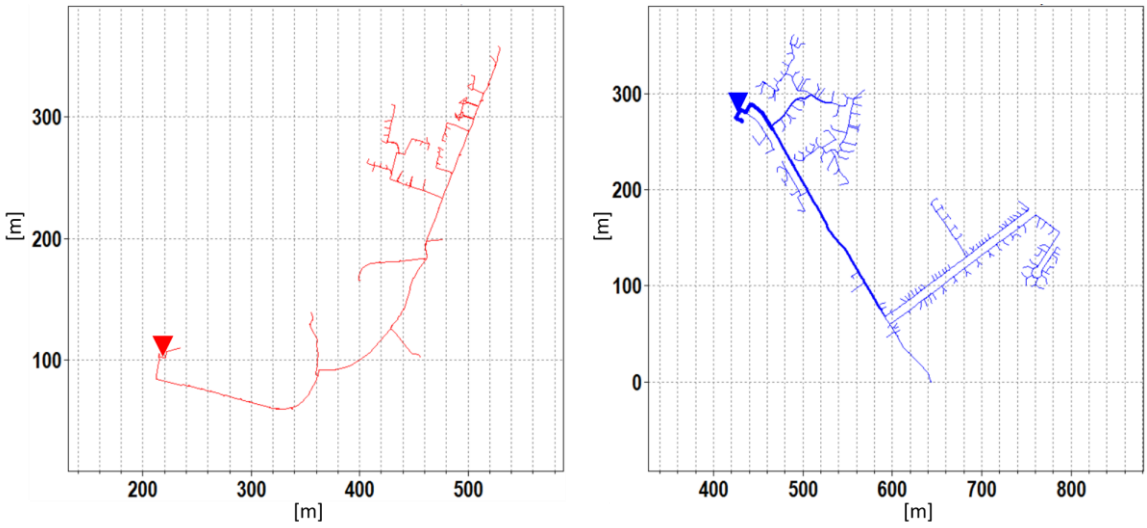

Figure 5.17 Visualization of LV feeder networks with 46 (left) and 142 (right) households

Table 5.1 Features of selected LV feeder network

Feeder	Total Cable Length (m)	Number of Households			
		Total	***Phase A***	***Phase B***	***Phase C***
1	1520	46	14 (30%)	15 (33%)	17 (37%)
2	3612	142	44 (31%)	53 (37%)	45 (32%)

5.5.2 Case study 1: The median network

The first feeder network to be investigated was the median network, serving 46 households with 1520 meters of cable. Following the Monte-Carlo simulation steps introduced in *Section 5.2.2*, four different control strategies were assessed against PV penetration levels from 0% to 100% at a 10% interval. The probabilistic assessment for the following metrics including percentage of households with EN 50160 voltage problems, network loading levels and cost of energy to heat water, are presented as follows:

Voltage problems

The percentage of households with EN 50160 voltage problems was calculated in each simulation (100 simulations with randomized inputs per PV penetration level). The results for four different control scenarios are presented in ***Figure 5.18***, where the average value ± one standard deviation is plotted. Furthermore, examples of network voltage responses at 100% PV penetration (every household has a PV panel) under four control scenarios are shown in ***Figure 5.19***.

It can be seen from the figure that percentage of customers with voltage problems tends to increase with higher penetration of PV installations. This is due to the voltage rise caused by surplus PV generation. No EHWTs is the worst-case scenario, where there is no energy consumption for surplus PV generation and all extra solar energy are fed back to the grid, resulting in a significant voltage rise (see ***Figure 5.19***). With 100% PV penetration, the percentage of customers with voltage problems would rise to 13%.

The Economy 7 control and instant electric heating scenarios could mitigate the voltage problems only to a limited extent (approximately 2% on average), because these two control scenarios do not have mechanisms to proactively absorb energy when there is excessive PV generation. The instant electric heating scenario performs slightly better than Economy 7 for voltage mitigation, mainly because the energy consumed to meet daytime hot water demand may offset some surplus PV generation. However, it is worth noting that instant heating could cause under-voltage problem if there is excessive hot water demand (shown in top right figure in ***Figure 5.19***).

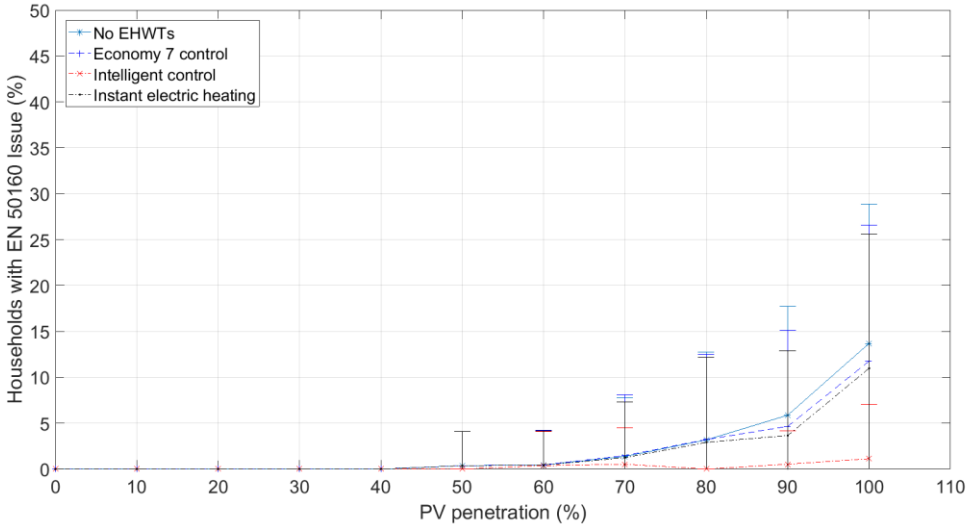

Figure 5.18 Percentage of households with voltage issues in the median network

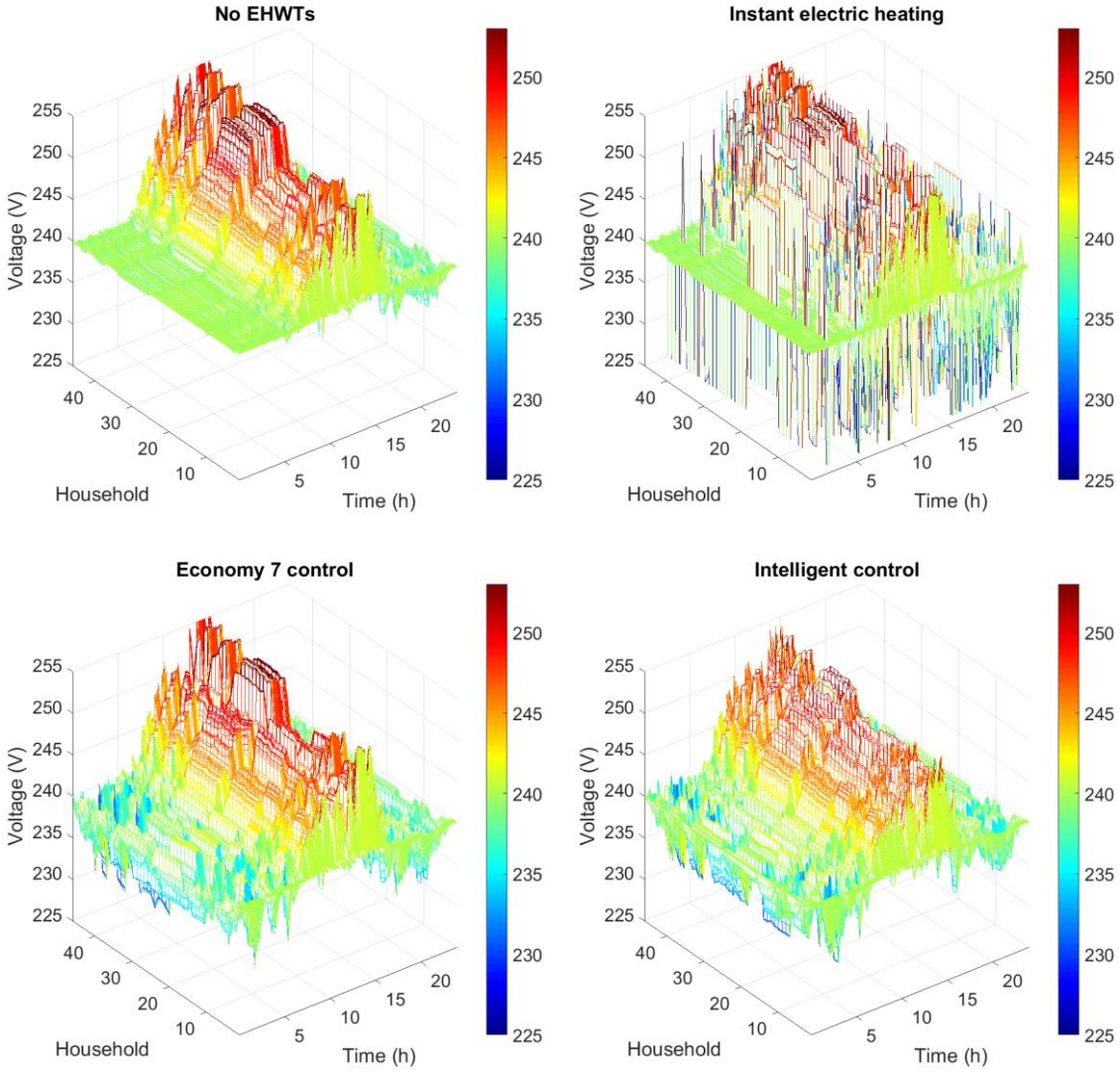

Figure 5.19 Median network voltage responses with 100% PV penetration under four control scenarios

Finally, the intelligent control scenario provides the best performance for voltage mitigation. After implementing intelligent control in the EHWTs as described in *Section 5.4.4*, the percentage of households with EN 50160 voltage problems drops from 13% with no EHWTs to less than 1%. Translated into the number of households, the figure of 1% is negligible because it represents less than half a household out of a total of 46 households in the network. It can therefore be concluded that by installing the intelligent EHWTs, the median LV network could avoid voltage problems which could otherwise have occurred under high PV penetration.

Thermal problems (loading level)

The thermal problem (loading level) is represented as the percentage of maximum current as compared with the ampacity (rated current) of the header of the feeder. In this median network, the first segment of the cable is specified as 300 mm^2 underground conductor. Assuming the cable is in ducts, the planning guide provided by UK Power Networks [164] specifies that the rated current for this cable is 345 *A*. The loading levels of average value ± one standard deviation for the four scenarios are calculated and illustrated in ***Figure 5.20***.

The first phenomenon worthy of notice is that the instant electric heating scenario has a much higher loading level (around 70%) than the other three. This is caused by high, intensive power consumption to meet instantaneous hot water demand. The other three scenarios start with a loading level between 20% and 30% at zero PV penetration, with the no EHWTs showing slightly lower figures than the Economy 7 and intelligent control. This is not, however, a 'fair' comparison because hot water service in the no EHWT scenario is provided by other means of energy, such as gas, rather than electricity. Even so, with a higher penetration of PV panels (> 70%), intelligent control outperforms the other two scenarios by a small margin, given that it limits net power in-feed from the PV panels and

consequently reduces maximum current. At a higher level of PV penetration, the degree of loading level is mainly affected by the highest PV generation. At 100% PV penetration, both the no EWHTs and the Economy 7 control scenarios have a 52% load level, while the intelligent control scenario shows slightly under 48%.

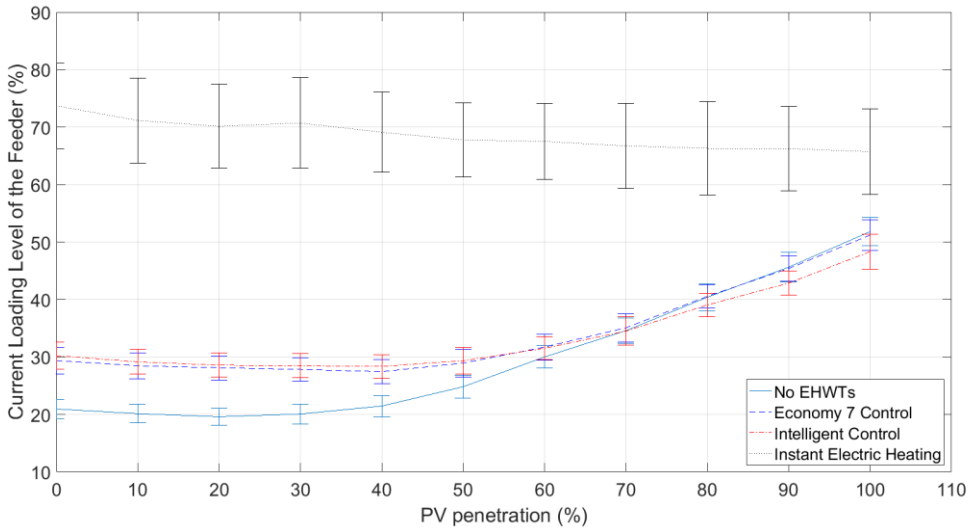

Figure 5.20 Loading level of feeder at different PV penetration levels (median network)

Cost of energy for water heating

This metric is calculated as follows: the total electricity price paid by the user divided by the total energy used to charge the tank, assuming the use of the Economy 7 tariff scheme. It should be noted that the surplus PV energy used to charge the tank is considered to be '*free*' energy, and therefore does not contribute to the electricity price paid by the user. Since the no EHWTs scenario does not use electricity as the source of energy to fulfil hot water demand, this scenario has been excluded from the analysis. ***Figure 5.21*** shows the average value ± one standard deviation of energy cost (in £/kWh) to heat water under the other three scenarios.

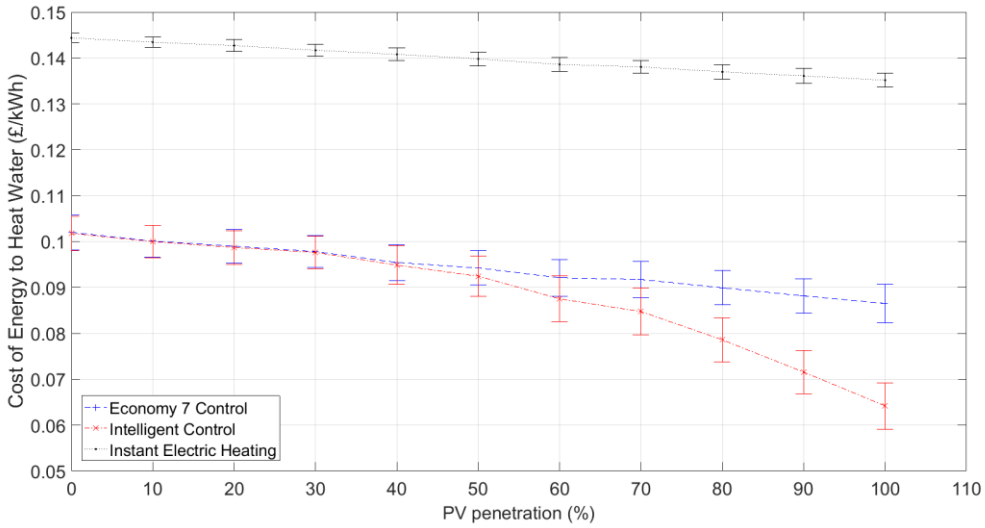

Figure 5.21 Cost of energy for water heating at different PV penetration levels (median network)

Instant electric heating results in the highest cost of energy, principally because it neither fully utilizes the cheap night-time tariff nor uses 'free' surplus PV generation during the day. Economy 7 and Intelligent control start with similar cost of energy where PV penetration is low. However, with a higher penetration of PV panels, the advantage of intelligent control (which utilizes 'free' surplus PV generation) begins to show its impact, resulting in a much lower cost of energy. At 100% PV penetration, the cost of energy under the intelligent control scenario is £0.065/kWh, compared to £0.087/kWh and £0.135/kWh under the Economy 7 control and instant electric heating scenarios respectively.

It remains arguable, however, that intelligent control could provide benefits for cost of energy due to the export tariff for PV generation. The export tariff is part of the feed-in tariff that the energy supplier would pay for each kWh of PV solar energy that the household exports back to the electricity grid. This is currently set at £0.041/kWh, but it is expected to decrease significantly in the future [165]. It might be argued that the surplus PV energy used to charge EHWTs could otherwise been exported back to grid for export

tariff arbitrage. However, two factors should be noted: 1. The tank is only charged with surplus energy, which would otherwise be spilled (not being generated) due to the voltage problem it would cause. This energy should therefore be considered as '*free bonus*' energy. 2. The proportion of export energy for the domestic PV system is currently only estimated by the energy supplier at 50% of total PV generation, instead of being accurately monitored [166]. The export tariff arbitrage would, therefore, not be affected by the generated PV being used to charge the tank or export back to the grid. This scheme may, however, be subject to change in the future with the rollout of smart meters.

Overall, if EHWTs were endowed with intelligent control, this would allow higher penetration of PV installations by mitigating both voltage and thermal problems which would occur in other scenarios. Intelligent control also has an economic impact, though the magnitude of this could be dependent on future tariff policy.

5.5.3 Case study 2: The large network

Following the same steps as in the previous section, the metrics were evaluated for the large network which serves 142 households with 3612 meters of cable.

Voltage problems

Figure 5.22 shows the percentage of households with voltage problem under different control scenarios and PV penetration levels. Similar to the median network, the percentage of households with voltage problem rises with increasing PV penetration, but unlike the median network, the large network would not, even with intelligent controlled EHWTs, accommodate a high PV penetration without encountering voltage problems. Voltage problems start to occur at 40% PV penetration, reaching to 60% of households at 100% PV

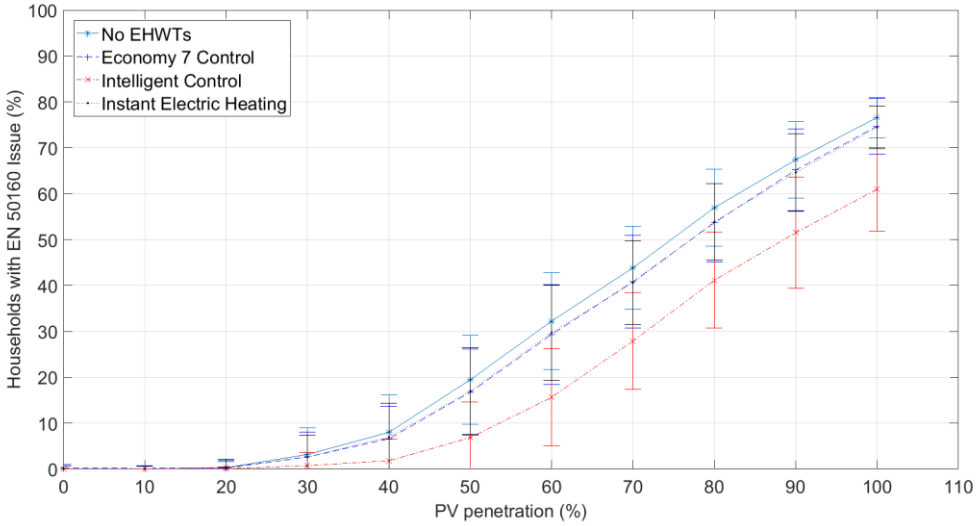

Figure 5.22 Percentage of households with voltage issues in the large network

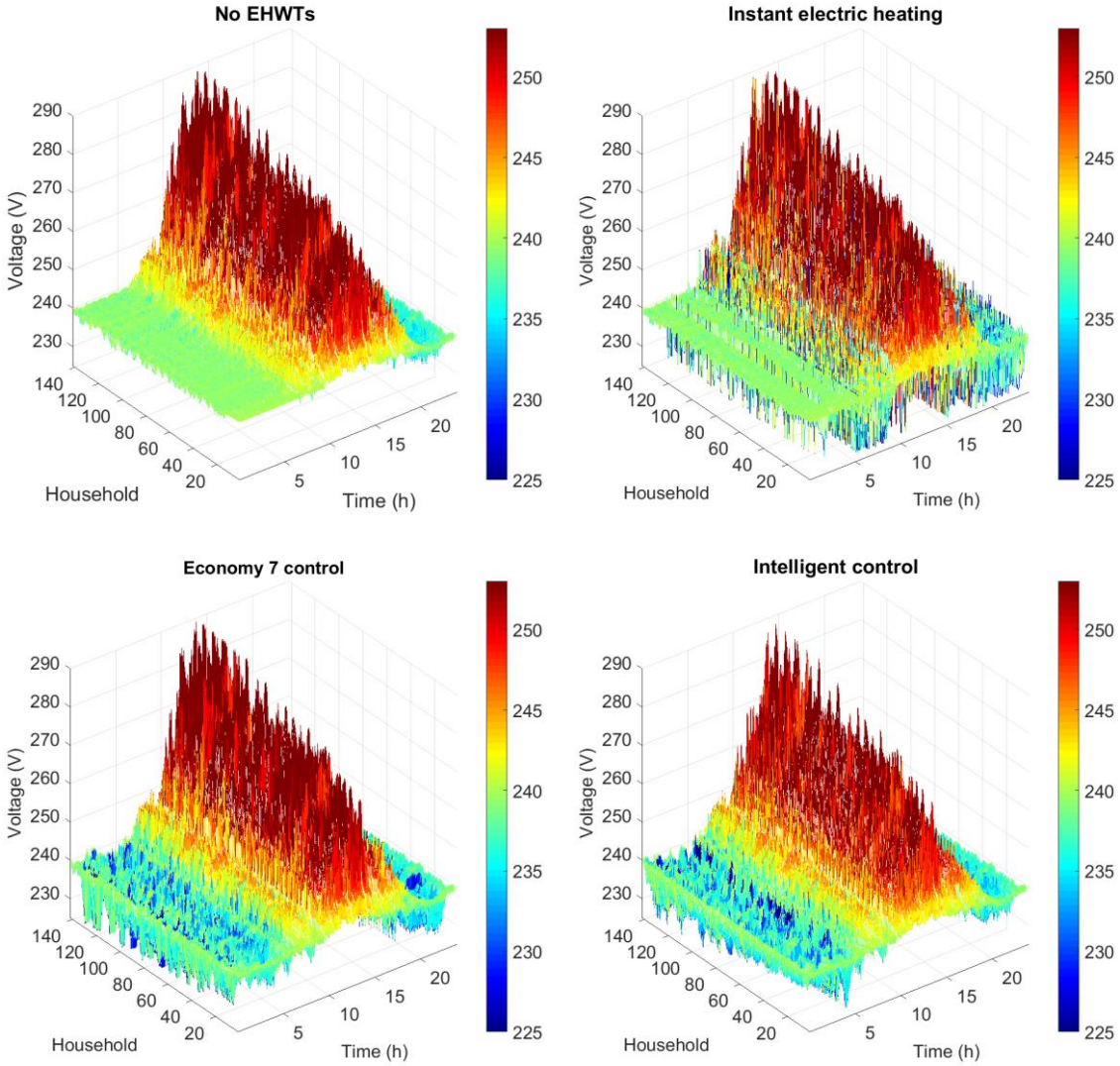

Figure 5.23 Large network voltage responses with 100% PV penetration under four control scenarios

penetration. This does, however, still outperform other control scenarios, under which voltage problems would arise at 30% PV penetration, and reach to about 75% of households at 100% PV penetration.

Examples of network voltage response with 100% PV penetration under four control scenarios are presented in ***Figure 5.23***. Although there are fewer red (over-voltage) regions under the intelligent control scenario than the other three, a significant part of the network still suffers from over-voltage problems, given the insufficient capacity of the EWHTs to store all the surplus energy generated from the PV panels. If the size of the tank was increased, there would be more capacity to store surplus energy, but this would entail an economic sacrifice for individual consumers given the higher capital costs. Further investigation of control strategies and tank size could be carried out in future for the networks which are too large for the proposed fleet of tanks to absorb surplus PV generation.

Thermal problems (loading level)

Based on the cable code, the large network uses the same first segment of cable as the median network rated at 345 *A*. The loading level for each scenario is plotted out in ***Figure 5.24***. Due to the higher number of households in the network, the loading level of the large network is three times higher than the median network. Implementing instant heating for hot water demand would not be feasible, because the maximum current would be around 1.5 times the rated current regardless of PV penetration level. Networks with Economy 7 control and no EHWTs reach 100% loading level at 65% PV penetration, whereas the network with intelligent EHWTs reaches 100% loading level at 70% PV penetration. At 100% PV penetration, the intelligent control scenario can reduce the loading level from 165% (as in the other two scenarios) to 150%.

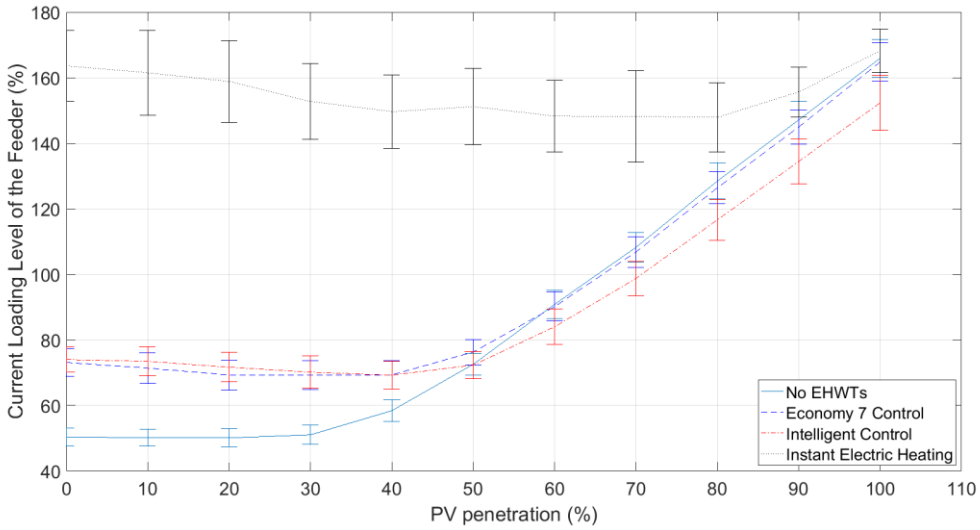

Figure 5.24 Loading level of the feeder under different PV penetration levels (large network)

Cost of energy for water heating

Figure 5.25 shows the cost of energy under 3 scenarios, excluding the one with no EHWTs. As can be seen from the figure, the large network has approximately the same cost of energy as the median network for the instant electric heating and Economy 7 control scenarios. However, under the intelligent control scenario, the large network has a lower cost of energy compared to the median network. This is primarily because intelligent control takes advantage of '*free*' surplus energy, and EHWTs in the large network absorbs more surplus PV energy in order to mitigate voltage problems. At 100% PV penetration, the cost of energy for intelligent EHWTs is reduced to £0.051/kWh, compared to £0.087/kWh for regular Economy 7 EHWTs.

Although intelligent EHWTs will not completely solve voltage or thermal problems caused by high PV penetration owing to their thermal capacity limits, they could in the large LV network (142 households in this case) accommodate higher level of PV generation before voltage and thermal problems occur.

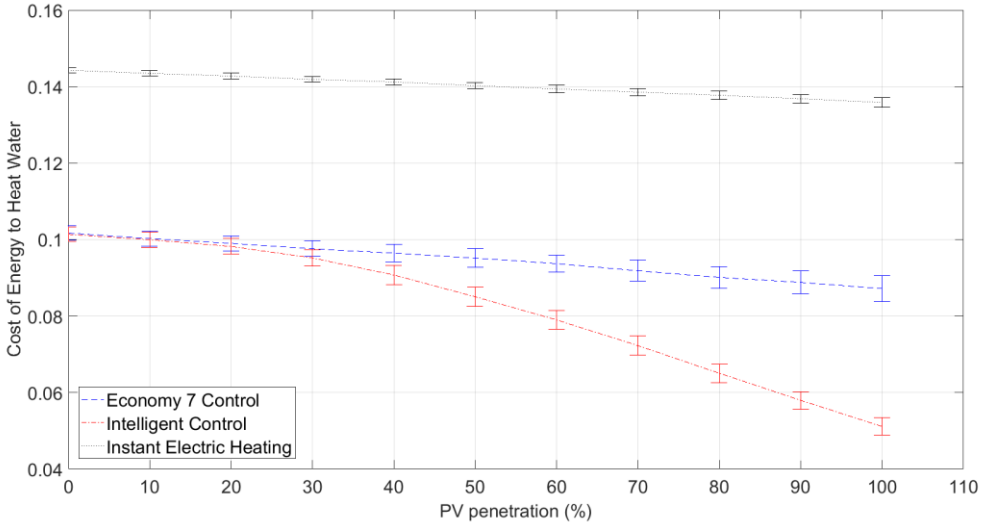

Figure 5.25 Cost of energy for water heating under different PV penetration levels (large network)

5.5.4 Overall analysis

The results of the median and large networks indicate that intelligent EWHTs can significantly improve the voltage performance and marginally improve the thermal performance of the network with the presence of PV systems. The degree of improvement could, however, be dependent on the size of the LV network (i.e. number of households in the network). For the median network with 46 households, the use of intelligent EWHTs would enable the network to accommodate 100% PV penetration, whereas for the large network with 142 households, the PV penetration would only increase from 30% (benchmark scenario) to 40% before voltage problems occurred. If 100% PV penetration is to be reached, other measures must also to be taken.

5.6 Summary

This chapter addressed the question: "*Could intelligent EHWTs be used to alleviate the voltage and thermal problems caused by excessive PV generation?*". The question was

answered by carrying out probabilistic assessment of intelligent EHWTs on real UK LV networks.

The software architecture for the simulation was based on OpenDSS and Matlab, with OpenDSS handling time series power flow calculation and Matlab processing input and output data as well as implementing control algorithms. Based on this architecture, a Monte-Carlo simulation approach was proposed for a probabilistic assessment of different scenarios, including networks with no EWHTs, instant electric heating, Economy 7 controlled EHWTs, and intelligent EWHTs incorporating with an over-voltage mitigation algorithm. The results are assessed against the following metrics: percentage of households with voltage problems, loading levels and cost of energy for water heating.

The household, hot water demand profiles used in the simulation were validated against the real-world data and proved to be consistent, and PV generation profiles were also produced from ground-truth parameters. Two representative real UK LV networks were used for the case study: a median-sized feeder network with 46 households and a large-sized feeder network with 142 households. Probabilistic analysis revealed that a fleet of intelligent tank could significantly improve the voltage performance of the network. The median LV network could allow 100% PV penetration if every household had an intelligent EHWT, while PV penetration level would drop to 60% with a regular or no EHWT. For the large LV network, the use of intelligent EHWTs would allow maximum PV penetration to increase from 20% to slightly above 30%. In overall terms, regardless of the size of the network, the presence of intelligent EHWTs in every household could enable 50% more PV installations beyond the network's existing maximum capacity.

Given the time constraints of this project, only 2 out of 128 feeder networks were analysed in this chapter. Future research work should cover all available networks with an extended OLTC model so that multi-feeder analysis could be performed. Network stress

detection algorithm should also be implemented in the simulation model. Furthermore, it might be worthwhile to explore more elaborate control algorithms (for instance, model predictive control), with a view to maximizing the ability of EHWT to absorb surplus local renewable generation.

Chapter 6. Conclusions and Future Work

This dissertation explores the potential of using smart appliances, particularly intelligent EHWTs, to alleviate the network stress caused by distributed renewable generation. *Chapter 1* and *2* introduced and identified three gaps in research, namely:

1. An effective network stress identification approach for smart appliances is needed for distributed and decentralised DSM scheme.
2. While the EHWT size has largely been considered within the context of combined hot water systems using tanks heated by various energy sources, understanding the optimal size of the EHWT in isolation within DSM has not been explored thoroughly.
3. A bottom-up network simulation approach integrated with intelligent EWHT model has not been fully investigated.

These gaps were translated into research questions and subsequently answered in *Chapter 3, 4 and* 5. *Section 6.1* summarises this thesis's contributions to answering the research questions posed, and *Section 6.3* supplements this with recommendations for future work.

6.1 Contributions against Research Objectives

Four research questions, framing the objective of this thesis, were stated in *Chapter 1, Section 1.3*. This section summarises the contributions made by the thesis to answering these questions, and outlines the work carried out throughout the thesis. The statements in bold represent the novel contributions claimed in this thesis.

1. *"Is there a technique that can enable domestic devices to perceive the stress across the network in real time without the need to further invest into the communication infrastructure?".* (Chapter 3)

This question is addressed in *Chapter 3*, where **an approach to identify three levels of stress, especially LV and MV network stress, using the information extracted from local mains voltage measurement was proposed and validated. This approach enables domestic appliances to perceive the network stress without the need for external communication**.

Voltage frequency was used to indicate system-wide stress. Zero-crossing detection method and third order Butterworth low pass filter were applied in order to extract frequency information from the measured voltage data. The results showed consistency with the system frequency data provided by the National Grid.

The tap changer position of 33/11kV OLTC in MV substations was used to infer MV network stress. The enabling technique was the tap change detection algorithm applied to the measured voltage. **A multi-layer perceptron neural network was used to classify voltage changes associated with the tap changing events, with a validated successful classification rate of 90% and 99.9% for tap change and non-tap change events respectively.**

The LV network stress was revealed by removing the voltage impact associated with upstream tap change events from the original measured mains voltage. The processed voltage showed a relatively inverse proportional relationship with the active and reactive power consumed at the same location.

By adopting the technique proposed in this chapter, smart appliances will be able to perceive the network stress without any need for communication. This would thus enable

a more cost- effective decentralised or distributed DSM scheme, and it would be practical to further exploit this method in domestic appliances.

2. *"How to determine the optimal tank size to provide customers with greater economic benefits, given the pattern of their hot water usage?"*. (Chapter 4)

With a view to answering this question, a sizing design of domestic EHWTs was carried out in *Chapter 4*. **A two-stage optimization method for sizing design of the EHWT with the target to minimize energy cost against given hot water usage was developed to address this question.**

In order to formulate the optimization problem, an EHWT energy model was proposed based on a patented topology, which is being commercialized in the UK market. The optimization was carried out in two stages: operation optimization using non-linear constrained optimization solver in Matlab, followed by sizing optimization using Brute-force method (gradient descent method can also be used). Overall, with a given hot water usage profile, the optimization process is able to determine the tank size that provides minimum energy costs.

3. *"What are the typical patterns of hot water usage and the most common optimal tank size for UK consumers?"*. (Chapter 4)

Also in *Chapter 4*, this question was addressed by analysing the usage profiles from the EST study and applying them to the optimization approach described earlier. **Four distinct hot water usage patterns and one optimal tank size (100-litre) for UK consumers have been revealed from the data analysis. The study also showed that there is no strong correlation between hot water usage patterns and different household occupancy features (such as number of residents or number of bedrooms**

in the house). Further analysis indicated that the 100-litre tank remained the most prevalent optimal size, regardless of type of household. The contributions made in *Chapter 4* is essential for the network simulation in the following chapter, because they provided guidelines on the modelling of network components such as size of EHWT model and hot water usage profile.

4. "*How can intelligent EHWTs be used to alleviate voltage and thermal (current) problems caused by excessive PV generation?*". (Chapter 5)

Chapter 5 addressed this question by performing a probabilistic assessment of intelligent EHWTs in real UK LV networks. **A Monte-Carlo simulation with two representative real UK networks was carried out, and it showed that the use of intelligent EHWTs would significantly improve voltage performance and marginally improve thermal (current) performance in the LV network.** The results revealed that the use of intelligent EHWTs in all households would allow an increase of 50% in PV installations as compared to the existing PV capacity of the network. Furthermore, the presence of intelligent EHWTs can reduce energy costs by between 24% and 44% owing to their ability to absorb free surplus PV generation.

6.2 Discussion

Modern power networks are becoming more complex with its changing infrastructure and a growing portfolio of generation and demand. A variety of control approaches, including centralised, distributed and decentralised approaches, have been proposed to tackle these challenges. The tap changing detection algorithm proposed in *Chapter 3* could be relevant and beneficial to all three types of control approach because it eliminates the need for real-time communication among different devices. In a centralised control scheme,

for example, a system controller needs to gather network stress information and send out control signals to devices in real time. With the adoption of the tap changing detection algorithm, each device can operate autonomously in response to the network stress perceived by the algorithm, and only report to or receive instructions from the system controller within a much longer time interval (i.e. daily).

As regards the PV to HWT system proposed in *Chapter 5*, from the perspective of carbon emission it may be argued that heating up the tank using electricity is less efficient than gas or other sources of energy such as ground source heat. Other assets such as EV could potentially be used to absorb surplus energy, but it is worth noting that surplus PV generation occurs during the daytime, when many EVs will likely not be connected to the grid, which therefore limits the use of EVs for absorbing surplus PV generation. Apart from domestic battery systems, there are hardly any other domestic appliances with s storage capacity comparable to HWTs. Given that hot water provision accounts for a large proportion of domestic energy consumption and HWTs already exist in many households in the UK, the use of HWTs remains attractive for absorbing surplus PV generation.

6.3 Future Work

This section identifies the limitations of the work carried out in this dissertation and recommends further work that could be pursued in future.

In *Chapter 3*, the core technique used for network stress identification approach was tap change detection using the MLP neural network. This neural network demonstrates a 90% success rate at detecting tap change events. Errors in the classification system may, however, lead to a deviation of measured network stress from actual stress (as shown in ***Figure 3.20***). This deviation could be resolved by increasing the classification accuracy of the neural network, and it was discovered that accuracy could be further improved should

more training data be obtained. Owing to limitations on resources, the training and validation data for the neural network is currently only available from three locations, with a duration of up to two weeks. In order to fully apply the algorithm in the real world, it is necessary to obtain further tap change training data which would then be used to train the neural network.

In *Chapter 5*, given the time constraints of the project, only two out of 128 real LV networks were simulated for impact assessment. Future work should involve an analysis of a full set of LV networks, with a view to providing more detailed statistical results on the impact of EHWTs. As this set of networks covers a wide range of features such as number of households and cable length, a full dataset study will allow us to better understand and correlate the impact of PVs and EHWTs with respect to the network features. We could, for example, establish the maximum number of household in a network so as to resolve the voltage problems caused by PV generation through solely introducing intelligent EHWTs.

Finally, it is important to point out that in this thesis EHWTs were considered as the only DSM assets. In a typical future modern power network scenario, though, there should be a portfolio of controllable DSM assets, including EVs, home batteries, and even heat pumps. It would therefore be practical to include all these load models in future work on network simulation. This will also lead to further work on the feeder level load disaggregation control. For instance, from the perspective of a DNO or aggregator, only a certain amount of load needs to be taken off or added at the feeder transformer, but there has so far been little research into the best approach for the distribution of this load into each household. The simulation platform proposed in *Chapter 5* has established a fundamental framework for carrying out such research in future.

Bibliography

[1] United States Environmental Protection Agency, “Overview of Greenhouse Gases.” 2016.

[2] NASA, “The consequences of climate change,” 2016. [Online]. Available: http://climate.nasa.gov/effects/. [Accessed: 30-Dec-2016].

[3] M. R. Allen, D. J. Frame, C. Huntingford, C. D. Jones, J. A. Lowe, M. Meinshausen, and N. Meinshausen, “Warming caused by cumulative carbon emissions towards the trillionth tonne,” *Nature*, vol. 458, no. 7242, pp. 1163–1166, Apr. 2009.

[4] International Energy Agency (IEA), “World Energy Outlook 2016,” 2016.

[5] Department of Energy and Climate Change, “2010 to 2015 government policy: greenhouse gas emissions,” 2015.

[6] Department of Energy and Climate Change, “Energy consumption in the UK,” 2016.

[7] P. E. Dodds and W. McDowall, “The future of the UK gas network,” *Energy Policy*, vol. 60, pp. 305–316, Sep. 2013.

[8] Department for Business Energy & Industrial Strategy, “Electricity: Chapter 5, Digest of United Kingdom Energy Statistics (DUKES),” 2016.

[9] G. Keane and O. Pearce, “Analysing Technical constraints on Renewable Generation to 2050 - A report to the Committee on Climate Change,” 2011.

[10] Department for Business Energy & Industrial Strategy, “Renewable sources of energy: Chapter 6, Digest of United Kingdom Energy Statistics (DUKES),” 2016.

[11] M. A. Zehir and M. Bagriyanik, “Demand Side Management by controlling refrigerators and its effects on consumers,” *Energy Convers. Manag.*, vol. 64, pp. 238–244, Dec. 2013.

[12] K. Kostková, Ľ. Omelina, P. Kyčina, and P. Jamrich, “An introduction to load management,” *Electr. Power Syst. Res.*, vol. 95, pp. 184–191, Feb. 2013.

[13] B. Davito, H. Tai, and R. Uhlaner, “The smart grid and the promise of demand-side management,” *McKinsey Co.*, pp. 38–44, 2010.

[14] S. H. Hierzinger Roland, Albu Mihaela, Elburg van Henk, Scott Alastair J., Łazicki Artur, Penttinen Lauri, Puente Francisco, “European Smart Metering Landscape Report 2012 – update May 2013,” 2013.

[15] Elexon, “Electricity Data Summary.” [Online]. Available: https://www.bmreports.com/bmrs/?q=eds/main. [Accessed: 01-Nov-2016].

[16] Elexon, “What is the balancing mechanism?” [Online]. Available: https://www.elexon.co.uk/knowledgebase/what-is-the-balancing-mechanism/. [Accessed: 01-Nov-2016].

[17] P. Balcombe, D. Rigby, and A. Azapagic, “Energy self-sufficiency, grid demand variability and consumer costs: Integrating solar PV, Stirling engine CHP and

battery storage," *Appl. Energy*, vol. 155, pp. 393–408, 2015.

[18] S. Anuphappharadorn, S. Sukchai, C. Sirisamphanwong, and N. Ketjoy, "Comparison the economic analysis of the battery between lithium-ion and lead-acid in PV stand-alone application," *Energy Procedia*, vol. 56, no. C, pp. 352–358, 2014.

[19] P. J. Boait, D. Dixon, D. Fan, and A. Stafford, "Production efficiency of hot water for domestic use," *Energy Build.*, vol. 54, pp. 160–168, Nov. 2012.

[20] T. Nowak, "Energy Use in Homes 2007: A series of reports on domestic energy use in England: Energy Efficiency," London, 2007.

[21] Elexon, "ISG187-System Price Analysis Report on March 2016," 2016.

[22] R. C. Dorf, *CRC Handbook of Engineering Tables*. CRC Press, 2004.

[23] B. M. Weedy, B. J. Cory, N. Jenkins, J. B. Ekanayake, and G. Strbac, *Electric power systems*. John Wiley & Sons, 2012.

[24] L. M. Cipcigan and P. C. Taylor, "Investigation of the reverse power flow requirements of high penetrations of small-scale embedded generation," *IET Renew. Power Gener.*, vol. 1, no. 3, p. 160, 2007.

[25] P. Suwanapingkarl, "Power quality analysis of future power networks," Northumbria University, 2012.

[26] L. Zhou, F.-Y. Xu, and Y.-N. Ma, "Impact of smart metering on energy efficiency," in *Machine Learning and Cybernetics (ICMLC), 2010 International Conference on*, 2010, vol. 6, pp. 3213–3218.

[27] Insitituion of Civil Engineers, "Energy Reports – Distributed Generation," 2002.

[28] V. Hamidi, K. S. Smith, and R. C. Wilson, "Smart Grid technology review within the Transmission and Distribution sector," in *2010 IEEE PES Innovative Smart Grid Technologies Conference Europe (ISGT Europe)*, 2010, pp. 1–8.

[29] J. Romero Aguero, "Improving the efficiency of power distribution systems through technical and non-technical losses reduction," in *PES T&D 2012*, 2012, pp. 1–8.

[30] S. J. Ranade, "Electric Transmission and Distribution Efficiency," 2010.

[31] International Energy Agency, *Cool Appliances: Policy Strategies for Energy-Efficient Homes*. OECD Publishing, 2003.

[32] N. Gudi, L. Wang, and V. Devabhaktuni, "A demand side management based simulation platform incorporating heuristic optimization for management of household appliances," *Int. J. Electr. Power Energy Syst.*, vol. 43, no. 1, pp. 185–193, 2012.

[33] M. Newborough and P. Augood, "Demand-side management opportunities for the UK domestic sector," *IEE Proc. - Gener. Transm. Distrib.*, vol. 146, no. 3, p. 283, 1999.

[34] J. A. Schachter, P. Mancarella, J. Moriarty, and R. Shaw, "Flexible investment under uncertainty in smart distribution networks with demand side response:

Assessment framework and practical implementation," *Energy Policy*, vol. 97, pp. 439–449, Oct. 2016.

[35] DECC (Department of Energy and Climate Change), "UK Renewable Energy Roadmap Update 2013," 2013.

[36] D. Quiggin, S. Cornell, M. Tierney, and R. Buswell, "A simulation and optimisation study: Towards a decentralised microgrid, using real world fluctuation data," *Energy*, vol. 41, no. 1, pp. 549–559, May 2012.

[37] International Energy Agency, *Distributed Generation in Liberalised Electricity Markets*. 2002.

[38] G. Pepermans, J. Driesen, D. Haeseldonckx, R. Belmans, and W. D'haeseleer, "Distributed generation: Definition, benefits and issues," *Energy Policy*, vol. 33, no. 6, pp. 787–798, 2005.

[39] C. L. Masters, "Voltage rise: the big issue when connecting embedded generation to long 11 kV overhead lines," *Power Engineering Journal*, vol. 16, no. 1. p. 5, 2002.

[40] S. Boljevic and M. Conlon, "Fault current level issues for urban distribution network with high penetration of distributed generation," *2009 6th Int. Conf. Eur. Energy Mark.*, pp. 1–6, 2009.

[41] BSI, "Nominal voltages for low voltage public electricity supply systems." Bristish Standards Institute, 2011.

[42] E. Demirok, D. Sera, R. Teodorescu, P. Rodriguez, and U. Borup, "Clustered PV inverters in LV networks: An overview of impacts and comparison of voltage control strategies," *2009 IEEE Electr. Power Energy Conf. EPEC 2009*, pp. 1–6, 2009.

[43] W. P. Distribution, "Western Power Distribution - Exporting Limiting," 2016. [Online]. Available: https://www.westernpower.co.uk/Connections/Generation/Alternative-Connections/Export-Capping.aspx. [Accessed: 01-Sep-2016].

[44] H. Bevrani, A. Ghosh, and G. Ledwich, "Renewable energy sources and frequency regulation: survey and new perspectives," *IET Renew. Power Gener.*, vol. 4, no. 5, p. 438, 2010.

[45] P. Tielens and D. van Hertem, "Grid Inertia and Frequency Control in Power Systems with High Penetration of Renewables," vol. 0, no. 2, pp. 1–6, 2012.

[46] The Royal Academy of Engineering, *Wind energy implications of large-scale deployment on the GB electricity system*, no. April. 2014.

[47] S. Dierkes, F. Bennewitz, M. Maercks, L. Verheggen, and A. Moser, "Impact of Distributed Reactive Power Control of Renewable Energy Sources in Smart Grids on Voltage Stability of the Power System," in *Electric Power Quality and Supply Reliability Conference (PQ), 2014*, 2014.

[48] R. J. Sarfi, M. M. A. Salama, and Y. Chikhani, "Practical aspects of performing a distribution system loss reduction study," in *Proceedings 1995 Canadian Conference on Electrical and Computer Engineering*, 1995, vol. 1, pp. 164–167.

[49] H. N. Tram and D. L. Wall, “Optimal conductor selection in planning radial distribution systems,” *IEEE Trans. Power Syst.*, vol. 3, no. 1, pp. 200–206, 1988.

[50] S. C. Vegunta, D. Hawkins, F. Clifton, A. Steele, and S. A. Reid, “Distribution Network Losses and Reduction Opportunities from a UK DNO’s Perspective,” in *23rd International Conference on Electricity Distribution*, 2015, pp. 15–18.

[51] J. Romero Aguero, “Improving the efficiency of power distribution systems through technical and non-technical losses reduction,” in *PES T&D 2012*, 2012, pp. 1–8.

[52] J. G. De Steese, J. E. Englin, and R. D. Sands, “Conservation Voltage Reduction Potential In The Pacific Northwest,” in *Proceedings of the 25th Intersociety Energy Conversion Engineering Conference*, 1990, vol. 4, pp. 43–47.

[53] The Aluminum Association, “Aluminum Electrical Conductor Handbook.” 1989.

[54] J. Dixon, L. Moran, J. Rodriguez, and R. Domke, “Reactive power compensation technologies: State-of-the-art review,” *Proc. IEEE*, vol. 93, no. 12, pp. 2144–2164, 2005.

[55] N. Leemput, F. Geth, J. Van Roy, J. Büscher, and J. Driesen, “Reactive power support in residential LV distribution grids through electric vehicle charging,” *Sustain. Energy, Grids Networks*, vol. 3, pp. 24–35, 2015.

[56] M. E. Baran and F. F. Wu, “Optimal sizing of capacitors placed on a radial distribution system.,” *IEEE Trans. Power Deliv.*, vol. 4, no. 1, pp. 735–743, 1989.

[57] M. E. Baran and F. F. Wu, “Optimal capacitor placement on radial distribution systems.,” *IEEE Trans. Power Deliv.*, vol. 4, no. 1, pp. 725–734, 1989.

[58] S. X. Chen, Y. S. F. Eddy, H. B. Gooi, M. Q. Wang, and S. F. Lu, “A centralized reactive power compensation system for LV distribution networks,” *IEEE Trans. Power Syst.*, vol. 30, no. 1, pp. 274–284, 2015.

[59] C. Gao and M. A. Redfern, “A review of voltage control techniques of networks with distributed generations using On-Load Tap Changer transformers,” in *Universities Power Engineering Conference (UPEC), 2010 45th International*, 2010, pp. 3–8.

[60] C. Long and L. F. Ochoa, “Voltage control of PV-rich LV networks: OLTC-fitted transformer and capacitor banks,” *IEEE Trans. Power Syst.*, vol. 31, no. 5, pp. 4016–4025, 2016.

[61] X. Liu, A. Aichhorn, L. Liu, and H. Li, “Coordinated control of distributed energy storage system with tap changer transformers for voltage rise mitigation under high photovoltaic penetration,” *IEEE Trans. Smart Grid*, vol. 3, no. 2, pp. 897–906, 2012.

[62] P. Wang, D. H. Liang, J. Yi, P. F. Lyons, P. J. Davison, and P. C. Taylor, “Integrating Electrical Energy Storage Into Coordinated Voltage Control Schemes for Distribution Networks,” *IEEE Trans. Smart Grid*, vol. 5, no. 2, pp. 1018–1032, 2014.

[63] Y. P. Agalgaonkar, B. C. Pal, and R. A. Jabr, “Distribution voltage control considering the impact of PV generation on tap changers and autonomous

regulators," *IEEE Trans. Power Syst.*, vol. 29, no. 1, pp. 182–192, 2014.

[64] L. F. Ochoa and G. P. Harrison, "Minimizing energy losses: Optimal accommodation and smart operation of renewable distributed generation," *IEEE Trans. Power Syst.*, vol. 26, no. 1, pp. 198–205, 2011.

[65] A. R. Dalmau, D. M. Perez, I. Diaz, D. C. Mendaza, and J. R. Pillai, "Decentralized Voltage Control Coordination of On-Load Tap Changer Transformers , Distributed Generation Units and Flexible Loads," *Smart Grid Technol. - Asia (ISGT ASIA), 2015 IEEE Innov.*, 2015.

[66] Cambridge Economic Policy Associates Ltd, Sinclair Knight Merz, and GL Noble Denton, "The Economic Lives of Energy Network Assets: A Report for Ofgem," 2010.

[67] I. D. De Cerio Mendaza, I. G. Szczesny, J. R. Pillai, and B. Bak-Jensen, "Flexible demand control to enhance the dynamic operation of low voltage networks," *IEEE Trans. Smart Grid*, vol. 6, no. 2, pp. 705–715, 2015.

[68] Ipsos MORI, "Consumer Experiences Of Time of Use Tariffs," 2012.

[69] S. J. Darby, "Load management at home: advantages and drawbacks of some 'active demand side' options," *Proc. Inst. Mech. Eng. Part A J. Power Energy*, vol. 227, no. 1, pp. 9–17, Oct. 2012.

[70] K. Worthmann, C. M. Kellett, P. Braun, L. Grüne, and S. R. Weller, "Distributed and Decentralized Control of Residential Energy Systems Incorporating Battery Storage," *IEEE Trans. Smart Grid*, vol. 6, no. 4, pp. 1914–1923, 2015.

[71] J. Wu and X. Guan, "Coordinated Multi-Microgrids Optimal Control Algorithm for Smart Distribution Management System," *Smart Grid, IEEE Trans.*, vol. 4, no. 4, pp. 2174–2181, 2013.

[72] L. C. Siebert, L. R. Ferreira, E. K. Yamakawa, E. S. Custodio, A. R. Aoki, T. S. P. Fernandes, and K. H. Cardoso, "Centralized and decentralized approaches to demand response using smart plugs," in *2014 IEEE PES T&D Conference and Exposition*, 2014, pp. 1–5.

[73] Quanyuan Jiang, Xingpeng Li, Bo Wang, and Haijiao Wang, "PMU-Based Fault Location Using Voltage Measurements in Large Transmission Networks," *IEEE Trans. Power Deliv.*, vol. 27, no. 3, pp. 1644–1652, Jul. 2012.

[74] H. A. Abdelsalam, A. Y. Abdelaziz, and V. Mukherjee, "Optimal PMU placement in a distribution network considering network reconfiguration," in *2014 International Conference on Circuits, Power and Computing Technologies [ICCPCT-2014]*, 2014, pp. 191–196.

[75] D. P. Shepard, T. E. Humphreys, and A. A. Fansler, "Evaluation of the vulnerability of phasor measurement units to GPS spoofing attacks," *Int. J. Crit. Infrastruct. Prot.*, vol. 5, no. 3–4, pp. 146–153, Dec. 2012.

[76] Q. Li, R. Negi, and M. D. Ilic, "Phasor measurement units placement for power system state estimation: A greedy approach," in *2011 IEEE Power and Energy Society General Meeting*, 2011, pp. 1–8.

[77] M. Music, A. Bosovic, N. Hasanspahic, S. Avdakovic, and E. Becirovic,

"Integrated Power Quality Monitoring Systems in smart distribution grids," in *2012 IEEE International Energy Conference and Exhibition (ENERGYCON)*, 2012, pp. 501–506.

[78] BBC News, "Warning over smart meters privacy risk," 2012. [Online]. Available: http://www.bbc.co.uk/news/technology-18407340. [Accessed: 12-Oct-2016].

[79] H. Ibrahim, A. Ilinca, and J. Perron, "Energy storage systems-Characteristics and comparisons," *Renew. Sustain. Energy Rev.*, vol. 12, no. 5, pp. 1221–1250, 2008.

[80] S. Shao, M. Pipattanasomporn, and S. Rahman, "Grid integration of electric vehicles and demand response with customer choice," *IEEE Trans. Smart Grid*, vol. 3, no. 1, pp. 543–550, 2012.

[81] I. Hadjipaschalis, A. Poullikkas, and V. Efthimiou, "Overview of current and future energy storage technologies for electric power applications," *Renew. Sustain. Energy Rev.*, vol. 13, no. 6–7, pp. 1513–1522, 2009.

[82] B. Kanenwisher, "Tesla unveils a battery to power your home, completely off grid," *Eat Tomorrow*. 10-Sep-2015.

[83] Q. Wang, P. Ping, X. Zhao, G. Chu, J. Sun, and C. Chen, "Thermal runaway caused fire and explosion of lithium ion battery," *J. Power Sources*, vol. 208, pp. 210–224, 2012.

[84] S. Amarakoon, J. Smith, and B. Segal, "Application of Life-Cycle Assessment to Nanoscale Technology: Lithium-ion Batteries for Electric Vehicles," 2013.

[85] H. Meier and K. Rehdanz, "Determinants of residential space heating expenditures in Great Britain," *Energy Econ.*, vol. 32, no. 5, pp. 949–959, 2010.

[86] R. Yao and K. Steemers, "A method of formulating energy load profile for domestic buildings in the UK," *Energy Build.*, vol. 37, no. 6, pp. 663–671, Jun. 2005.

[87] S. J. Darby and E. McKenna, "Social implications of residential demand response in cool temperate climates," *Energy Policy*, vol. 49, pp. 759–769, 2012.

[88] I. Stadler, "Power grid balancing of energy systems with high renewable energy penetration by demand response," *Util. Policy*, vol. 16, no. 2, pp. 90–98, Jun. 2008.

[89] S. Firth, K. Lomas, A. Wright, and R. Wall, "Identifying trends in the use of domestic appliances from household electricity consumption measurements," *Energy Build.*, vol. 40, no. 5, pp. 926–936, Jan. 2008.

[90] P. M. Armstrong, "Enhancing the energy storage capability of electric domestic hot water tanks," University of Oxford, 2015.

[91] Ofgem, "Demand Side Response: A Discussion Paper," Oct. 2011.

[92] P. M. Armstrong, M. Uapipatanakul, I. Thompson, D. Ager, and M. McCulloch, "Thermal and sanitary performance of domestic hot water cylinders: Conflicting requirements," *Appl. Energy*, vol. 131, pp. 171–179, Oct. 2014.

[93] M. Kim, M. S. Kim, and J. D. Chung, "Transient thermal behavior of a water heater system driven by a heat pump," *Int. J. Refrig.*, vol. 27, no. 4, pp. 415–421, Jun. 2004.

[94] J. B. A. Lima, R. T. A. Prado, and V. Montoro Taborianski, “Optimization of tank and flat-plate collector of solar water heating system for single-family households to assure economic efficiency through the TRNSYS program,” *Renew. Energy*, vol. 31, no. 10, pp. 1581–1595, Aug. 2006.

[95] Katherine Moore, “Learnings from Market Investment in Ripple Control and Smart Meters,” 2015.

[96] D. Saker, M. Vahdati, S. Millward, and E. Essah, “Uncovering the potential of domestic demand side management to maximise the diffusion of renewable energy,” in *World Renewable Energy Forum, WREF 2012*, 2012, vol. 4, pp. 2778–2785.

[97] N. Saker, M. Petit, and J. L. Coullon, “Demand side management of electrical water heaters and evaluation of the Cold Load Pick-Up characteristics (CLPU),” in *2011 IEEE Trondheim PowerTech*, 2011, no. i, pp. 1–8.

[98] D. Saker, P. J. Coker, M. Vahdati, S. Millward, and C. Carey, “Unlocking the demand response potential from domestic hot water tanks,” in *4th Annual TSBE EngD Conference Proceedings*, 2013.

[99] L. Hughes, “Meeting residential space heating demand with wind-generated electricity,” *Renew. Energy*, vol. 35, no. 8, pp. 1765–1772, Aug. 2010.

[100] D. S. Callaway, “Tapping the energy storage potential in electric loads to deliver load following and regulation, with application to wind energy,” *Energy Convers. Manag.*, vol. 50, no. 5, pp. 1389–1400, 2009.

[101] H. Hao, B. M. Sanandaji, K. Poolla, and T. L. Vincent, “Aggregate flexibility of thermostatically controlled loads,” *IEEE Trans. Power Syst.*, vol. 30, no. 1, pp. 189–198, 2015.

[102] J. Quiros-Tortos, L. F. Ochoa, S. W. Alnaser, and T. Butler, “Control of EV Charging Points for Thermal and Voltage Management of LV Networks,” *IEEE Trans. Power Syst.*, vol. 31, no. 4, pp. 3028–3039, Jul. 2016.

[103] R.-C. Leou, C.-L. Su, and C.-N. Lu, “Stochastic Analyses of Electric Vehicle Charging Impacts on Distribution Network,” *IEEE Trans. Power Syst.*, vol. 29, no. 3, pp. 1055–1063, May 2014.

[104] W. Shi, N. Li, X. Xie, C.-C. Chu, and R. Gadh, “Optimal Residential Demand Response in Distribution Networks,” *IEEE J. Sel. Areas Commun.*, vol. 32, no. 7, pp. 1441–1450, Jul. 2014.

[105] Y. Li and P. A. Crossley, “Monte Carlo study on impact of electric vehicles and heat pumps on LV feeder voltages,” in *12th IET International Conference on Developments in Power System Protection (DPSP 2014)*, 2014, p. 12.13-12.13.

[106] M. Al Essa and L. Cipcigan, “Reallocating Charging Loads of Electric Vehicles in Distribution Networks,” *Appl. Sci.*, vol. 6, no. 2, p. 53, Feb. 2016.

[107] A. N. Espinosa and L. Ochoa, “Dissemination Document: Low Voltage Networks Models and Low Carbon Technology Profile,” 2015.

[108] H. Bevrani, G. F. Ledwich, J. J. Ford, and Z. Y. Dong, “On power system frequency control in emergency conditions,” *J. Electr. Eng. Technol.*, vol. 3, no. 4,

pp. 499–508, 2008.

[109] National Grid, “Grid code: Frequency and voltage operating range,” 2010.

[110] M. Peydayesh and R. Baldick, “The Effects of Very Fast Response To Frequency Fluctuation,” *Int. Assoc. Energy Econ.*, 2012.

[111] M. Amin and J. Stringer, “The electric power grid: Today and tomorrow,” *MRS Bull.*, vol. 33, no. 4, pp. 399–407, 2008.

[112] National Grid Electricity Transmission, “Firm Frequency Response Tender Rules and Standard Contract Terms.” pp. 1–105, 2016.

[113] National Grid Electricity Transmission, “Enhance Frequency Response Full Results.” 2016.

[114] Cirrus Logic, “Three Channel Energy Measurement IC CS5480 Datasheet,” 2013.

[115] Analog Devices, “Six Current Channels , One Voltage Channel Energy Metering IC Data Sheet ADE7816.” 2013.

[116] T. Lobos and J. Rezmer, “Real-time determination of power system frequency,” *IEEE Trans. Instrum. Meas.*, vol. 46, no. 4, pp. 877–881, 1997.

[117] H. Karimi, M. Karimi-Ghartemani, and M. R. Iravani, “Estimation of Frequency and its Rate of Change for Applications in Power Systems,” *IEEE Trans. Power Deliv.*, vol. 19, no. 2, pp. 472–480, 2004.

[118] A. Routray, A. K. Pradhan, and K. P. Rao, “A novel Kalman filter for frequency estimation of distorted signals in power systems,” *IEEE Trans. Instrum. Meas.*, vol. 51, no. 3, pp. 469–479, 2002.

[119] M. B. Djurić and Ž. R. Djurišić, “Frequency measurement of distorted signals using Fourier and zero crossing techniques,” *Electr. Power Syst. Res.*, vol. 78, no. 8, pp. 1407–1415, 2008.

[120] A. K. Thota, S. C. Watson, E. Knapp, B. Thompson, and R. Jung, “Neuromechanical Control of Locomotion in the Rat,” *J. Neurotrauma*, vol. 22, no. 4, pp. 442–465, Apr. 2005.

[121] A. D. Georgoulis, A. Papadonikolakis, C. D. Papageorgiou, A. Mitsou, and N. Stergiou, “Three-Dimensional Tibiofemoral Kinematics of the Anterior Cruciate Ligament-Deficient and Reconstructed Knee during Walking*,” *Am. J. Sports Med.*, vol. 31, no. 1, pp. 75–79, 2003.

[122] M. Akke, “Frequency estimation by demodulation of two complex signals,” *IEEE Trans. Power Deliv.*, vol. 12, no. 1, pp. 157–163, 1997.

[123] National Grid, “Firm Frequency Response Tender Rules and Standard Contract Terms,” pp. 1–105, 2016.

[124] E. Styvaktakis, M. H. J. Bollen, and I. Y. H. Gu, “Automatic classification of power system events using RMS voltage measurements,” in *IEEE Power Engineering Society Summer Meeting*, 2002, vol. 2, pp. 824–829.

[125] J. J. Erbrink, *On-load Tap Changer Diagnosis on High-Voltage Power Transformers using Dynamic Resistance Measurements*. PhD Thesis, Delft

University of Technology, 2011.

[126] Northern PowerGrid, “NPS / 003 / 012 – Technical Specification for Continuous Emergency Rated (CER) Transformers.” 2016.

[127] O. A. Grigg, V. T. Farewell, and D. J. Spiegelhalter, “Use of risk-adjusted CUSUM and RSPRT charts for monitoring in medical contexts.,” *Stat. Methods Med. Res.*, vol. 12, no. 2, pp. 147–70, Mar. 2003.

[128] R. Kang and M. D. McCulloch, “Identification of Electric Power System Stress through Feeder Voltage Measurement,” in *Innovative Smart Grid Technologies Conference Europe (ISGT-Europe), 2014 IEEE PES*, 2014, pp. 1–6.

[129] J. Kim, S. Lee, and B. Cho, “Discrimination of battery characteristics using discharging/charging voltage pattern recognition,” in *2009 IEEE Energy Conversion Congress and Exposition, ECCE 2009*, 2009, pp. 1799–1805.

[130] M. J. Fuerstman, P. Garstecki, and G. M. Whitesides, “Scaled conjugate gradient and Bayesian training of neural networks for fault identification in cylinders,” *Science (80-.).*, vol. 79, pp. 828–832, 2001.

[131] C. Bishop, *Neural Networks for Pattern Recognition*. Clarendon Press, 1995.

[132] M. F. Møller, “A scaled conjugate gradient algorithm for fast supervised learning,” *Neural Networks*, vol. 6, no. 4, pp. 525–533, Jan. 1993.

[133] K. Heussen, S. Koch, A. Ulbig, and G. Andersson, “Energy storage in power system operation: The power nodes modeling framework,” in *2010 IEEE PES Innovative Smart Grid Technologies Conference Europe (ISGT Europe)*, 2010, pp. 1–8.

[134] K. Heussen, S. Koch, A. Ulbig, and G. Andersson, “Unified System-Level Modeling of Intermittent Renewable Energy Sources and Energy Storage for Power System Operation,” *IEEE Syst. J.*, vol. 6, no. 1, pp. 140–151, Mar. 2012.

[135] P. Armstrong, R. Kang, and M. McCulloch, “Improvements in systems for heating water,” 2015.

[136] British Standards Institute, “BS 1566-1:2002+A1:2011: Copper indirect cylinders for domestic purposes. Open vented copper cylinders. Requirements and test methods.” 2002.

[137] UK Power, “Economy 10 electricity heating tariff,” 2016. [Online]. Available: https://www.ukpower.co.uk/home_energy/economy_10. [Accessed: 20-Nov-2016].

[138] Wadebridge Renewable Energy Network, “Sunshine Tariff Trial,” 2016. [Online]. Available: http://wren.uk.com/sunshine. [Accessed: 20-Nov-2016].

[139] AA Electrical Services, “Night storage heaters, Economy 7 & Economy 10.” [Online]. Available: http://itshosting.me/aaes/night-storage-heaters-economy-7-economy-10/. [Accessed: 03-Nov-2016].

[140] E. Gunn, “Buying your energy at night to save on bills? Could Economy 7 tariffs make a comeback as electricity costs rise?,” 2014. [Online]. Available: http://www.thisismoney.co.uk/money/bills/article-2548171/What-Economy-7-

does-work.html. [Accessed: 03-Nov-2016].

[141] Tamas Borbely and M. Kerai, “Energy usage in households with Solar PV installations,” 2014.

[142] “Hot Water Cylinders and Accessories.” [Online]. Available: http://www.plumbcenter.co.uk/heating/cylinders-accessories/. [Accessed: 29-Jan-2015].

[143] Matlab Documentation Center, “Optimization Toolbox, Constrained optimization, fmincon.” 2016.

[144] MathWorks, “Search Results Choosing the Algorithm.” [Online]. Available: https://uk.mathworks.com/help/optim/ug/choosing-the-algorithm.html. [Accessed: 06-Nov-2016].

[145] Energy Saving Trust, “Measurement of Domestic Hot Water Consumption in Dwellings,” 2008.

[146] P. Crespo Del Granado, S. W. Wallace, and Z. Pang, “The value of electricity storage in domestic homes: a smart grid perspective,” *Energy Syst.*, vol. 5, no. 2, pp. 211–232, Jun. 2014.

[147] R. Granell, C. J. Axon, and D. C. H. Wallom, “Clustering disaggregated load profiles using a Dirichlet process mixture model,” *Energy Convers. Manag.*, vol. 92, pp. 507–516, Mar. 2015.

[148] A. N. Espinoza and L. F. Ochoa, “Deliverable 3.6 ‘What-if Scenario Impact Studies based on real LV networks,’” 2014.

[149] Electric Power Research Institute, “Introduction to the OpenDSS,” *Structure*, no. April. pp. 1–4, 2009.

[150] A. Navarro-Espinosa and L. F. Ochoa, “Probabilistic Impact Assessment of Low Carbon Technologies in LV Distribution Systems,” *IEEE Trans. Power Syst.*, vol. 31, no. 3, pp. 2192–2203, May 2016.

[151] Office for National Statistics, “Families and Households: 2015,” 2016. [Online]. Available: http://www.ons.gov.uk/peoplepopulationandcommunity/birthsdeathsandmarriages/families/bulletins/familiesandhouseholds/2015-11-05. [Accessed: 01-Jul-2016].

[152] Ofgem, “Feed-in Tariff Installation Report 31 December 2015,” 2016.

[153] British Standards Institution, “BS EN 50160: Voltage Characteristics of Electricity Supplied by Public Distribution Systems.” 2000.

[154] Elexon, “Load Profiles and their use in Electricity Settlement.” pp. 1–31, 2013.

[155] I. Richardson and M. Thomson, “Domestic electricity demand model - simulation example.” Loughborough University, 2010.

[156] T. Gozel, A. Navarro, and L. Ochoa, “Deliverable 3.5 ‘Creation of aggregated profiles with and without new loads and DER based on monitored data,’” 2014.

[157] Office for National Statistics, “Families and Households: 2015,” 2015. [Online]. Available:

http://www.ons.gov.uk/peoplepopulationandcommunity/birthsdeathsandmarriages/families/bulletins/familiesandhouseholds/2015-11-05. [Accessed: 01-Dec-2016].

[158] N. Kreutzer, "Electric Load in the Domestic Sector and its Modulation by Building Integrated Photovoltaic : Findings of a Detailed Monitoring Study of Energy Consumption in UK Buildings," University of Wales, 2010.

[159] Ofgem, "Feed-in Tariff Installation Report 30 September 2016," 2016.

[160] J. Davies, "A Guide To Roof Construction – Part 1." [Online]. Available: http://great-home.co.uk/a-guide-to-roof-construction/. [Accessed: 01-Dec-2016].

[161] "What is a kWp, and how does it relate to kW and kWh?," 2012. [Online]. Available: http://www.evoenergy.co.uk/blog/18514/what-is-a-kwp-and-how-does-it-relate-to-kw-and-kwh/. [Accessed: 01-Dec-2016].

[162] I. Knight, N. Kreutzer, M. Manning, M. Swinton, and H. Ribberink, "European and Canadian non-HVAC electric and DHW load profiles for use in simulating the performance of residential cogeneration systems," 2007.

[163] REDRING, "Powerstream 12kW," 2016. [Online]. Available: https://www.redring.co.uk/product/45793202/RP12-Powerstream-12kW. [Accessed: 15-Dec-2016].

[164] D. Croucher, "Design and Planning Framework for underground networks in UK Power Networks," *UK Power Networks*. pp. 1–20, 2011.

[165] Ofgem, "Feed-in Tariff (FIT): Generation & Export Payment Rate Table 01 October- 31 December 2016," 2016. [Online]. Available: https://www.ofgem.gov.uk/system/files/docs/2016/11/tariff_table_for_publishing.pdf. [Accessed: 18-Dec-2016].

[166] Energy Saving Trust, "Feed-in Tariffs," 2016. [Online]. Available: http://www.energysavingtrust.org.uk/scotland/grants-loans/renewables/feed-tariffs. [Accessed: 19-Dec-2016].

Appendix

Appendix 3.1

Photos of the OLTC transformer plate at SSE, Reading, where the OLTC and voltage data were recorded for the validation of the tap changing detection algorithm. Specification of 30% impendence drop has been highlighted.

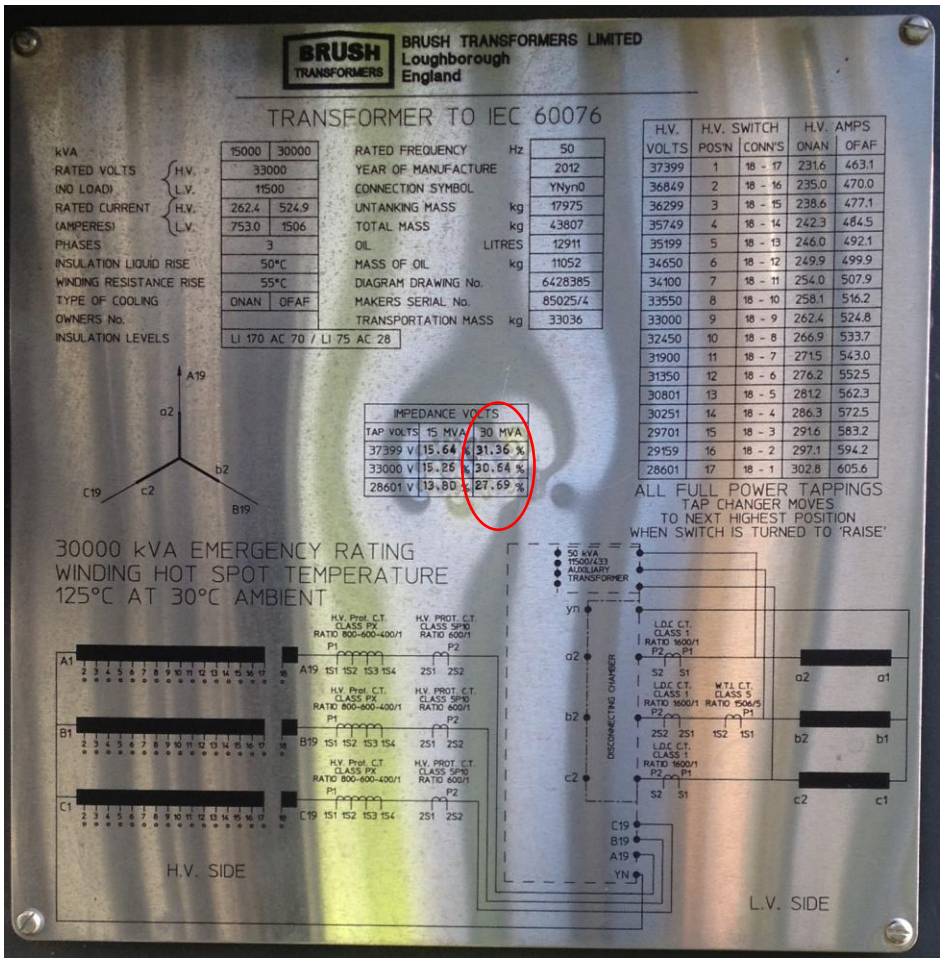

Appendix 3.2

132 kV voltage data between 19th of March to 20th of April, 2014, provided by SSE, showing a maximum voltage variation at around 3.5%.

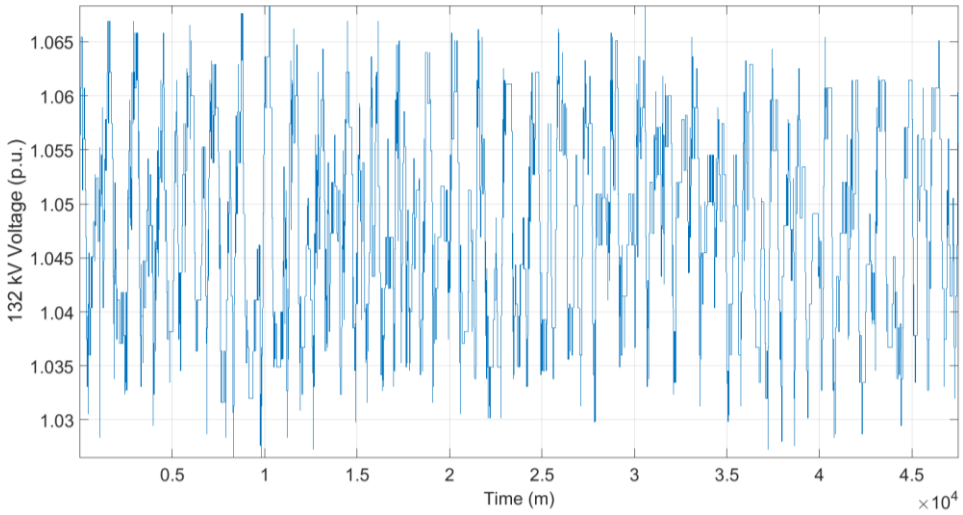

Appendix 3.3

Reading tap position provided by SSE between 12th and 18th of March, 2014, showing that tap position usually returns to the same position by the end of the day.

12-Mar-14 07:40:29	6
12-Mar-14 17:40:30	7
12-Mar-14 21:40:35	6
12-Mar-14 23:40:42	5
13-Mar-14 07:40:51	6
13-Mar-14 09:40:49	7
13-Mar-14 22:40:47	6
13-Mar-14 23:40:41	5
14-Mar-14 06:40:42	6
14-Mar-14 17:40:46	7
14-Mar-14 21:40:49	6
14-Mar-14 23:40:51	5
15-Mar-14 08:40:56	6
15-Mar-14 22:40:56	5
16-Mar-14 09:41:01	6
16-Mar-14 22:41:08	5
17-Mar-14 07:41:11	6
17-Mar-14 16:41:11	7
17-Mar-14 21:41:11	6
17-Mar-14 23:41:11	5
18-Mar-14 03:25:26	4
18-Mar-14 06:41:18	5
18-Mar-14 07:02:56	6
18-Mar-14 16:41:21	7
18-Mar-14 21:41:37	6
18-Mar-14 22:41:23	5

Appendix 4.1

Histograms of household occupancy feature distributions (boiler type, number of children, number of adults, region, house type) for each cluster determined in *Section 4.5* are shown in this appendix. No strong correlations between clusters and each household features are shown in these figures.

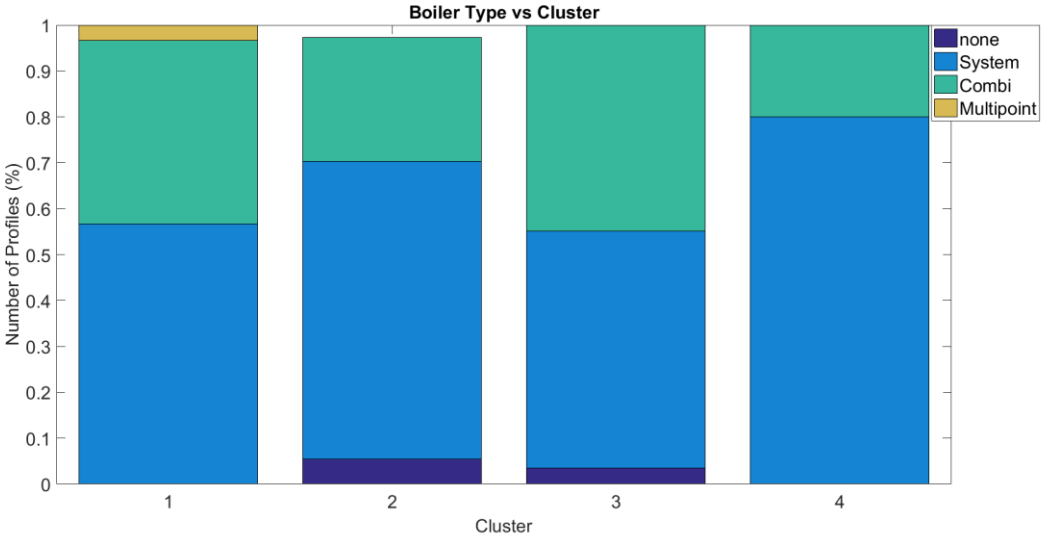

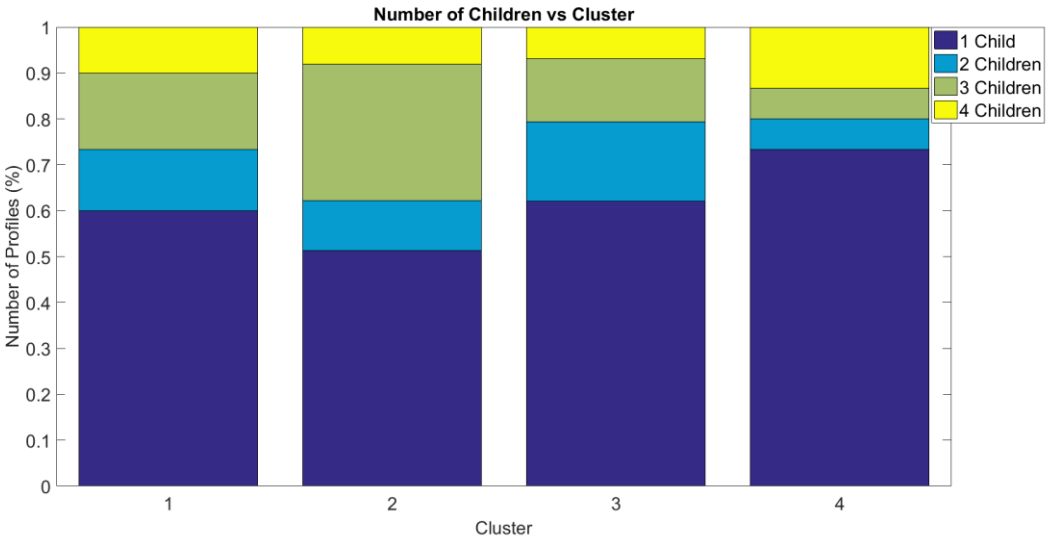

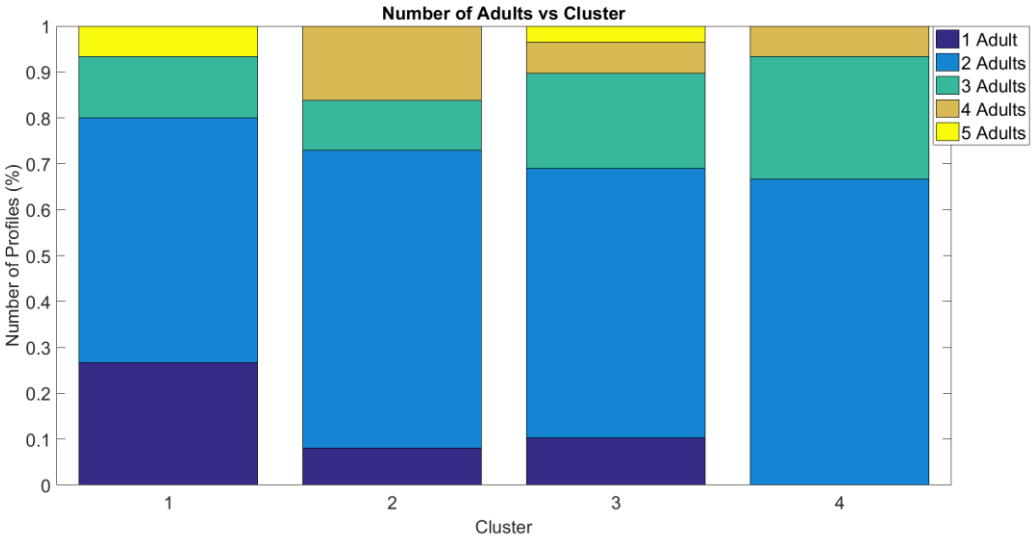
Number of Adults vs Cluster
Number of Profiles (%)
Cluster
1 Adult
2 Adults
3 Adults
4 Adults
5 Adults

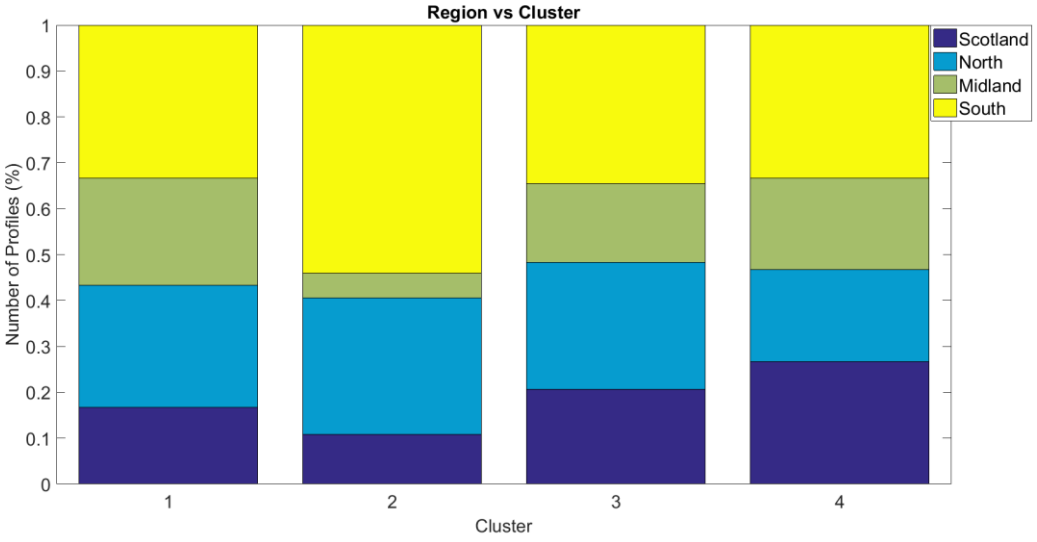
Region vs Cluster
Number of Profiles (%)
Cluster
Scotland
North
Midland
South

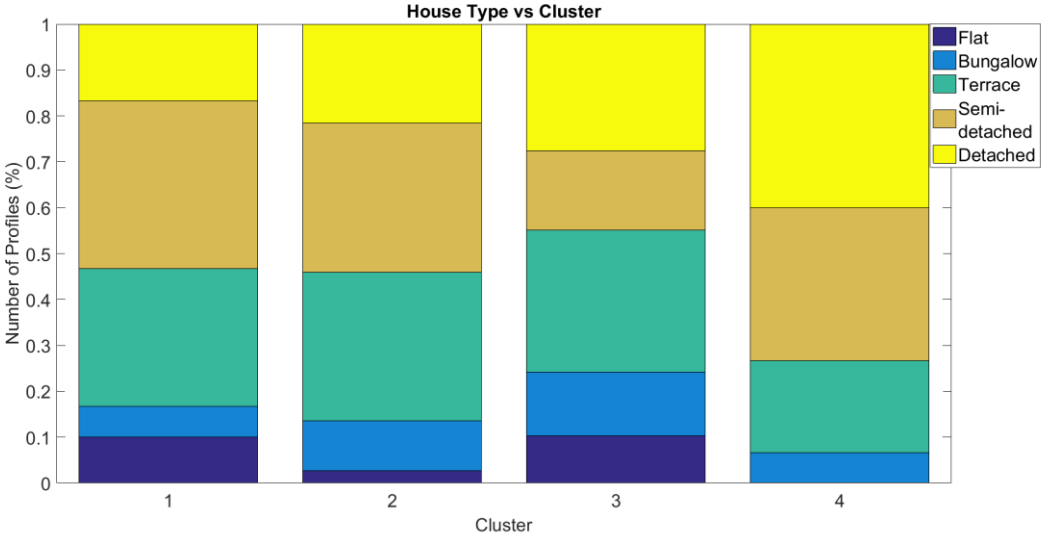
House Type vs Cluster
Number of Profiles (%)
Cluster
Flat
Bungalow
Terrace
Semi-detached
Detached